8-31-2024

Data driven decision making for sustainable planning and operations of large scale networks

Bahareh Kargar
New Jersey Institute of Technology, bk349@njit.edu

Copyright Warning & Restrictions

The copyright law of the United States (Title 17, United States Code) governs the making of photocopies or other reproductions of copyrighted material.

Under certain conditions specified in the law, libraries and archives are authorized to furnish a photocopy or other reproduction. One of these specified conditions is that the photocopy or reproduction is not to be "used for any purpose other than private study, scholarship, or research." If a, user makes a request for, or later uses, a photocopy or reproduction for purposes in excess of "fair use" that user may be liable for copyright infringement,

This institution reserves the right to refuse to accept a copying order if, in its judgment, fulfillment of the order would involve violation of copyright law.

Please Note: The author retains the copyright while the New Jersey Institute of Technology reserves the right to distribute this thesis or dissertation

Printing note: If you do not wish to print this page, then select "Pages from: first page # to: last page #" on the print dialog screen

ABSTRACT

DATA DRIVEN DECISION MAKING FOR SUSTAINABLE PLANNING AND OPERATIONS OF LARGE SCALE NETWORKS

by
Bahareh Kargar

This dissertation explores data-driven decision-making networks, focusing on sustainable planning and operations for large-scale systems such as healthcare supply chains and power systems. One significant application in healthcare is the optimization of vaccine supply chains. An agent-based simulation-optimization modeling framework is developed to enhance the efficiency and sustainability of vaccine distribution. First, an agent-based epidemiological model of COVID-19 is extended to capture disease transmission dynamics and forecast the number of susceptible individuals and infections. Then, a sustainable vaccine supply chain considering the impacts of greenhouse gases is developed and integrated with the simulation model to minimize total costs and environmental impacts. This framework is validated using a real-world COVID-19 scenario in the US, underscoring the importance of advanced modeling techniques in managing complex and dynamic public health challenges, ensuring effective and responsible responses. Another application is in incentive-based demand response programs in the residential sector. The residential sector often struggles with demand response due to a limited understanding of consumer-specific behavior patterns and demand elasticity. This project explores the incorporation of heterogeneous elasticity values in demand response to enhance the economic efficiency of Load Serving Entities. Three distinct models are introduced: aggregate elasticity, appliance-specific elasticity, and customer and appliance-specific elasticity. By assessing the impact

of tailored demand response incentives on energy consumption patterns, the model is applied to a test case in New Jersey. The results demonstrate that appliance-specific models and customer-specific elasticities significantly reduce operational costs, benefiting both customers and service providers. The study highlights the critical role of detailed elasticity information in optimizing demand response strategies and suggests future research directions towards leveraging advanced analytics for more effective demand management. Finally, the incentive-based demand response strategy is extended using Reinforcement Learning to optimize residential energy consumption. A Multi-Agent Reinforcement Learning framework is developed, leveraging multiple agents to dynamically adjust appliance usage based on incentive signals. Deep Q-Networks are employed to handle large state spaces. The effectiveness of this approach is demonstrated with real-world data while promoting consumer engagement through adaptive incentive-based strategies.

DATA DRIVEN DECISION MAKING FOR SUSTAINABLE PLANNING AND OPERATIONS OF LARGE SCALE NETWORKS

by
Bahareh Kargar

A Dissertation
Submitted to the Faculty of
New Jersey Institute of Technology
in Fulfillment of the Requirements for the Degree of
Doctor of Philosophy in Industrial Engineering

Department of Mechanical and Industrial Engineering

August 2024

APPROVAL PAGE

DATA DRIVEN DECISION MAKING FOR SUSTAINABLE PLANNING AND OPERATIONS OF LARGE SCALE NETWORKS

Bahareh Kargar

SangWoo Park, Dissertation Advisor — Date
Assistant Professor of Mechanical and Industrial Engineering, NJIT

Layek Abdel-Malek, Committee Member — Date
Professor of Mechanical and Industrial Engineering, NJIT

Sanchoy Das, Committee Member — Date
Professor of Mechanical and Industrial Engineering, NJIT

Golgen Bengu, Committee Member — Date
Associate Professor of Mechanical and Industrial Engineering, NJIT

Lian Qi, Committee Member — Date
Professor of Rutgers Business School, Rutgers University

BIOGRAPHICAL SKETCH

Author: Bahareh Kargar

Degree: Doctor of Philosophy

Date: August 2024

Undergraduate and Graduate Education:

- Doctor of Philosophy in Industrial Engineering,
  New Jersey Institute of Technology, Newark, NJ, 2024
- Master of Science in Industrial Engineering,
  Iran University of Science Technology, Tehran, Iran, 2017
- Bachelor of Science in Industrial Engineering,
  Payam-e Noor University, Shiraz, Iran, 2012

Major: Industrial Engineering

Presentations and Publications:

B. Kargar, P. MohajerAnsari, İ. E. Büyüktahtakın, H. Jahani, and S. Talluri, "Data-driven modeling for designing a sustainable and efficient vaccine supply chain: A COVID-19 case study," *Transportation Research Part E: Logistics and Transportation Review,* 184, 103494, 2024.

B. Kargar, S. Park, "Learning Heterogeneous Elasticity Values for Incentive Based Demand Response," *Oral Presentation, INFORMS Annual Meeting*, Phoenix, Arizona, USA, 2023.

B. Kargar, İ. E. Büyüktahtakın, "Sustainable Cold Vaccine Supply Chain Network Design: COVID 19 Case Study," *Oral Presentation, INFORMS Annual Meeting*, Indianapolis, Indiana, , USA, 2022.

This dissertation is dedicated to my beloved parents, whose love and support have been my guiding light. To my mother, the light of my life, my mentor, motivator, and inspiration: your kind hands have taught me kindness and compassion, and your patience was the sacrifice you made for my success. Your endless encouragement and care have been my strength. To my beloved father, who is looking down from above: although our time together on this earth was short, thank you for enduring life's difficulties with strength and resilience, teaching me to face adversity with courage. You continue to inspire me every day. I'm lost for words to express my gratitude for all your sacrifices. You are my lucky charm, my hero, and my joy

ACKNOWLEDGMENTS

I would like to express my sincere gratitude to my advisors and mentors, Dr. Esra Buyuktahtakin Toy and Dr. SangWoo Park. Their immense knowledge, guidance, motivation, and support have been invaluable. My PhD would not have been possible without them, and I am forever grateful for their contributions. It is truly a blessing to work with mentors whom I deeply admire.

I extend my deepest gratitude to my committee members: Drs. Layek Abdel-Malek, Sanchoy Das, Golgen Bengu, and Lian Qi. It has been a tremendous honor to work with such distinguished professionals, whose expertise and dedication have profoundly inspired me. Each of you has provided profound personal and professional guidance, enriching my understanding of scientific research and life.

I am also thankful to the Department of Mechanical and Industrial Engineering at NJIT, especially Dr. Sanchoy Das, the Graduate Advisor for IE Programs. His expertise and professionalism always guided me on the right path, and his advice was invaluable. I am grateful to all the friends and peers I have met at NJIT; I will never forget your contributions and look forward to maintaining our connections throughout my career.

A heartfelt thank you to my mother for her endless love, unwavering support, and the incomparable lessons in compassion and patience she has taught me. I also want to express my sincere appreciation to my brother, Ali, whose mentorship and inspiration have been crucial to my journey, and to my sisters for their encouragement in reaching my goals. Finally, I deeply value the support and belief of my dear friends Leila and Hamed, which has been a source of great strength for me.

TABLE OF CONTENTS

TABLE OF CONTENTS
(Continued)

Chapter **Page**

TABLE OF CONTENTS
(Continued)

Chapter **Page**

LIST OF TABLES

Table **Page**

LIST OF FIGURES

LIST OF FIGURES
(Continued)

Figure **Page**

CHAPTER 1

INTRODUCTION

1.1 Overview

Data-driven decision-making is increasingly being applied to large-scale and complex systems and domains. One example of such a system is a supply chain network, which has intricate microstructures, macro emergences, and dynamic evolutions [1]. Data-driven decision-making involves using evidence and insights derived from data to guide the decision-making process and verify a plan of action before committing to it [2]. Its importance cannot be overstated in the success of businesses, industries, and governments. Data-driven decision-making models are employed to analyze data, discover insights, and assist in effective decision-making.

Operations research (OR) is a problem-solving and decision-making approach that uses analytical methods to improve management in organizations. The concept of OR emerged during World War II and was initially used by military planners. OR involves the use of various problem-solving techniques and methods to achieve better decision-making and efficiency. This approach can be applied to a wide range of real-world problems in different fields such as manufacturing, finance, healthcare, and logistics. OR provides highly developed methodologies to model and solve these real-world problems, resulting in insights on optimal decision-making.

This dissertation is centered on data-driven decision-making networks, with a focus on proposing innovative data-driven models to support sustainable planning and operations in large-scale networks. The objective is to leverage data-driven models in diverse areas, including healthcare supply chains and power systems, to make more informed decisions and plans.

1.2 Data-Driven Models

Data-driven decision-making refers to the process of using data and insights derived from it to guide the decision-making process and validate a plan of action [2]. It is crucial for the success of businesses, industries, governments, and individuals, as it helps in achieving goals and avoiding failures. Data plays the most significant role in effective decision-making. The main component of effective decision-making is analyzing data to provide valuable insights. This approach is transforming various fields, including business, healthcare, and education, where experts gather and analyze data to inform their decision-making [3]. The adoption of data analytics has become widespread in industries, with businesses incorporating it in every stage of their operations, from managing supply chains to gaining a competitive advantage.

Data-driven models rely on statistical and machine learning techniques to develop the model. The process of data-driven modeling consists of three distinct steps, which involve the use of three different sets of data. Typically, these sets of data are created by dividing a main dataset into different subsets that contain the same input variables but with different combinations of values and for different periods [4]. The first step in this process is the training of the algorithm, where the model is run on the training dataset to produce results. These results are then

compared to the original training data, and the parameters of the algorithm can be adjusted accordingly to fit the training dataset better [5]. The second step in the data-driven modeling process is validation, which involves using a separate dataset to evaluate the algorithm's performance and adjust its key modeling parameters for better fitting. To prevent overfitting, the validation dataset must be distinct from the training dataset [6]. Overfitting can cause the model to perform well with specific data but poorly with other datasets. In the third step, the algorithm is tested on the remaining data to provide a final unbiased evaluation of the model's forecasting and modeling performances. It is generally accepted that the model's parameters and structure should not be changed based on the results of this final step [7].

The worldwide spread of COVID-19 has affected numerous countries and regions, creating a significant challenge for governments in managing crises [8]. Responding promptly and taking timely action is critical in combating COVID-19. The World Health Organization (WHO) declared the COVID-19 pandemic a public health emergency of international concern, and its impact has been felt in all aspects of life. Additionally, the COVID-19 epidemic is generating a substantial amount of data that could be utilized to guide decision-making in the COVID-19 response [9]. These emergency measures involve disease detection, prevention and control, and recovery from the potential largest global recession since the Great Depression, which is caused by the COVID-19 pandemic [10].

In addition, critical decisions must be made to protect communities and economies worldwide. These may include the postponement or cancellation of various events such as sports, religious, political, and cultural activities, as well as actions to address severe stock shortages resulting from panic buying [11].

According to a report, educational institutions such as schools, universities, and colleges in over 180 countries have been closed on either a national or local basis, affecting the majority of the student population globally [12].

As the epidemic continues to spread, various forms of COVID-19 related information and data are constantly being updated on the internet. This vast amount of information includes global epidemic data, statistics related to COVID-19 research, details of medical equipment, transportation information, and more. By integrating and categorizing these various forms of information, data-driven decision-making can be used to effectively manage and respond to this disease and any relevant emergencies.

Data-driven decision-making has proven to be crucial and successful in responding to the COVID-19 pandemic. Various countries and regions have implemented data-driven policies including prevention and control measures, financial assistance, psychological counseling, and reopening strategies. Policymakers have derived valuable information from various COVID-19 related data sources and utilized machine learning algorithms to make informed decisions, resulting in better and more suitable choices.

Furthermore, optimizing energy systems to reduce overall energy costs has become an important focus for large-scale industries worldwide. The U.S. power grid, operated by thousands of organizations, is recognized as the world's largest machinery for transporting electricity over vast distances through a complex and extensive network. The grid is essential for almost all aspects of daily life, making its reliability crucial to the nation's interests. The rising occurrence of severe weather events has posed significant challenges to safely operating electric power systems around the world.

The concept of demand response (DR), which refers to changes in electricity consumption during peak hours, has gained popularity as a way to address reliability and efficiency issues in the power grid [13]. DR provides a powerful alternative for homeowners looking to reduce costs and conserve energy while contributing to overall grid stability. According to the U.S. Department of Energy, residential electricity consumption accounts for over 38% of total U.S. electricity consumption. However, one of the main reasons why demand response has not been widely adopted in the residential sector is a lack of understanding of consumer behavior patterns. Therefore, the development of data-driven models to enhance the effectiveness of residential demand response programs is crucial for both consumers and utilities looking to optimize energy distribution plans. These data-driven models can help discover customer psychology patterns and the heterogeneous nature of elasticity from available datasets without requiring expert knowledge.

1.3 Motivation

The existing literature on epidemiology focuses mainly on either estimating disease transmission or optimizing the distribution of critical resources, neglecting the importance of addressing both simultaneously. In most cases, either agent-based simulations or optimization models are used separately to control an epidemic. Furthermore, previous studies on vaccine supply chains have overlooked crucial vaccination details, such as different vaccine types and the number of doses required for each vaccine type. To address these gaps, we are motivated by the goal of designing a data-driven large-scale network for optimal COVID-19 vaccine

distribution and epidemic control planning. This approach will consider different echelons and enable a macroscopic view of the distribution process.

Furthermore, demand response programs are crucial in reducing residential electricity demand, especially during peak hours. However, to our best knowledge, existing demand response schemes do not take full advantage of the reduction potential: (a) they do not consider customer psychology, (b) they do not consider appliance-specific demand elasticity, and (c) they do not consider customer-specific demand elasticity. Offering monetized rewards to customers for reducing demand is a widespread method for demand response [14, 15]. However, offering a constant reward for all types of appliances and all customers may not be the most effective way.

To enhance demand response and reduce electricity costs, power grid operators and load aggregators need to understand customer psychology and the heterogeneous nature of elasticity. Our research is motivated by the goal of establishing a framework for understanding the heterogeneous elasticity of electricity consumption in the face of monetary rewards, and utilizing that information for the dynamic pricing of such rewards. We aim to predict the elasticity of electricity demand for each customer and appliance based on factors such as the day of the week, time of day, temperature, humidity, lifestyle, and building characteristics. This information will be utilized to design a reward pricing mechanism that adjusts the amount of reward based on the current system state. The main goal of this project is to improve the stability and efficiency of power grid operations while reducing the environmental impact of residential buildings.

1.4 Contributions

Our proposed research could be broadly categorized in three parts:

- First, we introduce an agent-based simulation-optimization modeling framework, aimed at enhancing the efficiency and sustainability of vaccine supply chains. We first extend an agent-based epidemiological simulation model of COVID-19 to capture disease transmission and forecast the number of susceptible individuals and infections. We then develop a sustainable Vaccine Supply Chain (VSC) considering the impact of greenhouse gases and integrate the simulation model into the VSC model to minimize total costs and environmental impacts. The integrated modeling framework runs in a loop, dynamically optimizing resource allocation based on the continuous interchange of outputs between the simulation and VSC models, which refines the results with each iteration. The framework's effectiveness is validated through its application to a real-world COVID-19 vaccine distribution scenario in the United States. Our findings underscore the importance of strategically managing vaccine supplies to control the pandemic. The comprehensive analysis and robustness of the proposed framework make it a valuable tool for policymakers and health administrators, offering a scalable solution that can be adapted to various infectious disease outbreaks.

- Second, we explore the incorporation of heterogeneous elasticity values in Incentive-Based Demand Response (IBDR) programs to enhance the economic efficiency of Load Serving Entities (LSE). We present three distinct models—each increasing in granularity from aggregate elasticity, through appliance-specific, to both customer and appliance-specific elasticity. Energy loss and power flow equations are also considered in the proposed model as it is an essential part of the power grid. We assess the impact of tailored demand response incentives on energy consumption patterns using a test case in Essex County, New Jersey. Our results show that while appliance-specific models and incorporating customer-specific elasticities significantly reduce

operational costs, benefiting both customers and the service providers. Furthermore, the study highlights the critical role of detailed elasticity information in optimizing demand response strategies, suggesting a potential direction for future research towards leveraging advanced analytics for more effective demand management.

- Third, we present a Multi-Agent Reinforcement Learning (MARL) framework for dynamic pricing in IBDR programs, targeting residential energy consumption management. The proposed MARL-IBDR framework leverages the interaction of multiple agents to optimize energy consumption and pricing strategies, using Deep Q-Networks (DQNs) to handle large and continuous state spaces. A hierarchical architecture is employed, integrating multiple Residential Agents (RAs), which dynamically adjust their appliance usage based on incentive signals. The model employs a Markov Decision Process (MDP) framework to accommodate the inherent variability and uncertainty of energy demand. The effectiveness of the proposed framework is demonstrated using real-world data, highlighting its potential to enhance grid reliability and efficiency while promoting consumer engagement through adaptive incentive-based strategies.

CHAPTER 2

DATA-DRIVEN MODELING FOR DESIGNING A SUSTAINABLE AND EFFICIENT VACCINE SUPPLY CHAIN: A COVID-19 CASE STUDY

2.1 Introduction

The spread of COVID-19 overwhelmed healthcare systems in many countries, leading governments to implement various intervention strategies, such as mandatory mask-wearing, quarantine, and lockdowns, to slow down or stop the virus's spread [16, 17]. However, the most effective way to address the global COVID-19 crisis is to develop effective and efficient vaccines [18, 19].

The rapid spread of COVID-19 has emphasized the critical importance of vaccines in planning response activities in all regions during and post-pandemic. Vaccines play a pivotal role in saving lives and stopping this global threat. Increased vaccination rates have been shown to substantially decrease the number of cases and deaths, thereby protecting individuals from this disease. Consequently, all countries have urgently started scientific research and vaccine development efforts. Following unprecedented efforts, the scientific community has delivered good news, indicating that several vaccines have been developed and approved for emergency use. For example, on December 31, 2020, the Pfizer/BioNTech vaccine was listed for WHO Emergency Use Listing (EUL). The SII/Covishield and AstraZeneca vaccines were listed for EUL on February 16,

2021. On March 12, 2021, the Janssen vaccine developed by Johnson & Johnson was also approved [20]. The Moderna vaccine received Emergency Use Listing (EUL) approval on April 30, 2021, along with several other vaccines developed to combat the COVID-19 outbreak. This dissertation focuses on three vaccines that are predominantly used in the US: PfizerBioNTech, Moderna, and Johnson & Johnson (Janssen).

After the development of COVID-19 vaccines, the main challenge is distributing them on a large scale. To pilot COVID-19 vaccine distribution, governments and policymakers must prioritize the distribution to healthcare workers, front-line workers, and vulnerable populations [21]. This has become a prominent challenge in the US, where policymakers seek efficient guidelines to distribute vaccines effectively and equitably to states, clinics, pharmacies, and communities. The allocation of a limited vaccine supply to downstream demand while considering rapidly changing demand with the evolving pandemic, locating regional warehouses and distribution centers, and making shipping plans to achieve the optimal distribution strategy is also challenging. Furthermore, the distribution of COVID-19 vaccines at a macroscopic level has heightened the strategic importance of supply chain management practice in an emergency situation [22]. Therefore, we aim is to develop a simulation-based supply chain model to effectively optimize available resources and provide critical insights into the optimal vaccine location and allocation decisions.

Human interactions and contact networks play a crucial role in transmitting COVID-19. Therefore, developing an algorithm that models human behavior, interactions, and disease transmission is essential to predict the impact of vaccines on reducing infection rates. This approach is particularly important in optimizing

the distribution of vaccines by determining the best location for vaccination warehouses and making allocation decisions. Kerr et al. [23] developed a stochastic agent-based model (Covasim) that simulates person-to-person contact within various social layers. The agent-based Covasim model can estimate the number of infections and assess the effectiveness of various interventions, including physical distancing, testing, isolation, contact tracing, and quarantine.

This dissertation presents a mixed-integer programming (MIP) model that incorporates a general vaccine location-allocation as a key factor in disease control. The proposed Vaccine Supply Chain (VSC) is multi-echelon including four critical layers namely the manufacturer, the regional warehouse, the state repository, and the healthcare facilities. Our study, while using COVID-19 as the primary case study, offers insights applicable to a broad range of pandemic scenarios. Our model is not limited to any specific time or disease. The adaptability and flexibility of our model, evident in its ability to handle different vaccine types and manage varying dosage schedules, demonstrate its applicability beyond COVID-19. The recurrence of pandemics, from SARS to COVID-19 emphasizes the need for adaptable and efficient vaccine distribution models. The optimization model considers both strategic and tactical planning decisions to optimize the distribution of vaccines, including the location of regional and state warehouses at the strategic level, and the allocation of vaccines at the tactical level. Specifically, tactical planning decisions such as production, inventory, and capacity expansion are taken into account in addition to strategic planning decisions such as facility location and switching warehouses. Moreover, this research extends beyond the traditional cost-centric objectives, embedding environmental considerations as a pivotal aspect in our logistical network optimization. This

not only aspires to minimize the total logistical costs but also to reduce environmental impacts, establishing a blueprint for sustainable and responsible vaccine distribution. Unlike the previous studies on vaccine distribution, our optimization model considers the population dynamics constraints of susceptible individuals, infections, and vaccinated individuals to project the disease's growth. Specifically, we have combined the extended Covasim model with the vaccination center location-allocation MIP model into one simulation-optimization framework. This innovative framework operates iteratively, both forward and backward in time, to dynamically optimize vaccine allocation strategies in response to evolving disease dynamics. To solve the proposed VSC model, we use an augmented ϵ-constraint method, which incorporates inventory control, switching warehouses, and capacity expansion into the multi-period facility planning problem to address demand shortage.

The remainder of this research is structured as follows. In Section 2.2, we review of the most pertinent literature related to agent-based models, as well as vaccine and epidemic supply chain management, followed by a discussion of our main contributions. Section 2.3 presents the epidemic model, the VSC model, and the simulation-optimization model, along with the underlying assumptions and key features. Section 2.4 offers an analysis of the results obtained from the numerical case study and the validation of the model using COVID-19 infection data. Sensitivity analysis and managerial implications are discussed in Sections 2.5 and 2.6, which provide valuable insights for policymakers and decision-makers. Finally, in Section 2.7, we conclude the research study and outline directions for future research.

2.2 Literature Review and Contributions

In the context of disease control, particularly with regard to COVID-19, resource allocation becomes a crucial aspect due to the scarcity of resources during a pandemic. In this section, we will briefly review the relevant literature on agent-based modeling, vaccines, and epidemic SC networks, specifically focusing on the COVID-19 pandemic. We will also highlight this study's critical contributions to the existing body of knowledge.

2.2.1 Agent-based models

Models for examining COVID-19 transmission and control measures can be broadly divided into two main types: compartmental models and agent-based models. A computational model that simulates the actions and interactions of autonomous agents to analyze a system's behavior and governing factors is known as an agent-based model. On the other hand, compartment models serve as a simpler mathematical framework that delineates the flow of entities between discrete compartments within a system. These models are particularly suited for scenarios where the population or system can be segregated into separate groups or states with clear transition phases [24].

While both agent-based and compartmental models have their strengths in studying epidemic dynamics, we chose agent-based models due to several key reasons aligned with our research's objectives. Although agent-based models can be more complex and computationally expensive, their ability to encapsulate intricate individual-level interactions and behaviours in complex systems offers a depth of analysis that is essential to our research. They excel at capturing heterogeneous behaviors and nonlinear relationships, providing flexibility to

represent a wide array of scenarios by adjusting agent rules. This flexibility is beneficial in our work where situations may not fit into predefined compartments. Finally, these models facilitate scenario testing and sensitivity analysis, enabling us to explore potential outcomes of various policies or interventions. Therefore, their adaptability and realism make them particularly suited for our study, where individual decision-making and emergent patterns significantly influence the results. Recently, many studies on epidemic control have employed agent-based simulation models to estimate the disease transmission rate and predict infectious disease progression [25, 26, 27, 23]. For instance, Müller et al. [27] have developed a methodology that combines transportation modeling with a mechanical infection model and a person-centric disease progression model into an epidemiological simulation model. Shamil et al. [26] have proposed an agent-based model to simulate the transmission of COVID-19 among the inhabitants of New York City. Li et al. [25] utilize advanced computational services to develop open-sourced agent-based simulation models, analyzing various allocation strategies and accurately simulating virus transmission patterns.

The utilization of vaccines in controlling the spread of COVID-19 has been recognized as a crucial intervention and has been incorporated into the agent-based simulation literature. For instance, Kerr et al. [23] introduced the COVID-19 Agent-based Simulator (Covasim) to estimate the transmission and disease dynamics of COVID-19. Covasim includes demographic information on population size and age structure, all levels of transmission contact networks, and age-specific disease outcomes, along with a comprehensive set of interventions, such as vaccination intervention, to control the epidemic. Li and Giabbanelli [28] developed an agent-based simulation model to investigate the effectiveness of a

nationwide vaccine campaign, considering different vaccine efficacies, acceptance rates, and daily vaccine capacity. Jahn et al. [29] presented a dynamic agent-based population model to compare vaccination strategies for five age groups. They employed stepwise optimization to derive a prioritization sequence that maximizes the reduction in total hospitalizations and deaths compared to no vaccination.

2.2.2 Vaccine and epidemic supply chain network

Mathematical optimization models have been integrated with epidemiological disease models to manage the logistics and operations of controlling infectious diseases, such as COVID-19. Critical resources such as personal protective equipment (PPE), test kits, ventilators, and vaccines should be effectively distributed during the COVID-19 pandemic [30, 31, 32].

The existing literature focuses extensively on VSC to control COVID-19 and other infectious diseases [33, 34, 35, 36]. VSC operations for infectious disease control include vaccine composition [37, 38, 39], vaccine production to manage supply and demand sides [40, 41], vaccine allocation [42, 43], and finally, vaccine delivery which involves distribution operations and optimizing inventory [44, 45]. A comprehensive literature review that focuses on resilient VSC has been done in the study of Golan et al. [46]. The lack of network-based, modeling-based, and quantitative analysis, according to Golan et al. [46], is a fundamental gap that must be filled to develop decision tools for the COVID-19 VSC network.

In the context of COVID-19, several studies have developed mathematical models to determine vaccine prioritization strategies for different population groups [47, 48, 49]. Bubar et al. [47] compared COVID-19 vaccine prioritization strategies among five population groups and assessed their impacts. Babus et

al. [48] developed a model to estimate occupation-based infection risks and allocate vaccine priorities accordingly. Vahdani et al., [49] present a multi-vaccine distribution model for the COVID-19 pandemic, addressing diverse vaccination challenges and prioritizing different age groups.

However, most studies on COVID-19 vaccine distribution focus on operational issues related to vaccine allocation, with few studies dedicated to developing mathematical models for vaccine distribution [50, 51, 52, 53]. For instance, Basciftci et al. [53] proposed a distributionally robust optimization model for optimally locating distribution centers and allocating resources such as test kits and vaccines, accounting for spatiotemporal demand uncertainties for these resources. Bertsimas et al. [51] developed a prescriptive framework to optimize vaccine site location, population assignment to different sites, and vaccine allocation. They embedded the predictive epidemiological model DELPHI-V into a mathematical model to optimize vaccine distribution. Yin et al. [54] proposed a modeling framework to optimize vaccination center locations and vaccines allocated to these centers, pharmacies, and health centers, considering a limited budget and health population dynamics. Zhang et al. [52] introduce a framework for emergency logistic network design, incorporating an improved short-term epidemic prediction model and a robust optimization approach for reliable facility resource allocation during the pandemic. Unlike most current COVID-19 vaccine distribution literature, this dissertation covers a wide range of vaccine-related operational problems, including vaccine acceptance rates and population dynamics constraints to predict disease growth. It also includes location-allocation decisions such as facility location, subsequent vaccine allocation

to health facilities, and capacity planning, accounting for inventory and unmet demand.

The VSC presents unique challenges that have both environmental and societal implications, especially given its requirement for low-temperature storage and transportation. This not only necessitates different transportation modes but also leads to increased energy consumption and refrigerant gas leakage. With increasing awareness of sustainability, it is essential to design supply chains that balance economic, environmental, and social factors. While numerous studies have examined the economic aspects of the VSC [55, 53, 52], recent literature has started to emphasize environmental considerations. For example, Saif and Elhedhli [56] introduced a hybrid optimization approach for eco-sustainable cold supply chain design in Canada, focusing on minimizing costs and global warming impact for perishable products like meat and vaccines. Sazvar et al. (2021) proposed a multi-objective model to achieve a sustainable and resilient influenza VSC in Iran, minimizing costs and CO_2 emissions while maximizing resilience. In another paper, Jahani et al. [19] developed a bi-objective queuing model in Australia to optimize vaccine distribution, focusing on minimizing wait time and total investment in vaccine holding and ordering.

One of the critical aspects of the VSC network is its flexibility in adapting to any changes in demand, particularly in response to the continuous change in the behavior of COVID and its emerging variants. This makes the VSC network resilient to fluctuations in virus behavior and demand for vaccines. To address changes in demand and subsequent costs, the VSC should be dynamically reconfigured over time by opening/closing facilities, switching facilities, or expanding capacity [57]. This dynamic supply chain reconfiguration can be achieved by

considering facility opening/closing, capacity expansion, and facility switching at each potential location in a multi-period and multi-echelon supply chain. Studies have shown that dynamic reconfiguration of the supply chain can lead to improved performance and cost savings [57, 58].

Despite some literature on the dynamic facility location problem ([57], there has been little attention given to the design of sustainable SCs with capacity expansion over the planning horizon. Thanh et al. (2008) proposed a mixed-integer linear program to design a multi-product, multi-echelon, production-distribution network, considering the opening, closing, and expansion of facilities. Pimentel et al. [58] developed a model for stochastic capacity planning and dynamic network design, considering facility location and capacity planning decisions under demand uncertainty. Wilhelm et al. [57] introduced a mathematical model for multi-period, multi-product, multi-echelon dynamic supply chain networks, considering capacity expansion, contraction, and closures. Fattahi et al. [59] proposed a mixed-integer model to design a dynamic, multi-echelon supply chain with price-sensitive demand, incorporating modular capacity options for production plants.

In most dynamic supply chain models [60, 61, 57, 58], facilities that are operational at the beginning of the planning horizon can be either closed or switched, but once a facility is closed, it must remain closed until the end of the planning horizon. On the other hand, facilities that are not operational at the beginning of the planning horizon can be opened and subsequently expanded; after opening, they must remain operational until the end of the planning horizon. As a result, in such models, a facility with excess capacity cannot be closed or switched. Our proposed model addresses this limitation by allowing for capacity expansion, as well as closure or switching of facilities.

2.2.3 Key contributions

Existing epidemiological literature typically focuses on one aspect of epidemic control. More specifically, to control the pandemic, most studies utilize either agent-based simulations (e.g., Covasim) or compartment models (e.g., SIR) to estimate disease transmission or optimization models separately to distribute the critical resources. Moving beyond the typical focus of epidemiological studies, our research uniquely integrates both agent-based simulations and optimization models. This combined approach offers a comprehensive and adaptable pandemic control strategy, merging the depth of agent-based simulations with the key strategies derived from optimization models. Our dissertation seeks to address the limitations in the field of vaccine distribution during the pandemic by making the following contributions:

- Our study addresses a gap in VSC research by offering a macroscopic-level model for COVID-19 vaccine distribution and inventory management, ensuring an optimal balance across all supply chain echelons. Unlike existing models like Yin et al. [54], which focus only on the state level, our model expands its scope to a macroscopic, US-wide scale. It includes not only manufacturers, warehouses, state repositories, and healthcare facilities but also emphasizes the limited shelf-life of vaccines to align production and distribution with capacity, reducing wastage and optimizing resources. This multi-echelon VSC model captures the intricate vaccine distribution dynamics across diverse geographies and population densities.

- The VSC design accommodates the unique challenges of cold chain management, including low-temperature storage, transportation, and specialized packaging, ensuring efficient vaccine delivery. Simultaneously, our model recognizes the broader environmental impact by considering the global warming potential of various greenhouse gases (GWP), not just CO_2 emissions. This approach, which extends beyond economic considerations, is especially pertinent in cold supply chains, as highlighted by Saif and Elhedhli [56]), demonstrating our commitment to sustainability in supply chain optimization.

- Another significant contribution in VSC management is the model's dynamic adaptability. It features the capability for capacity expansion, enabling manufacturers to adjust production efficiently in response to fluctuating vaccine demands. This ensures that vaccine production remains agile and aligned with real-time needs. Furthermore, the model's iterative simulation-optimization framework continuously updates with the latest pandemic data. This adaptability allows for accurate estimations of vaccine demand and strategic responses to evolving pandemic dynamics. This flexibility is crucial in managing the complexities and uncertainties inherent in global health crises.

- Our model, inspired by Kerr et al. [23], effectively integrates vaccination compartments for different vaccine types, considering specific dosages to control the epidemic outbreak. This comprehensive approach ensures our optimization model benefits from accurate inputs derived from the simulation model. Consequently, our strategies are tailored to the unique vaccine-specific strategies, leading to more efficient distribution plans. We also incorporate key vaccination factors like vaccine effectiveness, acceptance rates, and transmission rates, essential in any pandemic response. These factors are not only crucial for planning effective vaccine distribution strategies but also for achieving herd immunity.

2.3 Problem Formulation

This section provides a detailed description of the agent-based simulation and optimization models and their integration. It includes specific features and assumptions incorporated into both models, the notation used, and the formulation of our VSC model.

2.3.1 Model features and assumptions

Epidemic model features. The Covasim model, introduced by Kerr et al. [23], is an open-source agent-based simulation model used to forecast COVID-19 pandemic trends, evaluate various intervention strategies, and estimate resource needs to control the epidemic. This model incorporates country-specific

demographics based on age and population size, realistic transmission networks among different contact layers (e.g., households, schools, and workplaces), disease outcomes based on age, and viral dynamics of the disease. Additionally, the model includes human behaviors with daily activities to estimate COVID-19 transmission, considering various interventions such as testing, isolation, contact tracing, quarantine, and vaccination.

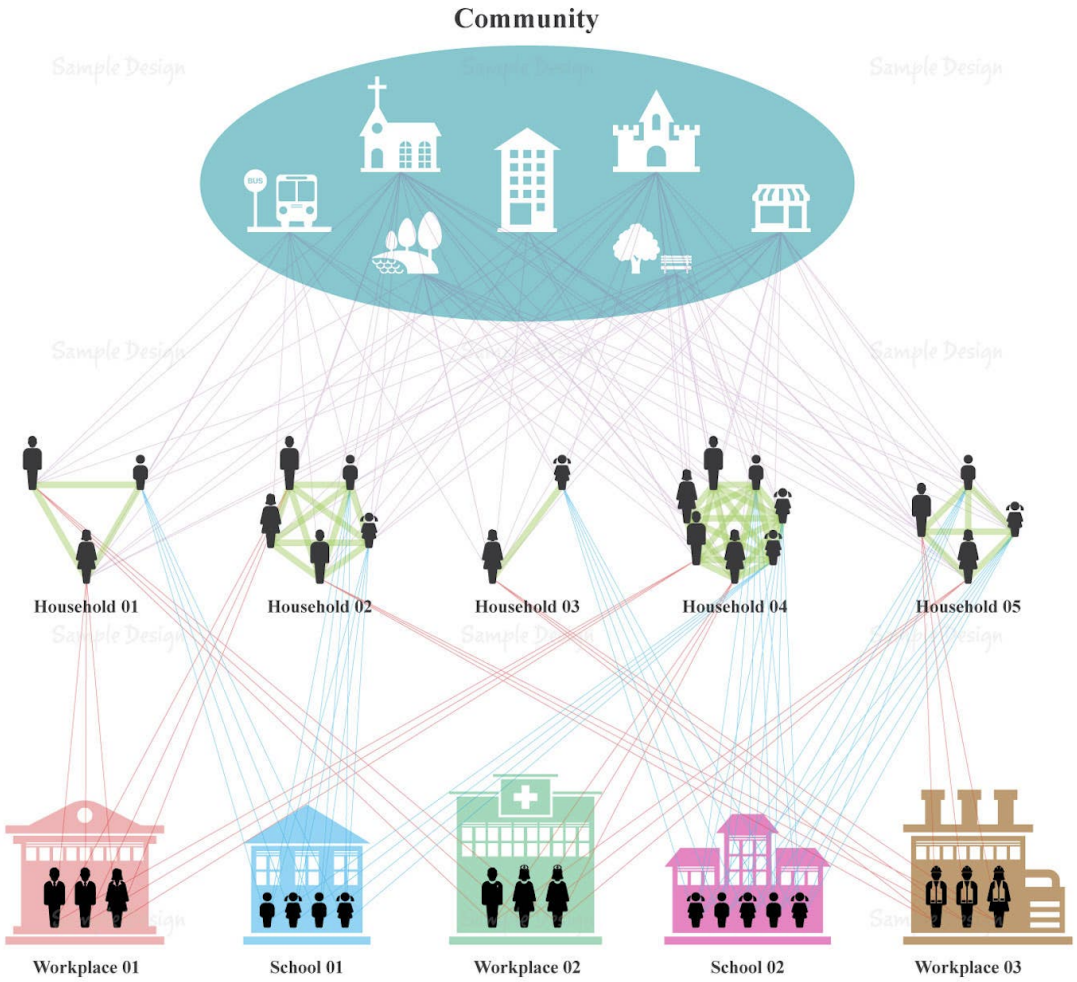

Figure 2.1 Contact networks with multiple layers in Covasim.
Source: Inspired by Kerr et al. [23].

In our proposed simulation-optimization modeling framework, Figures 2.1, 2.2, 2.3, and 2.4 are interconnected, each playing a pivotal role in illustrating our comprehensive approach to vaccine supply chain management. Figure 2.1 (Contact networks in Covasim) provides for understanding how individual interactions across various social layers influence disease transmission, which is vital for vaccine distribution planning. Figure 2.2 (Structure of Covasim) further details the health status classifications crucial for modeling the epidemic's progression. Figure 2.3 (Structure of the VSC model) shows the multi-echelon supply chain, essential for understanding the logistical aspects of vaccine distribution. Finally, Figure 2.4 (Disease transmission optimization modeling) integrates these elements, to demonstrate the application of disease transmission data in optimizing vaccine distribution strategies.

The Covasim agent-based simulation model depicted in Figure 2.1 captures the movement of individuals among various social layers where they interact and potentially increase the risk of infection. For instance, individuals may carry out daily activities in public places or interact with family members and friends in the community. Students may interact with their classmates and teachers in school, and adults may interact with their colleagues in the workplace. These dynamic contacts are approximated as static average daily contacts between different layers, as illustrated in Figure 2.1, with individuals having different connections (lines) and connection weights (line widths) for each layer.

The Covasim model considers different health statuses of individuals based on disease symptoms and transmission. Specifically, each individual is classified as susceptible, exposed, asymptomatic, presymptomatic, recovered, or dead. Notably, infectious individuals are categorized into asymptomatic, presymp-

tomatic, mild, severe, or critical groups based on their symptoms. The asymptomatic compartment represents infected individuals who never develop symptoms, while the presymptomatic compartment denotes those who have been infected but have not yet developed symptoms. Figure 2.2 illustrates a schematic diagram of disease transmission and the different health statuses of individuals.

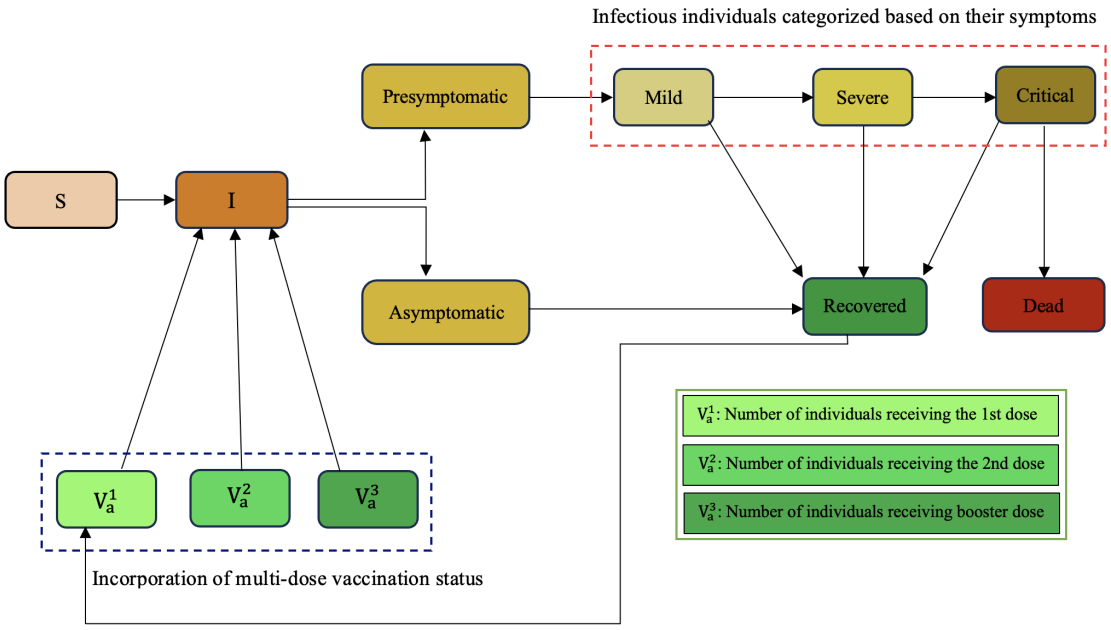

Figure 2.2 Structure of the Covasim simulation model
Source: Inspired by Kerr et al.[23].

Susceptible individuals may become infected by encountering infected individuals, leading to exposure. Exposed individuals can be further categorized as asymptomatic (i.e., individuals who do not exhibit symptoms) or presymptomatic (i.e., individuals who develop symptoms later). Presymptomatic individuals may experience symptoms ranging from mild to severe or critical. Asymptomatic individuals typically recover from the disease on their own, but those with critical symptoms may die because of a weakened immune system or delays in treatment.

In our research, we have expanded upon the simulation model developed by Kerr et al. [23] by introducing three additional categories to account for vaccination status. As shown in Figure 2.2, these categories are denoted as V_{a1}, V_{a2}, and V_{a3}, which correspond to individuals who have received their first, second, and third vaccine doses, respectively. Incorporating the three additional vaccine dose categories into our model addresses key challenges by significantly increasing the complexity of both the COVASIM simulation and VSC models. Managing these complexities involves handling specific requirements for each vaccine category, such as different dosages for each vaccine type, the time intervals between doses, and tracking the number of individuals receiving each dose. Additionally, the introduction of these categories increases logistical challenges, such as ensuring appropriate transportation for each vaccine type, which vary in their storage and handling requirements. These aspects add complexity to our model, making it more comprehensive and reflective of real-world vaccine distribution scenarios. For individuals who have chosen to receive the Pfizer or Moderna vaccines, the second dose is typically administered a few weeks after the first dose, and a third booster shot is given after a few months. It is important to mention that we assumed of the same vaccine acceptance rate across all states in the United States.

Vaccine supply chain features. The VSC under consideration is a multi-echelon supply chain comprising four layers: the manufacturer, the regional warehouse, the state repository, and the healthcare facilities, as depicted in Figure 2.3. The manufacturers produce vaccines, which are then transferred to the regional warehouses. From there, the vaccines are dispatched to the state repositories in different states, ultimately deliver them to various healthcare

facilities. The healthcare facilities, such as clinics, pharmacies, hospitals, and vaccine centers, constitute the last echelon in the VSC and are responsible for fulfilling customer demands directly.

In our VSC, the locations of the manufacturer and health facilities are predetermined and fixed. However, the locations of the regional warehouses and state repositories can be chosen from available potential locations through the network design. The quantity of vaccine flow between successive layers is also determined through network design. It is assumed that each vaccine supply at time t will be distributed from the manufacturer to the end user (health facility) during each period t.

The optimization model comprises three vaccine types, namely Pfizer, Moderna, and Janssen. We assume that each health facility administers only one type of vaccine. The Pfizer and Moderna vaccines require two doses, followed by a booster shot, while the Janssen vaccine involves a single dose, followed by a booster shot. Due to the high supply volumes (Statista, 2022), the Pfizer vaccination center has a higher vaccine capacity (e.g., 6,000 daily capacity) than the Moderna and Janssen vaccination centers, which have a lower vaccine capacity (e.g., 2,000 daily capacity).

The storage and transportation of vaccines require special cold chain equipment. Therefore, different vehicle types, such as freezers for Pfizer and Moderna and refrigerators for Janssen should be considered in the VSC. Thus, we assume that the transportation cost of Pfizer and Moderna with trucks equipped with freezers is higher than the cost of Janssen with trucks equipped with a refrigerator. Consequently, we assume that each health facility administers only one type of vaccine to streamline the logistical and operational dynamics significantly.

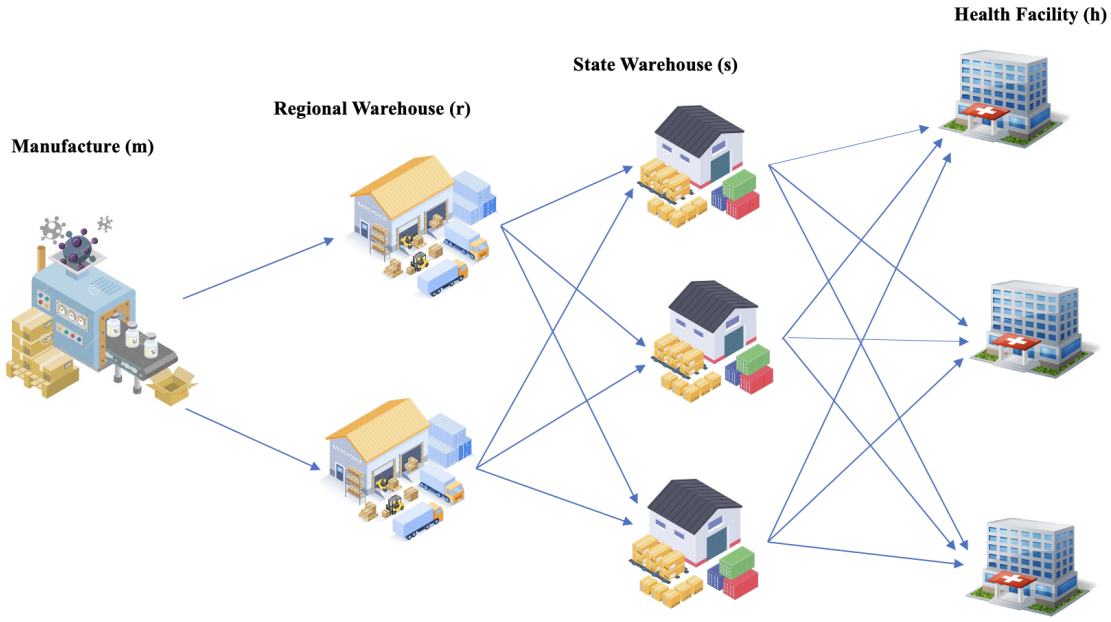

Figure 2.3 Structure of the VSC model and its flow.

This assumption mitigates the complexities and potential challenges associated with handling different vaccines multiple vaccine types with different requirements at a single facility, ensuring a smoother, more efficient operation. Furthermore, adopting such a strategy aligns with potential real-world approaches that favor specialization to facilitate the vaccination process. By focusing on a singular vaccine type, healthcare facilities can optimize their storage and administration protocols, minimizing potential errors and enhancing the vaccination campaign's overall efficiency and safety.

Incorporating disease transmission equations into our optimization model at each time period and in each state allows us to make optimal vaccine location-allocation decisions while taking into account their impact on disease growth. These equations are based on agent states flow in the simulation model, as shown in Figure 2.4. The S and I agent states represent the Susceptible and

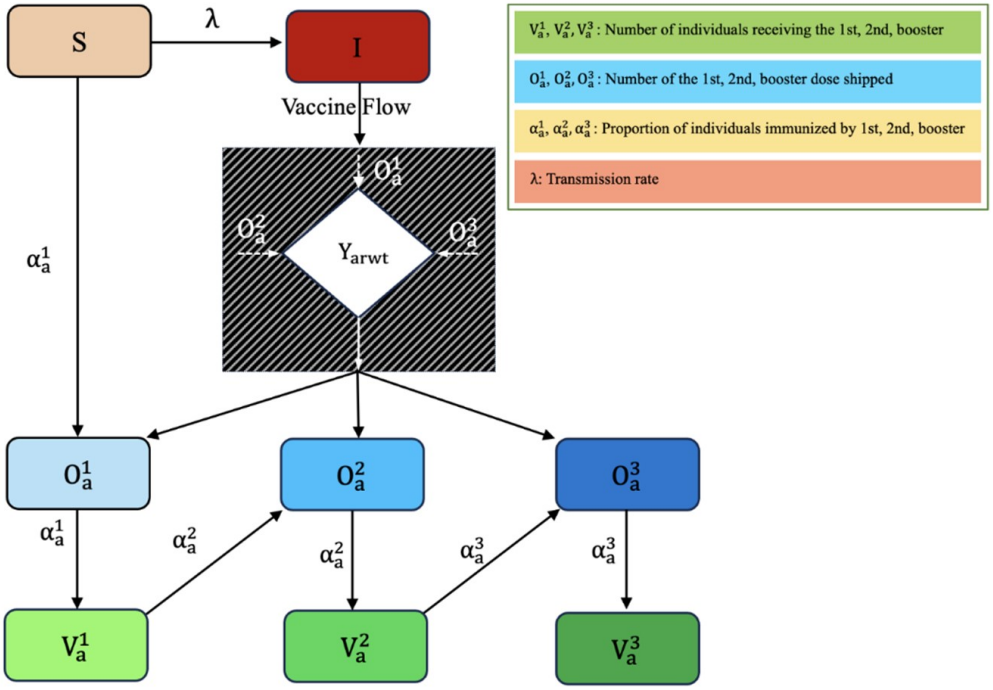

Figure 2.4 Disease transmission optimization modeling.

Infected populations, respectively. Individuals in state S are prone to infection and move to Infected state I, which includes both Asymptomatic and Presymptomatic individuals. The grey box illustrates the vaccine flow from the regional warehouse to the state repository, denoted as Y_{artw}, with O_{a1}, O_{a2}, and O_{a3} representing the quantities of first, second, and third doses shipped, respectively. V_{a1}, V_{a2}, and V_{a3} represent people who have received the first, second, and third (booster) doses of different vaccine types. Furthermore, α_{a1}, α_{a2}, and α_{a3} represent the proportion of individuals who get immunization by V_{a1}, V_{a2}, and V_{a3}, respectively. Susceptible individuals can receive vaccines and move to the V_{a1}, V_{a2}, and V_{a3} agent states. The results for the S, I, V_{a1}, V_{a2}, and V_{a3} agent states in each state at each time are used as inputs in the optimization model to generate vaccine center location and allocation decisions.

2.3.2 Model notation

The following are the notations used in the mathematical model.

Table 2.1 Sets and Indices

Symbol	Description
m	Index of manufacturer, $m = 1, \ldots, M$
r	Index of potential regional warehouse sites located in region, $r = 1, \ldots, R$
w	Index of potential state repository sites located in state, $w = 1, \ldots, W$
h	Index of health facilities, $h = 1, \ldots, H$
a	Index of vaccine type, $a = 1, \ldots, A$
d_a	Index of the number of vaccine doses for each vaccine type a, $d_a = 1, \ldots, \ldots D_a$
t	Index of time, $t = 1, \ldots, \overline{T}$

Table 2.2 Parameters

Parameter	Description
N	Number of regional warehouses to be deployed in location r
M	Number of state repositories to be deployed in location w
ϕ	Percentage of capacity of warehouse
cap_{rt}	Capacity of regional warehouse r at time t
cap_{wt}	Capacity of state repository w at time t
Capi_amt	Initial capacity of manufacturer m for producing vaccine type a at time period t
$\text{Cap}_m^{\max}$	Maximum capacity of manufacturer m
CF_{rt}	Fixed cost of opening a regional warehouse r at time t
CF_{wt}	Fixed cost of opening a state repository w at time t
CT_{amrt}	Transportation cost per unit of vaccine type a from manufacturer m to regional warehouse r at time t
CT_{arwt}	Transportation cost per unit of vaccine type a from regional warehouse r to state repository w at time t
CT_{awht}	Transportation cost per unit of vaccine type a from state repository w to health facility h at time t
CP_{amt}	Production cost of vaccine type a produced by
Continued on next page	

Table 2.2 – continued from previous page

Parameter	Description
	manufacturer m at time t
CH_{amt}	Holding inventory cost per unit of vaccine type a in manufacturer m at time t
CH_{art}	Holding inventory cost per unit of vaccine type a in regional warehouse r at time t
CH_{awt}	Holding inventory cost per unit of vaccine type a in state repository w at time t
CC_{amt}	Cost of capacity increments of manufacturer m for producing vaccine type a at time t
CS_{rt}	Fixed cost of switching a regional warehouse r for other cold products at time t
CS_{wt}	Fixed cost of switching a state repository w for other cold products at time t
EF_{rt}	Annual fixed CO_2-equivalent emissions from a regional warehouse r at time t
EF_{wt}	Annual fixed CO_2-equivalent emissions from a state repository w at time t
e_{amrt}	CO_2-equivalent emissions per unit of vaccine type a shipped between manufacturer m and regional warehouse r at time t
e_{arwt}	CO_2-equivalent emissions per unit of vaccine type a shipped between regional warehouse r and state repository w at time t
e_{awht}	CO_2-equivalent emissions per unit of vaccine type a between state repository w and health facility h at time t
λ_{wt}	Disease transmission rate from S_{wt} to I_{wt} in state w at time t
$\alpha_a^{d_a}$	Proportion of individuals who get immunization by the vaccine dose d_a for each vaccine type a
π_w	The initial number of susceptible individuals in state w, inputted from the agent-based simulation model
ϖ_w	The initial number of infections in state w, inputted from the agent-based simulation model

Continued on next page

Table 2.2 – continued from previous page

Parameter	Description
$\theta_{aw}^{d_a}$	The initial number of individuals who have received the vaccine dose d_a for each vaccine type a in state w
$\beta_{aw}^{d_a}$	The vaccine acceptance rate of dose d_a for each vaccine type a, i.e., willingness to get vaccinated, in state w
k_{d_a}	Number of days completed after dose d_a of each vaccine type a, $k_i = 1, \ldots, K_{d_a}$
σ	Specific limitation percentage of infections

2.3.3 Mathematical MIP model formulation

Our proposed model is inherently general, designed to be applicable across a wide range of pandemic scenarios beyond COVID-19. It provides the flexibility to handle a variety of vaccine types along with their specific dosing requirements, an essential aspect for addressing the diverse needs of different pandemics. In our problem formulation, we have modelled the dynamics of population infection and vaccinated population constraints to be applicable to a range of pandemics, not just COVID-19. The constraints for balancing susceptible, infected, and vaccinated individuals are deliberately designed to be general. By fine-tuning specific parameters, these constraints can be applied effectively to different pandemic scenarios. Moreover, the model's framework to vaccine logistics and demand constraints is characterized by its adaptability. These aspects have been formulated to allow for easy adjustment in response to the fluctuating conditions of pandemics and the diverse nature of vaccines. This adaptability is crucial for effective management of both initial and subsequent vaccine allocations, adapting

Table 2.3 Decision Variables and Descriptions

Variable	Description
I_{wt}	Infected individuals in state w at time t.
S_{wt}	Susceptible individuals in state w at time t.
$V_{awt}^{d_a}$	Number of people who receive the vaccine dose d_a for each vaccine type a in state w at time t.
X_{rt}	1 if a regional warehouse is opened in location r at time t; 0 otherwise.
X_{wt}	1 if a state repository is opened in location w at time t; 0 otherwise.
Z_{rt}	1 if a regional warehouse is switched for other cold products in location r at time t; 0 otherwise.
Z_{wt}	1 if a state repository is switched for other cold products in location w at time t; 0 otherwise.
Y_{amrt}	Number of vaccine type a shipped from manufacturer m to regional warehouse r at time t.
Y_{arwt}	Number of vaccine type a shipped from regional warehouse r to state repository w at time t.
Y_{awht}	Number of vaccine type a shipped from state repository w to health facility h at time t.
$O_{arwt}^{d_a}$	Number of vaccine dose d_a for each vaccine type a shipped from regional warehouse r to state repository w at time t.
L_{amt}	Inventory level of vaccine type a in manufacturer m at time t.
L_{art}	Inventory level of vaccine type a in regional warehouse r at time t.
L_{awt}	Inventory level of vaccine type a in state repository w at time t.
P_{amt}	Production quantity of vaccine type a produced by manufacturer m at time t.
$Capt_{amt}$	Total capacity of manufacturer m for producing vaccine type a at time period t.
$Capc_{amt}$	Capacity increments of manufacturer m for producing vaccine type a at time period t.

to the dynamic needs of pandemics where vaccine requirements and distribution strategies can vary significantly.

In the critical endeavor to manage the pandemic effectively, a multifaceted approach is paramount. The primary objective remains to minimize the spread of infections across all regions, which is encapsulated in our model through Constraint 2.33. This constraint limits infections, aligning our supply chain strategies with crucial public health goals. However, the vaccine distribution process presents significant logistical and environmental challenges. In addressing these, our focus extends to the entire vaccine supply chain, where operational efficiency and environmental responsibility are crucial. From an operational perspective, the cost objective is instrumental in streamlining processes and identifying cost-effective strategies. Simultaneously, by minimizing CO_2-equivalent emissions, our model promotes a more environmentally responsible vaccine supply chain (VSC). This holistic approach seeks to balance immediate public health concerns with long-term economic and environmental sustainability. The mathematical formulation for the optimization model is provided.

Objective functions

$$\begin{aligned}
\min Z_1 = & \sum_r \sum_t CF_{rt} X_{rt} + \sum_w \sum_t CF_{wt} X_{wt} \\
& + \left[\sum_a \sum_t \left(\sum_m \sum_r CT_{amrt} Y_{amrt} + \sum_r \sum_w CT_{arwt} Y_{arwt} + \sum_w \sum_h CT_{awht} Y_{awht} \right) \right] \\
& + \sum_a \sum_m \sum_t CP_{amt} P_{amt} \\
& + \left[\sum_a \sum_t \left(\sum_m CH_{amt} L_{amt} + \sum_r CH_{art} L_{art} + \sum_w CH_{awt} L_{awt} \right) \right] \\
& + \sum_a \sum_m \sum_t CC_{amt} Capc_{amt} \\
& + \sum_r \sum_t CS_{rt} Z_{rt} + \sum_w \sum_t CS_{wt} Z_{wt} \quad (2.1)
\end{aligned}$$

The objective function 2.1 aims to minimize the total supply chain costs. Specifically, the first and second terms in the objective function represent the total fixed costs of opening regional warehouses and state repositories, respectively. The following three terms represent the shipping costs of vaccines among different echelons of the vaccine network. The following four terms represent the production and inventory costs in the manufacturer, regional warehouse, and state warehouse. Subsequently, costs associated with capacity increments of the manufacturer and switching the regional and state warehouses are formulated. Finally, the last term is associated with vehicle costs, including fixed and transportation costs.

$$\begin{aligned}
\min Z_2 = & \sum_r \sum_t EF_{rt} X_{rt} + \sum_w \sum_t EF_{wt} X_{wt} \\
& + \left[\sum_a \sum_t \left(\sum_m \sum_r e_{amrt} Y_{amrt} + \sum_r \sum_w e_{arwt} Y_{arwt} + \sum_w \sum_h e_{awht} Y_{awht} \right) \right] \quad (2.2)
\end{aligned}$$

The objective function 2.2 aims to minimize the environmental impacts of the logistics chain network. Specifically, the first two terms represent the fixed CO_2-equivalent emissions from a regional warehouse and a state repository, respectively. The next three terms represent the total global warming impacts of vaccine transportation between the manufacturer and regional warehouse, regional warehouses and state repositories, and state repositories and health facilities.

Network constraints

$$\sum_{t}\sum_{r} X_{rt} \leq N \tag{2.3}$$

Constraint 2.3 imposes a total budget of N regional warehouses.

$$\sum_{t}\sum_{w} X_{wt} \leq M \tag{2.4}$$

Constraint 2.4 imposes a total budget of M state repositories.

$$\sum_{w} Y_{arwt} \leq \sum_{m} Y_{amrt} \quad \forall a \in A, r \in R, t \in T \tag{2.5}$$

Constraint 2.5 ensures that the quantity of vaccine transferred from a regional warehouse to a state repository does not exceed the amount transferred from a manufacturer to the regional warehouse.

$$\sum_{h} Y_{awht} \leq \sum_{r} Y_{arwt} \quad \forall a \in A, w \in W, t \in T \tag{2.6}$$

Constraint 2.6 enforces the constraint that the number of vaccines dispatched from a state repository to a health facility must not exceed the number of vaccines dispatched from a regional warehouse to the corresponding state repository.

$$\sum_{a}\sum_{m} Y_{amrt} + \sum_{a} L_{art} \leq \text{cap}_{rt} \sum_{j=1}^{t} X_{rj} \quad \forall r \in R, t \in T \tag{2.7}$$

Constraint 2.7 indicates that if a potential location is not opened for a regional warehouse, there will be no flow of vaccines. Additionally, the total vaccines transferred from the manufacturer to this regional warehouse, plus its held stock, must not exceed the regional warehouse's capacity at time t.

$$\sum_{a}\sum_{r} Y_{arwt} + \sum_{a} L_{awt} \leq \text{cap}_{wt} \sum_{j=1}^{t} X_{wj} \quad \forall w \in W, t \in T \tag{2.8}$$

Constraint 2.8 states that if a potential location is not opened for a state repository, then there is no vaccine flow, but if it is opened, the total vaccines transferred from the regional warehouse to this state repository and its current inventory cannot exceed its capacity at period t.

Inventory constraints

$$L_{amt} = L_{am,t-1} + P_{amt} - \sum_{r} Y_{amrt} \quad \forall a \in A, m \in M, t \in T \tag{2.9}$$

$$L_{art} = L_{ar,t-1} + \sum_{m} Y_{amrt} - \sum_{w} Y_{arwt} \quad \forall a \in A, r \in R, t \in T \tag{2.10}$$

$$L_{awt} = L_{aw,t-1} + \sum_{r} Y_{arwt} - \sum_{h} Y_{awht} \quad \forall a \in A, w \in W, t \in T \tag{2.11}$$

Constraints 2.9-2.11 imply inventory balance in each manufacturer, regional warehouse, and state repository, respectively.

$$L_{amt} \leq \sum_{r} Y_{amrt} \quad \forall a \in A, m \in M, t \in T \tag{2.12}$$

$$L_{art} \leq \sum_{w} Y_{arwt} \quad \forall a \in A, r \in R, t \in T \tag{2.13}$$

$$L_{awt} \leq \sum_{h} Y_{awht} \quad \forall a \in A, w \in W, t \in T \tag{2.14}$$

Constraints 2.12-2.14 indicate that the inventory policy at the manufacturer, regional warehouse, and state repository are made based on the limited shelf-life of the vaccines.

Capacity expansion constraints

$$Capt_{amt} = Capi_{amt} + \sum_{j=1}^{t} Capc_{amj} \quad \forall a \in A, m \in M, t \in T \tag{2.15}$$

$$\sum_{a}\sum_{t} \text{Capc}_{amt} \leq \text{Cap}_{m}^{\max} \quad \forall m \in M \tag{2.16}$$

$$P_{amt} + I_{amt} \leq Capt_{amt} \quad \forall a \in A, m \in M, t \in T \tag{2.17}$$

Constraint 2.15 calculates the total capacity of the manufacturer, which includes the initial capacity and the capacity increments for producing more vaccines. The increment capacity of manufacturing is constrained by constraint 2.16, which means that each manufacturing process cannot exceed its maximum capacity at each time. Constraint 2.17 ensures that the inventory level and production quantity of vaccines produced at each time do not exceed the total capacity of the manufacturer in that period.

Switching warehouses constraints

$$Z_{rt} \leq \sum_{j=1}^{t-1} X_{rj} \quad \forall r \in R, t \in \{2, 3, \ldots, T\} \tag{2.18}$$

$$Z_{wt} \leq \sum_{j=1}^{t-1} X_{wj} \quad \forall w \in W, t \in \{2, 3, \ldots, T\} \tag{2.19}$$

$$\sum_{t} X_{rt} \leq 1 \quad \forall r \in R \tag{2.20}$$

$$\sum_{t} X_{wt} \leq 1 \quad \forall w \in W \tag{2.21}$$

Constraints 2.18 and 2.19 stipulate that a regional warehouse and a state repository can only be switched at each period if they have already been opened earlier. Constraints 2.20 and 2.21 ensure that a regional warehouse and a state repository can only be opened once during the planning horizon, respectively.

Conditional constraints related to switching warehouses

$$\sum_{a} \sum_{m} Y_{amrt} \leq (1 - Z_{rt}) \text{cap}_{rt} \quad \forall r \in R, t \in T \tag{2.22}$$

$$\sum_{a} \sum_{r} Y_{arwt} \leq (1 - Z_{wt}) \text{cap}_{wt} \quad \forall w \in W, t \in T \tag{2.23}$$

$$\left(\sum_{a} \sum_{m} \frac{Y_{amrt}}{\text{cap}_{rt}} \right) + Z_{rt} \geq \sum_{j}^{t} X_{rj} \phi \quad \forall r \in R, t \in T \tag{2.24}$$

$$\left(\sum_{a} \sum_{r} \frac{Y_{arwt}}{\text{cap}_{wt}} \right) + Z_{wt} \geq \sum_{j}^{t} X_{wj} \phi \quad \forall w \in W, t \in T \tag{2.25}$$

Constraints 2.22-2.25 address the conditions for switching the regional warehouse and state repository for other cold products. Specifically, constraints 2.22 and 2.23 ensure that no vaccines should be shipped to the regional or state warehouses if they are switched. Constraints 2.24 and 2.25 ensure that if the regional or state warehouses are established, they can be switched, or the vaccines should be shipped at more than ϕ percent of their capacity.

Population Infection Dynamics and Vaccinated Population Constraints

$$\sum_{w} Y_{arwt} = \sum_{w} \left(\sum_{d_a} O^{d_a}_{arwt} \right) \quad \forall a \in A, r \in R, t \in T \tag{2.26}$$

Constraint 2.26 indicates the vaccine dose d_a for each shipment from regional warehouse r to state repository w.

$$S_{w1} = \pi_w, \quad I_{w1} = \omega_w, \quad V^{d_a}_{aw1} = \theta^{d_a}_{aw} \quad \forall d_a \in D_a \quad \text{st.} \quad a \in A \tag{2.27}$$

Constraint 2.27 displays the initial number of susceptible individuals and infections obtained from the real dataset, as well as the initial number of individuals who have received the vaccine dose d_a for each vaccine type a.

$$S_{w,t} = S_{w,t-1} - \lambda_{w,t} S_{w,t} - \sum_{a} \sum_{r} O^{1}_{arwt} \alpha^{1}_{a} \quad \forall d_a = 1 \quad \text{st.} \quad a \in A, w \in W, t \in 1, 2, \ldots \tag{2.28}$$

$$I_{w,t} = I_{w,t-1} + \lambda_{w,t} S_{w,t} - \sum_{a} \sum_{d_a} \sum_{r} O^{d_a}_{arwt} \alpha^{d_a}_{a} \quad \forall w \in W, t \in 1, 2, \ldots \tag{2.29}$$

Constraints 2.28 and 2.29 represent the number of susceptible individuals and the number of infected individuals, respectively. Specifically, the number of susceptible individuals in state w at time t equals the number of susceptible individuals from the previous period minus the number of infected individuals in state w at period t and minus the number of susceptible individuals who have received the vaccine dose d_a for each vaccine type a in state w at period t. Constraint 2.29 shows that the number of infected individuals in state w at time t equals the number of

infected individuals from the previous stage plus newly infected individuals minus the number of individuals saved by the vaccine doses.

$$V_{awt}^{d_a} = V_{awt-1}^{d_a} + \sum_r O_{arwt}^{d_a} - \sum_r \left(\sum_{d_a+1}^{D_a} O_{arwt}^{d_a} \right)$$

$$\forall a \in A, d_a \in D_a \quad \text{st.} \quad a \in A, w \in W, t \in 1, 2, \ldots \tag{2.30}$$

Constraint 2.30 indicates that the number of individuals who receive the vaccine dose d_a for each vaccine type a in state w at time t is equal to the number of individuals who received the vaccine dose d_a for each vaccine type a in state w from the previous stage, plus the newly vaccinated people with the vaccine dose d_a, minus the number of people who have received the next dose(s) of vaccine type a.

Vaccine logistics and demand constraints

$$\sum_r O_{arwt}^1 \geq S_{wt} \beta_{aw}^{d_a} \quad \forall a \in A, d_a = 1 \quad \text{St.} \quad a \in A, w \in W, t \in T \tag{2.31}$$

$$\beta_{aw}^{d_a} \sum_r O_{arw,t-k_{d_a}}^{d_a-1} \leq \sum_r O_{arwt}^{d_a} \leq \sum_r O_{arw,t-k_{d_a}}^{d_a-1}$$

$$\forall a \in A, d_a \in \{2, \ldots, D_a\} \quad \text{St.} \quad a \in A, w \in W, t \in \{k_{d_a}+1, \ldots, T\} \tag{2.32}$$

Constraint 2.31 ensures that the total number of first doses of vaccine type i shipped from regional warehouse r to state repository w at time t is greater than or equal to the number of people willing to be vaccinated. Constraint 2.32 ensures that the total number of next doses d_a of vaccine type a is greater than or equal to the lower bound of the number of people willing to be vaccinated but smaller than or equal to the previous dose d_{a-1} shipped from regional warehouse r to state repository w at time $t - k_{d_a}$, (k_{d_a} days before the dose d_a).

$$I_{wt} \leq \sigma_t S_{wt} \quad \forall w \in W, t \in T \tag{2.33}$$

Constraint 2.33 is designed to align the VSC strategy with public health goals during the pandemic. It imposes a limit on the number of infections that can occur. Specifically, it ensures that the total number of infections across all regions during the planning horizon does not exceed a certain threshold for newly infected individuals.

$$X_{rt}, X_{wt}, Z_{rt}, Z_{wt} \in \{0, 1\} \tag{2.34}$$

$$Y_{amrt}, Y_{arwt}, Y_{awht}, L_{amt}, L_{art}, L_{awt}, P_{amt}, Capt_{amt}, Capc_{amt}, I_{wt}, S_{wt} \geq 0 \tag{2.35}$$

$$V^{d_a}_{aw,t+1}, O^{d_a}_{arwt} \geq 0 \tag{2.36}$$

Constraints 2.34- 2.36 define the domain of all decision variables.

2.3.4 Solution method

Various methods have been employed in generating Pareto solutions for multi-objective optimization models, including Lp-metrics, lexicographic, weighted sum, goal programming, and ε-constraint [62, 63]. The augmented ε-constraint method—an improved version of the ε-constraint method—is a commonly used technique to solve multi-objective optimization problems. This method allows the user to easily explore the trade-offs between the different objectives, by varying the value of the constraint and observing how the optimal solution changes [64, 65]. Furthermore, it can handle a wide range of problem types, including linear, nonlinear, and mixed-integer optimization problems [66]. Thus, in this research, we utilized the augmented ε-constraint, to obtain optimal solutions for the proposed VSC optimization model. There are several reasons why this approach is suitable for the proposed VSC optimization model. Firstly, while weighted approaches only generate extra efficient solutions for linear problems, the augmented ε-constraint approach generates non-extreme efficient solutions.

Secondly, it can be time-consuming to determine the best weights to utilize goal programming. Lastly, it is a posterior method that can obtain the exact Pareto set for multi-objective integer programming problems, provided the step size is appropriately selected [67]. As traditional ε-constraint approaches have some limitations, which are partially addressed in improved versions of the method [66], we chose to implement the augmented ε-constraint method in this study.

The primary concept of this approach is to select one of the objective functions as a constraint while optimizing the remaining objective functions. The method aims to calculate the Payoff Table in lexicographic order. The augmented ε-constraint approach addresses several issues of the traditional ε-constraint method. One advantage of this method over the traditional ε-constraint approach is that it solves the problem with a more logical number of iterations than the ε-constraint approach, making it more computationally efficient [64, 65]. The general form of the augmented ε-constraint is as follows:

$$\begin{aligned} Z_{(k)}(x) + s_{(k)} &= \varepsilon_{(k)} \quad \forall k \neq j \\ \varepsilon_{(k)} &= Z_k^{\max}(x) - \left(\frac{Z_k^{\max}(x) - Z_k^{\min}(x)}{q_{(k)}} \right) n_{(k)} \quad \forall k \neq j \\ x \in X, &\quad s_{(k)} \in \mathbb{R}^+ \end{aligned} \tag{2.37}$$

Where s_k is the value of the covariate variable related to the constraint of the objective function k, and q_k and n_k are interval and iteration parameters corresponding to the k-th objective function, respectively.

Our solution method using the augmented ε-constraint approach, proceeds as follows:

- **Step 1:** We begin by selecting one of the objective functions as the main objective function. In our case, we chose the first objective function (Z_1),

which is to minimize the total costs of VSC while applying additional constraints to the secondary objective (Z_2).

- **Step 2:** The problem is solved for each objective function as a single objective each time, determining both optimum values of each objective function and its worst values. The worst value of the objective function is achieved by changing the minimization to maximization and vice versa for each function.

- **Step 3:** We then divide the range between the optimal values of the secondary objective functions into a certain number of sections. A table of ε values (ε_2, ε_3, ...) is created based on these divisions.

- **Step 4:** For each iteration, the problem is solved by focusing on the primary objective while applying one of the ε values (ε_2, ..., ε_k).

- **Step 5:** The optimal Pareto solutions are then obtained and presented.

The augmented ε-constraint method efficiently generates non-dominated solutions, effectively overcoming the limitations of the simple ε-constraint method. This approach ensures our optimization model comprehensively addresses its multi-objective nature, producing solutions that are cost-effective and environmentally sustainable.

2.3.5 Simulation-optimization model

We propose a simulation-optimization modeling framework to address the challenges associated with COVID-19 vaccination facility location and vaccine allocation. Firstly, we extend Covasim, an agent-based model of COVID-19, and integrate it with a proposed VSC model. The VSC and agent-based simulation models interact iteratively in a loop with forward and backward in the planning horizon. The loop of the simulation-optimization model is shown in Figure 2.5. It is an ongoing loop where outputs from one model continually serve as inputs to the other, refining the results with each iteration. The primary objective

behind this iterative approach is to harmonize the vaccination strategy with the ever-evolving progression of the disease. In our simulation-optimization framework, the 'forward' process involves the Covasim agent-based model forecasting the number of susceptible and infected individuals, which then serves as input for the optimization model. The 'backward' process, on the other hand, is the feedback mechanism where the optimization model's vaccine allocation results are used to refine the simulation's future disease progression predictions. This iterative forward-backward interaction enhances the model's responsiveness to changing pandemic dynamics, ensuring that vaccine allocation strategies are continuously optimized based on the most current data.

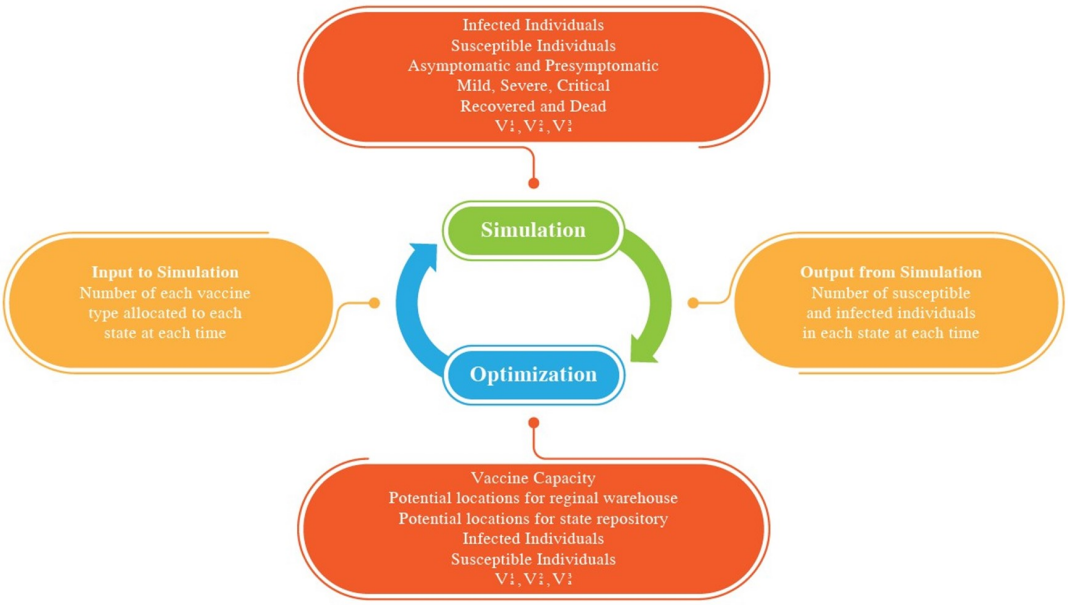

Figure 2.5 Loop of simulation-optimization model.

The integrated modeling framework runs in a loop, where the simulation model forecasts disease transmission inputs. Constraint 2.27 sets the initial

parameters, including the number of susceptible individuals and infections, as well as the initial number of individuals who have received the vaccine dose for each vaccine type, which are obtained from real datasets. Specifically, the simulation model uses these initial parameters to forecast the number of susceptible and infected individuals for each state in the current planning horizon. These forecasted numbers are then imported into the proposed VSC model. Unlike traditional models that rely merely on static parameters, our VSC model adapts to dynamic updates about disease progression and vaccination coverage. Subsequent parameters for the VSC model are determined by this iterative interaction between the simulation and VSC models, allowing the system to respond to evolving scenarios.

The VSC model incorporates potential locations for regional and state warehouses, vaccine capacity for each warehouse, and switching the established warehouses for other cold products. The VSC model then generates optimal vaccine location and allocation decisions while minimizing total costs and environmental impacts throughout the planning horizon. The VSC model outputs include the number of people who are expected to be vaccinated with the first dose, second dose, and booster shots in each state for each future period. These outputs are then fed back into the Covasim simulation model to estimate the number of susceptible and infected individuals for subsequent periods.

2.4 Results

We implemented the simulation-optimization framework proposed in Subsection 2.3.5 to address the challenges of COVID-19 vaccination facility location and vaccine allocation in the US. Specifically, we applied the agent-based simulation

to each state separately to fine-tune disease dynamics and integrated it with the VSC optimization model, which was applied to all states and healthcare facilities simultaneously to generate the optimal regional and state warehouse locations and vaccine allocation decisions. After solving the VSC model, we used the obtained results as inputs for the simulation model. The vaccination schedule incorporated the first, second, and booster shots for the Pfizer and Moderna vaccines and the first and booster shots for the Janssen vaccine. The model was solved for a six-month planning horizon from January 4, 2021, to June 7, 2021.

We first present a detailed case study of the simulation optimization framework proposed for resource allocation in COVID-19 vaccination. In Subsection 2.4.1, the COVID-19 vaccine case study in the US is presented. In Section 2.4.2, we present the validation results of the simulation-optimization model. Further, in Section 2.4.3, pareto solutions of VSC model is provided. In Section 2.4.4, we consider location decisions for vaccination centers based on real-world COVID-19 infection data in the relevant states and regions, which we will describe later. In section 2.4.5, the distribution of various types of vaccines to regional warehouses and state repositories across the US is discussed.

2.4.1 Case study

We applied the proposed model to all 51 states (the 50 states plus the District of Columbia) in the United States. Each period in the model represents a 14-day period, which corresponds to a six-month timeframe. We solved the model for 12 periods, a planning horizon from January 4, 2021, to June 7, 2021. We consider 10 Department of Health and Human Services (DHHS) regions listed [53].

- Region 1: Boston (Connecticut, Maine, Massachusetts, New Hampshire, Rhode Island, and Vermont);
- Region 2: New York (New Jersey, New York, and Puerto Rico);
- Region 3: Philadelphia (Delaware, District of Columbia, Maryland, Pennsylvania, Virginia, and West Virginia);
- Region 4: Atlanta (Alabama, Florida, Georgia, Kentucky, Mississippi, North Carolina, South Carolina, and Tennessee);
- Region 5: Chicago (Illinois, Indiana, Michigan, Minnesota, Ohio, and Wisconsin);
- Region 6: Dallas (Arkansas, Louisiana, New Mexico, Oklahoma, and Texas);
- Region 7: Kansas City (Iowa, Kansas, Missouri, and Nebraska);
- Region 8: Denver (Colorado, Montana, North Dakota, South Dakota, Utah, and Wyoming);
- Region 9: San Francisco (Arizona, California, Hawaii, Nevada);
- Region 10: Seattle (Alaska, Idaho, Oregon, and Washington).

We have selected the representative cities in the DHHS regions as candidate locations for regional warehouses [53]. The candidate locations for regional warehouses are Boston, New York City, Philadelphia, Atlanta, Chicago, Dallas, Kansas City, Denver, San Francisco, and Seattle. We have also pre-defined the locations of vaccine manufacturers in three main regions in the US, including Kalamazoo, Waltham, and Bloomington. For the state repository, we have considered one for each of the 51 states (the 50 states plus the District of Columbia). However, due to differences in population size, certain states, such as California, Texas, Florida, and New York, require more potential locations for state repositories. Therefore, we have made 75 potential locations available for the

establishment of state repositories, from which we will choose 51 by solving the optimization model. In addition, we have selected H = 200 healthcare facilities from the 500 most populated cities in the United States. Table 1 shows the number of potential manufacturers, regional warehouses, state repositories, and healthcare facilities and the total number of those selected via solving the model. Notably, the number of manufacturers and healthcare facilities is pre-defined and fixed.

We consider three types of COVID-19 vaccines, namely Pfizer, Moderna, and Janssen, with production costs of $1.18, $2.85, and $0.98 per dose, respectively [68]. The fixed opening cost for establishing a regional warehouse and a state repository is estimated as 10,000 times the local unit warehouse rental price per square foot [53].

Table 2.4 The Number of Potential Warehouses and Repositories

Category	**Potential Numbers**	**Selected Numbers**
Manufacturer	3	-
Regional Warehouse	10	6
State Repository	75	51
Healthcare Facility	200	-

It is noteworthy that the remaining cost parameters are adjusted by utilizing the relative cost of living index of the respective locations to account for the fluctuations in costs due to geographical location. In this research, the cost of living indexes obtained from World Population Review [69] are normalized by dividing them by the cost of living index at the base location (New Jersey). The unit inventory costs, CH_{amt}, CH_{art}, CH_{awt}, are calculated by summing up the low-temperature inventory costs and energy costs of common refrigerators for storing

vaccines, which are equal to 0.00008 multiplied by the relative cost of living index for 2022 at each state location. The unit transportation costs, CT_{amrt}, CT_{arwt}, CT_{awht}, are estimated as 3 per mile multiplied by the distance traveled in miles divided by $230,400$, assuming that each truck can carry an average of $230,400$ vaccine doses [53]. It is worth mentioning that we consider different transportation costs for different types of vaccines due to different cold storage requirements. Specifically, Pfizer and Moderna vaccines require "minus 70 degrees Celsius" and "minus 20 degrees Celsius" as the storage temperature, respectively [70]. Thus, for Pfizer and Moderna, the unit transportation cost is set to 3 per mile [53], as both are considered ultra-cold vaccines. For the Janssen vaccine, we assume the unit transportation cost is 2 per mile, as it should be transported using refrigerated trucks, not freezer trucks. We then adjust the transportation costs using the cost-of-living index.

The sustainability parameters (EF_{rt}, EF_{wt}) are determined by considering the base annual GHG emissions of each regional warehouse and state repository, which is 112 tons of CO_2-equivalent emissions, and volume-dependent GHG emissions following the function $g_r(Q_r) = 11.1Q_r^{0.76}$ tons of CO_2-equivalent emissions [56]. For long-haul trucks, the GHG emissions per kilometer are set at 6.3 kilograms [56]. Therefore, CO_2-equivalent emissions per unit of each vaccine type shipped (e_{amrt}, e_{arwt}, e_{awht}) are calculated by multiplying 10.08 per mile with the distance traveled in miles, divided by 230400.

Regarding the Covasim model parameters, we independently estimate the parameters for each state using historical data on new cases and deaths obtained from the CDC [71, 72]. We collect the population data for each state from the U.S. Census Bureau [73] and gather the number of initial susceptible individuals and

infections from JHU [74]. We make the assumption that the vaccine acceptance rate is the same for each state in the US. Moreover, we set the disease transmission rate ($\lambda_{w,t}$) to the default value of 0.16 in the Covasim model.

2.4.2 Model validation

In this section, we present the validation results of the simulation-optimization model. The purpose of this validation is to compare the predicted and actual number of new infections, which serves as a key input in the optimization of vaccine supply chain decisions. This comparison is crucial because the predicted infections (the output from the simulation), directly feed into our optimization model. It plays a key role in the optimization of vaccine supply chain decisions, especially in the allocation of vaccines to each state. By ensuring the accuracy of infection predictions, we can enhance the reliability of our vaccine distribution strategies, making the model's recommendations more effective and aligned with real-world scenarios.

To adhere to political and fairness considerations, the administration set up at least one vaccination repository center per state in the United States [51]. Thus, we used these actual vaccination repository center locations in our model for validation. The number of state repositories in our model is 51, which includes the 50 states plus the District of Columbia, one location in each state. The VSC model also determined the number of vaccines for each vaccine type allocated to each state and used these values as inputs in the Covasim model. We present the number of estimated infections over a 12-planning horizon, equal to six months, and compare it with the actual outbreak data. The results for the first 6 states

are displayed in Figure 2.6, and the validation results for the remaining 45 states of the US are presented in Appendix 5.2.

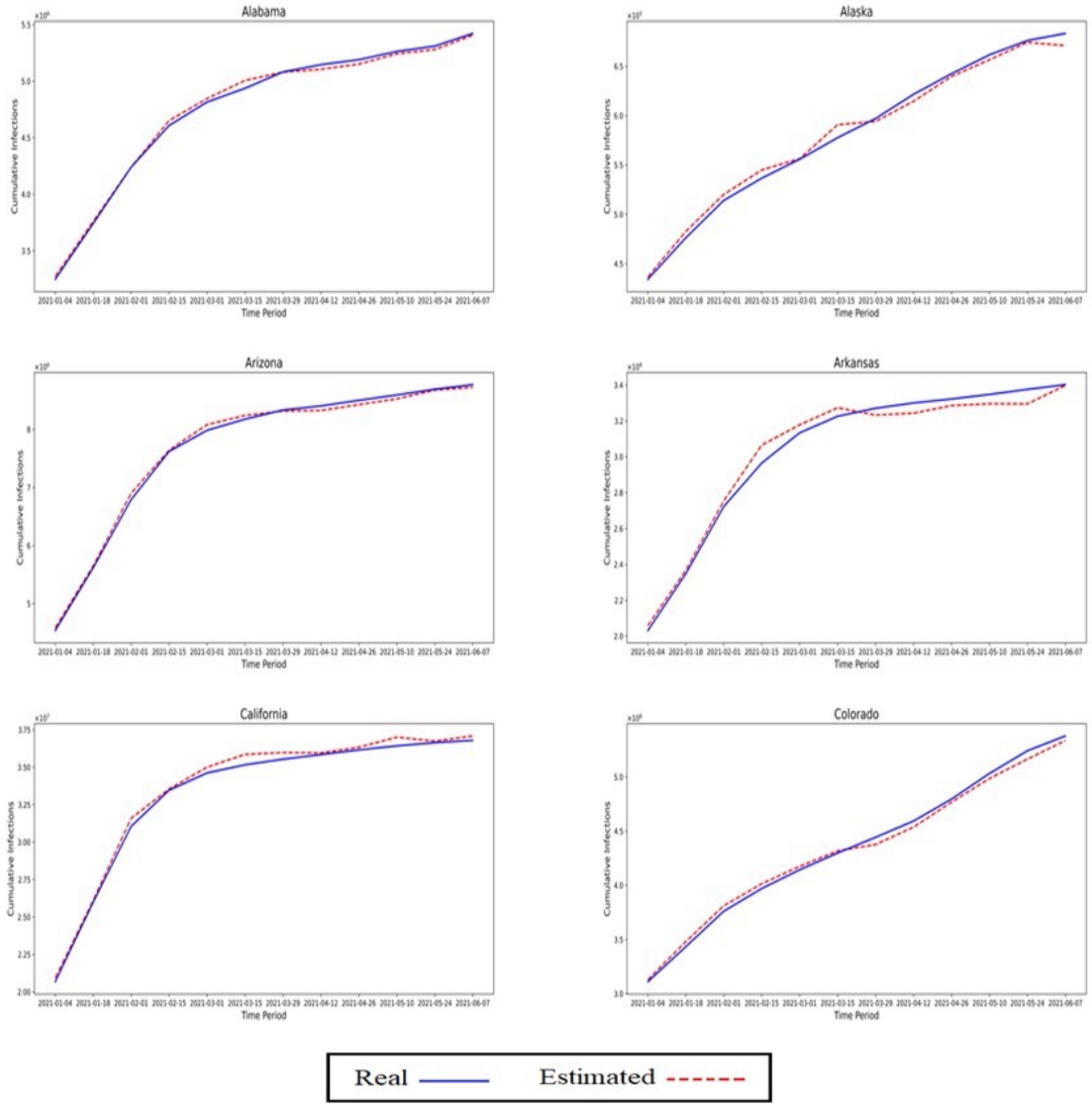

Figure 2.6 Model validation against real outbreak data in the US.

The simulation-optimization model described is validated by comparing the estimated number of new infections with the real outbreak data. The model starts from zero infections at the beginning of the simulation, while the real data is in

the middle of the pandemic. As a result, the model estimated a slightly higher number of infections at the start of the simulation and a lower estimated number in later periods. The fit between the estimated and actual data is visually good, as shown in Figure 2.6. The results presented in Table 2.5 and Figure 2.6 indicate that the proposed model provides similar predictions to the real data for 51 states in the US over the six-month planning horizon.

Table 2.5 Statistical Analysis Comparing Predicted New Infections and Real Outbreak Data in the US

State	**Mean Outbreak**	**Mean Predicted**
Alabama	475070	475597
Alaska	58137	58169
Arizona	766964	767978
Arkansas	303706	303717
California	3319879	3351343
Colorado	435048	426561
Connecticut	279355	279556
Delaware	86073	86042
Florida	1882215	1889920
Georgia	779948	780051
Hawaii	27572	27614
Idaho	169741	169820
Illinois	1185842	1193317
Indiana	651356	649848
Iowa	332826	332840
Kansas	283769	283700
Continued on next page		

Table 2.5 continued from previous page

State	Mean Outbreak	Mean Predicted
Kentucky	386087	386907
Louisiana	412591	416294
Maine	871037	871573
Maryland	380477	380893
Massachusetts	538426	543518
Michigan	719166	719940
Minnesota	500731	501106
Mississippi	282192	280127
Missouri	544779	545749
Montana	98567	99039
Nebraska	197603	196445
Nevada	282299	284184
New Hampshire	639120	637146
New Jersey	796630	797185
New Mexico	179640	180752
New York	1616936	1618842
North Carolina	821595	816546
North Dakota	100728	100241
Ohio	940829	943579
Oklahoma	401052	403741
Oregon	155757	157271
Pennsylvania	936863	936917
Rhode Island	119786	118652

Continued on next page

Table 2.5 continued from previous page

State	Mean Outbreak	Mean Predicted
South Carolina	487090	481761
South Dakota	112849	113014
Tennessee	755650	749500
Texas	2512873	2539931
Utah	358158	361723
Vermont	16119	15706
Virginia	550525	552248
Washington	340714	343491
West Virginia	128921	127293
Wisconsin	608739	605713
Wyoming	53471	53841
District of Columbia	40373	40434

2.4.3 Pareto solutions of VSC model

The VSC model is solved using a single objective function through the augmented ε-constraint approach. As mentioned earlier, the results of the VSC model are Pareto optimal solutions that represent a set of points on the Pareto frontier. The values of the objective functions, which include the economic and environmental objectives, are presented in Table 2.6. The augmented ε-constraint method produced five efficient Pareto solutions. It should be noted that the first Pareto solution is utilized for showcasing the outcomes and discussion.

The trade-off between the total costs and emissions is depicted in Figure 2.7, which displays the Pareto frontier curve. It shows that there is a trade-off between the two objectives, such that a decrease in the second objective results in

Table 2.6 The Values of the Pareto Points of Augmented ε-constraint Approach

Pareto solution	Objective 1 (Billion $)	Objective 2 (Thousand Tone)
1	5.78	337
2	5.87	335
3	5.90	333
4	6.07	331
5	6.57	329

an increase in the cost objective and vice versa. Therefore, if the decision-makers prioritize sustainability, higher costs are incurred in the VSC since costs increase when emissions decrease. This finding is a significant contribution of our model, as it equips decision-makers with the necessary insights to make better-informed decisions that enhance the sustainability of the VSCs.

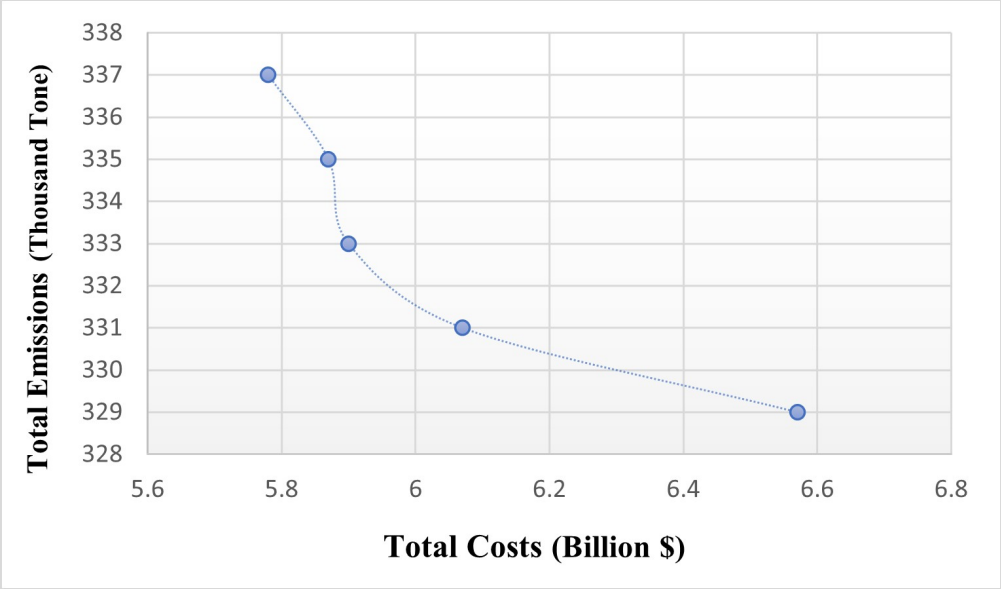

Figure 2.7 Pareto solutions of VSC model by augmented ε-constraint approach.

2.4.4 Warehouse location decisions

In this subsection, we present the results of the modeling framework developed in this research, specifically the location and allocation decisions of the regional warehouse and state repository. Our focus is primarily on the location decisions, as these need to be made immediately, in contrast to the vaccine allocation decisions, which can be revised over time as more information becomes available. To be more precise, we consider $N = 6$ regional warehouses as candidate locations out of the 10 main regions in the United States. Additionally, we set the number of state repositories to 51, one per state in the United States.

Figure 2.8 Regional warehouse and State repository locations in the US.

Figure 2.8 presents the locations of the regional warehouse and state repository locations across the United States, as determined by the optimization

model. From Figure 2.8, out of 10 candidate locations, the model selected six regional warehouses as the optimal solution. All of these warehouses are located in regions with high population density and high infection rates, as seen in the map. Figure 2.8 shows that the regional warehouses are allocated in Massachusetts, Wisconsin, Georgia, Texas, California, and Washington. Moreover, the model allocated one repository site per state (total 51 sites) out of 75 potential candidate locations, as designed, one repository location in each state.

In Figure 2.9, the vaccine shipments from the selected regional warehouses to the selected state repositories are shown. From Figure 2.9, the proposed model locates the regional warehouses in Massachusetts, Texas, Illinois, and California states, which is the same decision the government has taken in the real situation. It is important to note that vaccine distribution decisions may be influenced by transportation costs and environmental impacts. As shown in Figures 2.8 and 2.9, the distance between the regional warehouse and the state repository is the primary factor in selecting their respective locations. Therefore, the proposed model selects the state repository geographically closest to the designated regional warehouse to minimize transportation costs and mitigate the negative environmental effects of global warming.

2.4.5 Warehouse allocation decisions

Table 2.7 shows the allocation of vaccines to each state repository, including the number of first, second, and booster doses for Pfizer and Moderna and first and booster doses for Janssen, as well as the total number of vaccines allocated to each state. It is worth noting that the findings are expressed in units of 100,000 vaccine doses to improve readability. In Table 2.8, the vaccination proportions in

each state are presented and compared to their population shares. The columns in Table 2.8 display the state name, population, vaccination proportion in each state with respect to all states, and the percentage difference between the population and vaccination proportions.

Figure 2.9 Vaccine shipments from the regional warehouses to selected state repositories.

Figure 2.10 presents the total proportion of vaccines for the three types of vaccines in the US based on the optimal solution. As demonstrated in Table 2.7 and Figure 2.10, when there are no logistic or economic limitations on the vaccine allocation strategy, vaccine efficacy becomes the primary consideration for administering and distributing the vaccine. Therefore, based on the results, Pfizer vaccines have a higher priority for allocation to the states compared to Moderna and Janssen. Furthermore, from Table 5, the vaccine allocation percentage is almost the same as the population percentage. For example,

Alabama and Delaware receive 1.6% and 0.3% of the total administered vaccines, respectively, which are equivalent to their population percentages. This is because all individuals who are willing to receive the vaccine doses get vaccinated when the vaccine supply is sufficient to meet the vaccination needs. It is worth noting that we assumed the same vaccine acceptance rate in each state in the US.

One interesting finding is that the difference between the population and vaccination proportions becomes more significant for the most populous states. For instance, Texas, California, and New York have about a 0.2% difference between their vaccine allocation proportions and population proportions. This is because the total number of vaccines allocated is still insufficient to meet the vaccination needs of individuals in these states.

Table 2.7 Vaccine Allocation to State Repository in the US

State	First Dose Pfizer	Second Dose Pfizer	Booster Dose Pfizer	First Dose Moderna	Second Dose Moderna	Booster Dose Moderna	First Dose Janssen	Booster Dose Janssen	Total Vaccine Dose
Alabama	8.22	6.85	0	7.35	5.65	0	1.48	0	29.56
Alaska	3.00	2.38	0	2.55	1.96	0	0.32	0	5.62
Arizona	11.71	9.76	0	10.46	8.05	0	2.14	0	42.11
Arkansas	4.99	4.16	0	4.41	3.39	0	0.85	0	17.81
California	65.05	54.21	0	58.31	44.85	0	11.45	0	228.50
Colorado	9.08	7.56	0	8.05	6.19	0	1.37	0	32.25
Connecticut	6.22	5.18	0	5.49	4.22	0	1.08	0	22.19
Delaware	1.70	1.42	0	1.44	1.11	0	0.27	0	5.94
Florida	36.51	30.43	0	32.91	25.31	0	7.36	0	127.36
Georgia	16.86	14.05	0	15.05	11.57	0	2.90	0	60.44
Hawaii	2.50	2.09	0	2.17	1.67	0	0.42	0	8.85
Idaho	2.80	2.33	0	2.43	1.87	0	0.48	0	9.90
Illinois	16.88	14.07	0	15.08	11.60	0	2.92	0	60.55
Indiana	10.74	8.95	0	9.53	7.33	0	1.62	0	38.17

State	First Dose Pfizer	Second Dose Pfizer	Booster Dose Pfizer	First Dose Moderna	Second Dose Moderna	Booster Dose Moderna	First Dose Janssen	Booster Dose Janssen	Total Vaccine Dose
Iowa	5.23	4.36	0	4.64	3.57	0	0.89	0	18.70
Kansas	4.79	3.99	0	4.23	3.25	0	0.80	0	17.06
Kentucky	7.60	6.34	0	6.74	5.19	0	1.41	0	27.27
Louisiana	8.31	6.93	0	7.44	5.72	0	1.93	0	30.34
Maine	2.45	2.05	0	2.17	1.67	0	0.49	0	8.83
Maryland	10.18	8.48	0	9.06	6.97	0	1.79	0	36.48
Massachusetts	12.52	10.43	0	11.31	8.70	0	2.87	0	41.21
Michigan	16.83	14.03	0	15.09	11.60	0	3.00	0	60.55
Minnesota	9.24	7.70	0	8.26	6.35	0	1.63	0	33.19
Mississippi	4.68	3.90	0	4.06	3.12	0	0.49	0	16.25
Missouri	10.30	8.59	0	9.22	7.09	0	1.90	0	37.11
Montana	1.90	1.59	0	1.66	1.28	0	0.38	0	6.81
Nebraska	3.03	2.52	0	2.62	2.02	0	0.34	0	10.54
Nevada	5.17	4.31	0	4.64	3.57	0	1.15	0	18.84

State	First Dose Pfizer	Second Dose Pfizer	Booster Dose Pfizer	First Dose Moderna	Second Dose Moderna	Booster Dose Moderna	First Dose Janssen	Booster Dose Janssen	Total Vaccine Dose
New Hampshire	2.09	1.74	0	1.78	1.37	0	0.07	0	7.06
New Jersey	15.00	12.50	0	12.54	9.64	0	2.65	0	52.32
New Mexico	3.73	3.11	0	4.17	3.21	0	0.78	0	15.01
New York	19.22	16.02	0	17.26	13.28	0	3.57	0	106.76
North Carolina	16.25	13.54	0	14.38	11.06	0	2.05	0	57.28
North Dakota	1.24	1.04	0	1.07	0.82	0	0.14	0	4.31
Ohio	19.89	16.57	0	17.83	13.71	0	3.79	0	71.78
Oklahoma	6.86	5.71	0	6.14	4.72	0	1.55	0	24.97
Oregon	7.24	6.04	0	6.46	4.97	0	1.45	0	26.16
Pennsylvania	19.18	15.98	0	17.15	13.19	0	3.29	0	68.79
Rhode Island	1.71	1.42	0	1.47	1.13	0	0.13	0	5.85
South Carolina	7.62	6.35	0	6.61	5.09	0	0.53	0	26.20

State	First Dose Pfizer	Second Dose Pfizer	Booster Dose Pfizer	First Dose Moderna	Second Dose Moderna	Booster Dose Moderna	First Dose Janssen	Booster Dose Janssen	Total Vaccine Dose
South Dakota	1.50	1.25	0	1.29	1.00	0	0.27	0	5.31
Tennessee	10.29	8.58	0	8.98	6.90	0	0.87	0	35.62
Texas	44.11	36.76	0	39.45	30.35	0	7.33	0	158.00
Utah	5.17	4.31	0	4.69	3.60	0	1.39	0	19.16
Vermont	1.14	0.95	0	0.92	0.71	0	0.12	0	3.84
Virginia	14.40	12.00	0	12.89	9.92	0	2.71	0	46.82
Washington	12.78	10.65	0	11.48	8.83	0	2.58	0	46.31
West Virginia	2.96	2.47	0	2.56	1.97	0	0.27	0	10.23
Wisconsin	9.33	7.77	0	8.24	6.34	0	1.16	0	32.83
Wyoming	1.10	0.92	0	0.93	0.71	0	0.23	0	3.88
Columbia Dist	1.32	1.10	0	1.11	0.85	0	0.22	0	4.60
Total	**522.60**	**435.41**	**0**	**465.75**	**358.27**	**0**	**90.89**	**0**	**1885.50**

Table 2.8 Vaccination Proportions of Each State Repository in the US

State	**Population** (%)	**Vaccine Proportion** (%)	**Difference** (%)
Alabama	1.6	1.6	0
Alaska	0.2	0.3	0.1
Arizona	2.2	2.2	0
Arkansas	0.9	0.9	0
California	12.2	12	-0.2
Colorado	1.7	1.7	0
Connecticut	1.2	1.3	0.1
Delaware	0.3	0.3	0
Florida	6.8	6.7	-0.1
Georgia	3.2	3.2	0
Hawaii	0.5	0.5	0
Idaho	0.5	0.5	0
Illinois	3.4	3.2	-0.2
Indiana	2	2	0

Continued on next page

Table 2.8 continued from previous page

State	Population (%)	Vaccine Proportion (%)	Difference (%)
Iowa	1	1	0
Kansas	0.9	0.9	0
Kentucky	1.4	1.4	0
Louisiana	1.5	1.5	0
Maine	0.5	0.5	0
Maryland	1.9	1.9	0
Massachusetts	2.1	2.2	0.1
Michigan	3.2	3.2	0
Minnesota	1.8	1.8	0
Mississippi	0.9	0.9	0
Missouri	1.9	1.9	0
Montana	0.3	0.4	0.1
Nebraska	0.6	0.6	0
Nevada	1	1	0

Continued on next page

Table 2.8 continued from previous page

State	Population (%)	Vaccine Proportion (%)	Difference (%)
New Hampshire	0.4	0.4	0
New Jersey	2.8	2.8	0
New Mexico	0.7	0.8	0.1
New York	5.9	5.7	-0.2
North Carolina	3	3.1	0.1
North Dakota	0.2	0.2	0
Ohio	3.6	3.7	0.1
Oklahoma	1.3	1.3	0
Oregon	1.3	1.4	0.1
Pennsylvania	3.7	3.7	0
Rhode Island	0.3	0.3	0
South Carolina	1.4	1.4	0
South Dakota	0.3	0.3	0
Tennessee	2	2	0

Continued on next page

Table 2.8 continued from previous page

State	Population (%)	Vaccine Proportion (%)	Difference (%)
Texas	8.6	8.4	-0.2
Utah	1	1	0
Vermont	0.2	0.2	0
Virginia	2.5	2.5	0
Washington	2.4	2.4	0
West Virginia	0.5	0.5	0
Wisconsin	1.8	1.8	0
Wyoming	0.2	0.2	0
District of Columbia	0.2	0.3	0.1

The data presented in Figure 2.10 reveals that the number of second doses for Pfizer and Moderna vaccines is considerably smaller than that of the first dose. This outcome is attributed to the prioritization of administering the first doses of those vaccines when the total vaccination capacity or vaccine supply is limited. This approach aims to maximize the benefit by allowing more individuals to receive the first dose, which is highly effective.

Additionally, the number of booster shots for all types of vaccines is zero because, in our planning horizon, which spans from January 4, 2021, to June

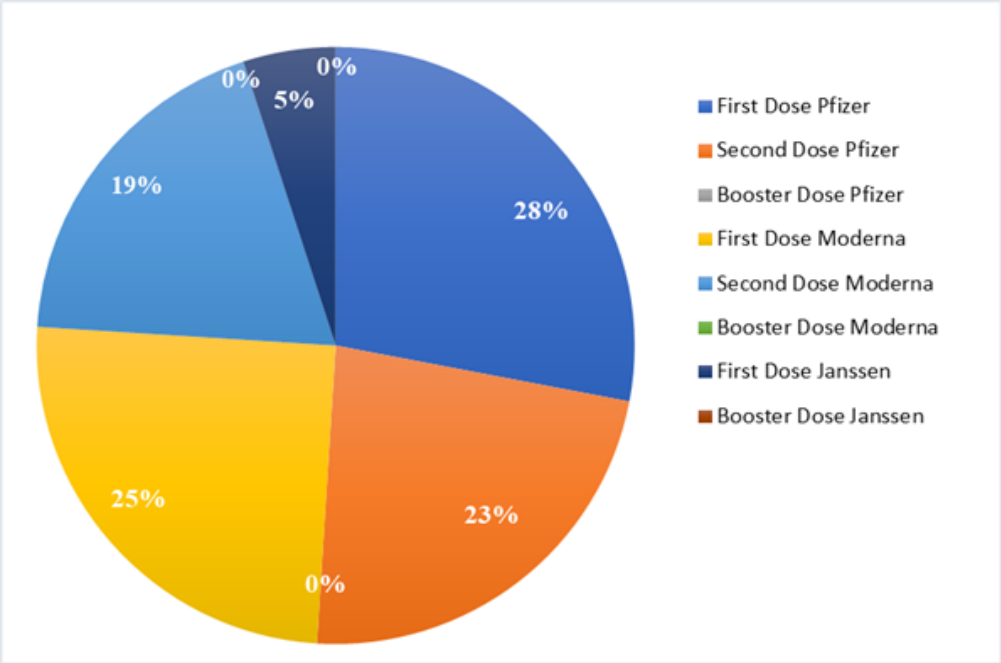

Figure 2.10 Proportion of each type of vaccine allocated to each state.

7, 2021, no booster shots are administered during that time. It is important to note that the decision to administer booster shots for vaccines is based on various factors, including the duration of immunity provided by each type of vaccine, the prevalence of the virus, the emergence of new COVID-19 variants, and the overall effectiveness of each vaccine type against these variants. During our planning horizon, the COVID-19 vaccine rollout was still in its early stages, and the US was still in the process of vaccinating its populations with the first and second doses of the vaccine. More specifically, only two doses of Pfizer and Moderna vaccines, and a single dose of Janssen vaccine, are distributed at this period. Moreover, the guidance provided by public health authorities during this period did not include recommendations for booster shots. As per the results, the Pfizer vaccine is generally more widely distributed than the other two vaccines due to its high effectiveness and longer duration of immunity.

2.4.6 Capacity expansion decisions

Our proposed model illustrates dynamic adaptability in VSC management, particularly in responding to fluctuating demand driven by changes in infection rates. This key feature of adaptability ensures that our approach stays aligned with real-world needs and vaccine production remains agile and responsive. Figure 2.11 presents the capacity expansion decision within our model.

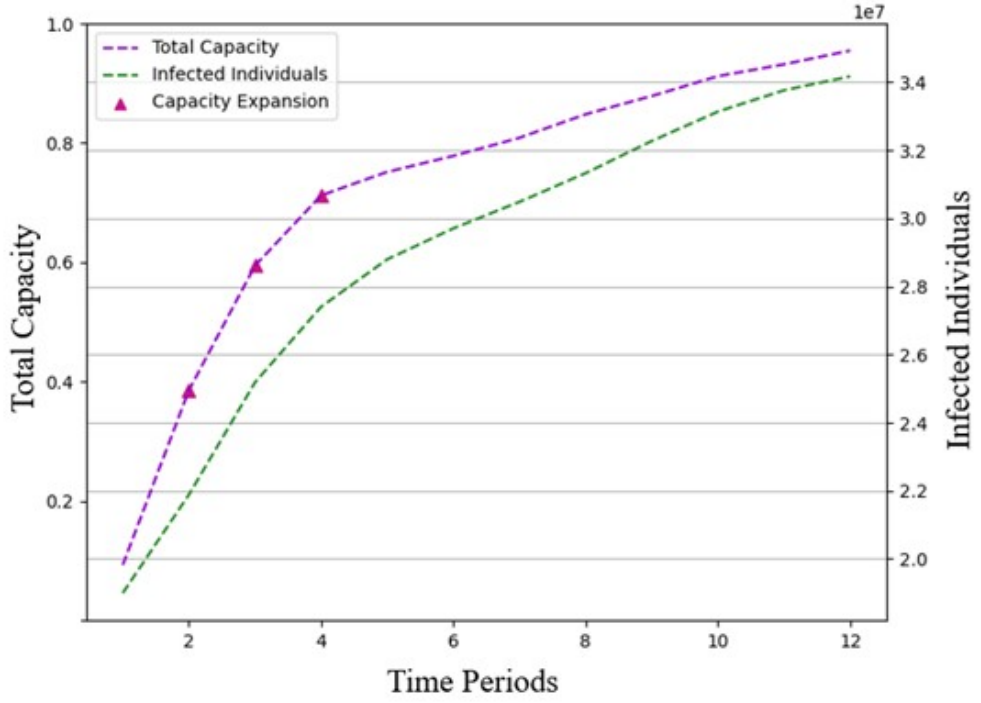

Figure 2.11 Total capacity and capacity expansion decision during the time periods.

Figure 2.11 reveals a progressive increase in vaccine production capacity which aligns with the trend in infected individuals. The pink markers highlight the time periods 2, 3, and 4 where capacity expansions are implemented. This increment in capacity indicates a strategic response to an increasing demand for vaccine production. Specifically, the notable increases in these periods correspond

to a significant rise in infections, suggesting a responsive increase in vaccine production to meet the escalating demand due to the surge in cases.

Overall, our model's dynamic adaptability is pivotal for efficient and responsive management of VSC, particularly in unpredictable pandemic conditions. By proactively adjusting to rapid changes in demand, it ensures effective mitigation of virus spread and adept management of public health crises, demonstrating a robust approach to global health challenges.

2.5 Sensitivity Analysis

In vaccine distribution, a main challenge arises from the uncertainties regarding the pandemic's dynamics and vaccination effects. As the pandemic evolves, the importance of a model capable of adapting to the evolving dynamics becomes increasingly evident. Our goal is to provide a comprehensive view of how the model performs under different scenarios, explaining the implications of these variations in real-world applications. To address the challenge, our sensitivity analysis assesses the robustness of the optimized solution when the structure of the Covasim model and some of its key parameters are perturbed. Specifically, we change the base values of these parameters and observe significant changes in results.

In considering the uncertainties of future pandemics, it is essential to recognize that they are likely to share common aspects with past health crises, including vaccine effectiveness, vaccine acceptance rate, transmission rates, and production costs. These parameters are fundamental in any pandemic response, directly impacting the success of vaccination campaigns. The effectiveness of a vaccine, regardless of the disease, remains a primary concern that dictates

distribution strategy. Similarly, public acceptance of vaccines, influenced by cultural, social, and educational factors, is crucial in planning effective distribution and achieving herd immunity. Understanding transmission rates is also pivotal for prioritizing vaccine distribution areas and determining the urgency of response.

Additionally, the cost of vaccine production, a key factor in affordability and accessibility, is especially vital in global health strategies. Thus, we did the sensitivity analysis from the perspective of vaccine effectiveness, vaccine acceptance rate, vaccine price, and disease transmission rate. Our sensitivity analysis demonstrates how our model adapts to diverse scenarios, thereby affirming its robustness and practical applicability. This analysis is not just theoretical; it is a vital tool in preparing for the challenges of future unknown vaccination distribution pandemics.

Initially, we vary the two main drivers of the vaccination campaign, that are the vaccine effectiveness (parameter $\alpha_a^{(d_a)}$) and the vaccine acceptance rate (parameter $\beta_{aw}^{(d_a)}$). In our sensitivity analysis, we test vaccination effectiveness rates varying from 0.75 to 0.95 in increments of 0.05. Furthermore, we change the value of the acceptance rate parameter $\beta_{aw}^{(d_a)}$ from low to high, enabling us to simulate the impact of varying vaccination acceptance rate on the total number of vaccines allocated.

Figure 2.12 presents the percent increase in both the total number of vaccines allocated and the total SC costs, highlighting the impact of varying vaccine effectiveness and acceptance rates on these parameters. Specifically, Figure 2.12a implies that when the vaccine effectiveness increases to 0.95, fewer vaccines are allocated compared to the number of vaccines allocated under vaccine effectiveness of 0.85, 0.8, and 0.75. As expected, a higher vaccine effectiveness enhances the

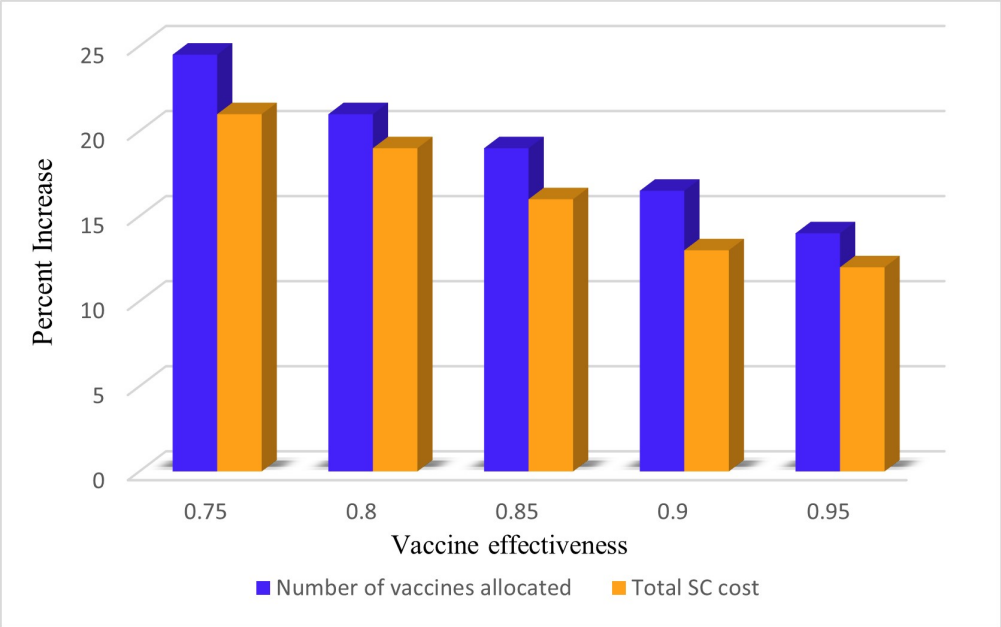

(a) Vaccine effectiveness

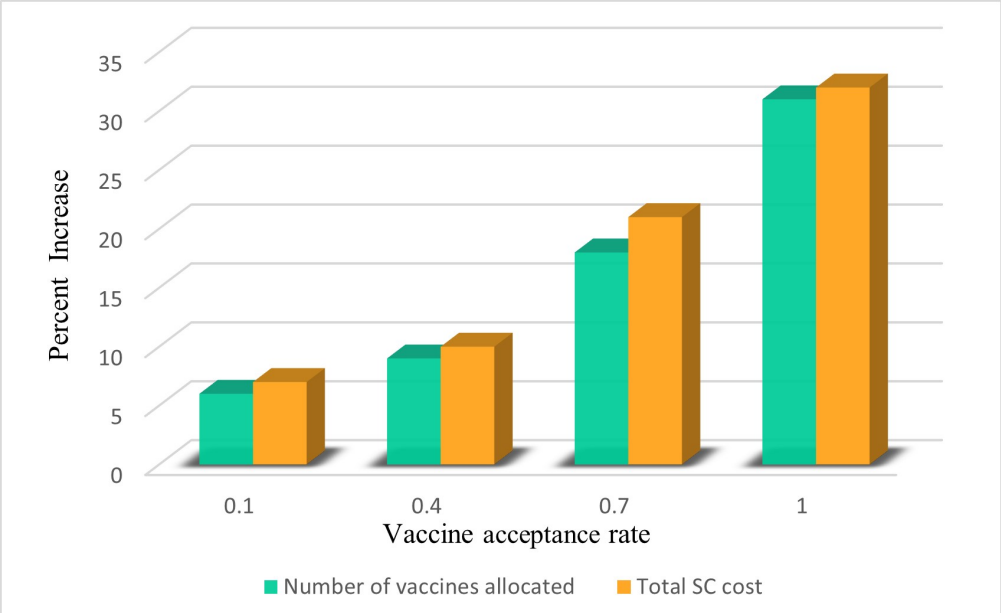

(b) Vaccine acceptance rate

Figure 2.12 Sensitivity of results with varying vaccine effectiveness and vaccine acceptance rate.

impact of all allocation strategies. Notably, in extreme scenarios where the vaccine effectiveness rate is null (represented by the parameter $\alpha_a^{(d_a)} = 0$), all allocation strategies have a consistent, non-efficacious performance. This trend of reduced vaccine allocation with increased effectiveness rate naturally extends to SC cost implications. Figure 2.12 illustrates that higher vaccine effectiveness not only refines the allocation process but also contributes to a more cost-efficient SC operation. Enhanced effectiveness at 0.95 leads to an obvious decrease in SC costs, reflecting the efficiency gains from needing fewer vaccines to achieve public health goals.

Figure 2.12b shows the percent changes in both the optimal number of vaccines allocated and total SC costs under different vaccine acceptance rates when the vaccination effectiveness rate is fixed. The results reveal that as the acceptance rate increases, the vaccine allocation witnesses a proportional increase. This trend reflects the model's responsiveness to dynamic public demand and emphasizes its drive toward achieving herd immunity. It is also worth noting that the model's optimization benefits become more pronounced with increasing acceptance rates. This suggests that as more individuals show willingness to get vaccinated, the model's allocation strategies become increasingly crucial in ensuring the most impactful and efficient distribution. Furthermore, we observe the same trend where higher vaccine acceptance rates lead to increased total SC costs. This trend underscores the necessity for strategic resource planning to navigate the challenges of increasing vaccine demand while balancing public health goals with the imperative of cost-effective distribution.

Then, we extended our sensitivity analysis by employing a multi-parametric approach that simultaneously varies key parameters, specifically vaccine effec-

tiveness and vaccination acceptance rates. This comprehensive analysis is vital for guiding policy formulation and operational strategies in vaccine distribution, particularly for resource allocation planning during pandemics. We defined five distinct scenarios to explore the interplay between vaccine effectiveness and acceptance rates, and their combined impact on vaccine allocation and SC costs. Scenario A is characterized by high vaccine effectiveness (0.95) and high acceptance rate (1), representing an ideal vaccination context. Scenario B represents a situation of high vaccine effectiveness (0.95) with low acceptance (0.1), whereas Scenario C explores the converse scenario, with low vaccine effectiveness and high acceptance rate. Scenario D presents a more challenging case with both low vaccine effectiveness and acceptance rates. Lastly, Scenario E investigates a scenario with moderate levels of both vaccine effectiveness (0.85) and acceptance (0.5). Figure 2.13 describes the critical influence of both vaccine effectiveness and acceptance rates under these scenarios.

The analysis reveals a detailed landscape where each scenario influences vaccine distribution and associated costs distinctly. According to Figure 2.13, Scenario C exhibits the highest vaccine allocation, a consequence of its lower vaccine effectiveness combined with a high acceptance rate. This scenario necessitates an increased allocation of vaccines to fulfill public health objectives due to vaccine's low efficacy, leading to increased SC costs. In contrast, Scenario B demonstrates the lowest vaccine allocated, suggesting that acceptance rate significantly influences the extent of vaccine distribution efforts. It is also observed the increase in total vaccine allocated aligns directly with the SC costs. For example, Scenario C experienced the most significant rise in costs due to its extensive distribution requirements. This observation indicates that higher vaccine

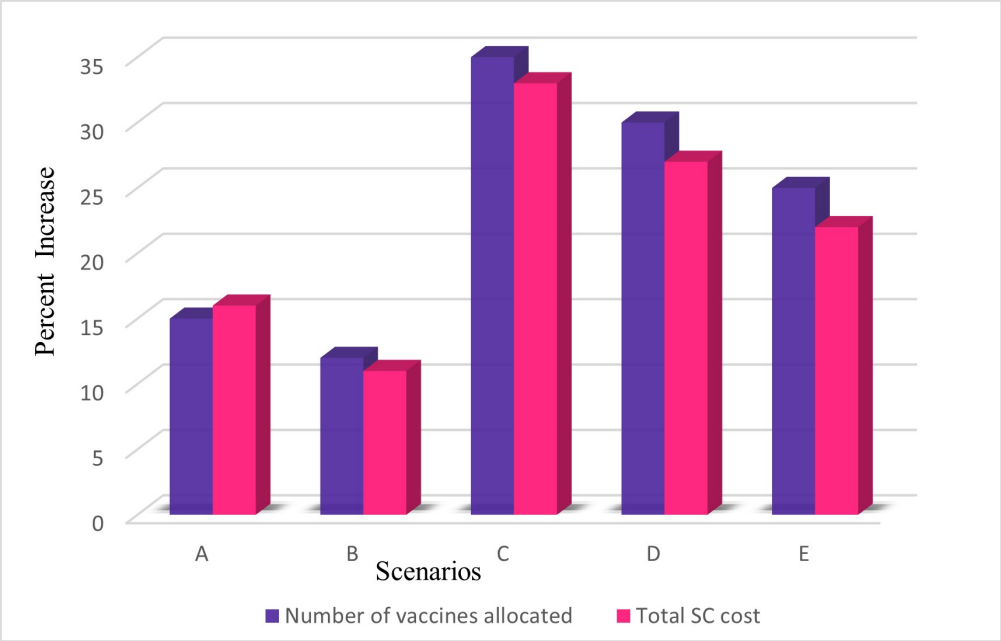

Figure 2.13 Sensitivity analysis with varying both vaccine effectiveness and acceptance rate.

effectiveness can enhance cost-efficiency across the vaccine distribution network. Furthermore, the scenario with moderate effectiveness and acceptance presents a balanced approach, incurring higher logistical costs than minimal scenarios but remaining more manageable compared to the most challenging scenarios.

Then we change the base values of the vaccine production cost (parameter CP_amt) to observe the changes in results. This analysis is paramount to understand how cost fluctuations in real-world scenarios might influence vaccine allocation strategies. Specifically, we propose three scenarios by changing the cost of three types of vaccines. Scenario "A1": This serves as our baseline, representing the simulation-optimization outcomes when vaccine costs are at their original values. Scenario "A2" represents a case where Pfizer's cost increased 50% while keeping all other vaccines' costs at their original price. Scenario "A3" represents a case in which Moderna's cost increased 50% while the costs for other vaccines

remain unchanged. Scenario "A4" represents a case where Janssen vaccine's cost witnesses a 50% increase, with other vaccine costs kept at their initial values. Figure 2.14 shows the proportion of vaccines allocated for each type of vaccine namely, Pfizer, Moderna, and Janssen under these scenarios.

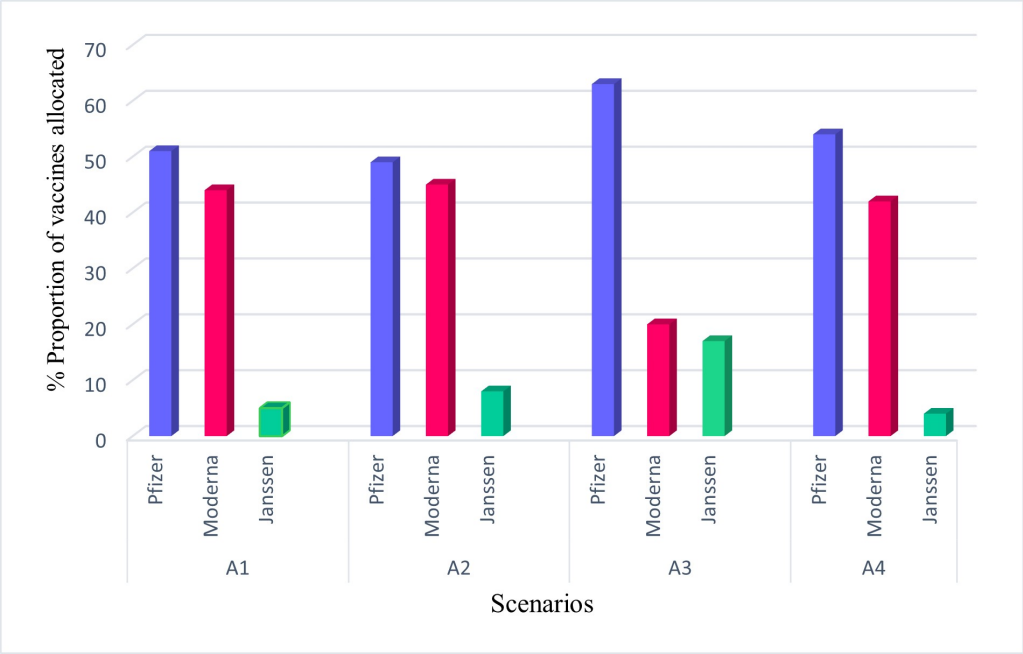

Figure 2.14 Sensitivity analysis under varying vaccine cost.

From the results presented in Figure 2.14, we observe the consistent allocation patterns for scenarios A2 and A4 when compared with the baseline scenario A1. This consistency suggests that despite the cost modifications, the costs for Pfizer and Janssen remain competitive, keeping their allocation levels largely unchanged. In contrast, scenario A3 reveals a distinct change in allocation dynamics when Moderna is expensive than the two other vaccines. Under this scenario, Pfizer vaccines are more allocated due to less cost. Janssen's allocation also witnesses a marginal increase, likely as a compensatory strategy to offset the

reduced Moderna allocations. Overall, the proportion of vaccines allocated for each type is more when the cost of vaccines is reduced, as expected.

We further vary the main parameter within the COVASIM model: the infection transmission rate. While this parameter is meticulously calibrated from historical data, considerable inherent uncertainties remain about the evolving dynamics of the pandemic and people's behaviors during mass vaccination periods. Therefore, we define three scenarios to observe substantial changes in results. Scenario "B1" represents a case in which the transmission rates are the same across all states. Scenario "B2" represents a case where the transmission rates for highly populated states are doubled while keeping other states rates the same as in Scenario B1. Similarly, Scenario "B3" indicates that the transmission rates for less populated states are halved, with rates for the remaining states unchanged from Scenario B1. Figure 2.15 presents the total number of vaccines allocated under these three scenarios, with perturbed transmission rates.

From the results presented in Figure 2.15, it becomes evident that there is a pronounced increase in the total number of vaccines allocated under Scenario B2, a direct consequence of increased transmission rates in densely populated states. In contrast, Scenario B3 does not exhibit significant changes in allocation strategy. This substantial allocation in Scenario B2 can be attributed to the increased transmission rates in highly populated states, leading to an increased demand for vaccines to address the larger number of infections. The results highlight the transmission probability plays a significant role, especially in areas with dense populations. This analysis suggests that the impact of the pandemic is largely determined by the efficacy of vaccination campaigns in curbing infections at the early phases of transmission.

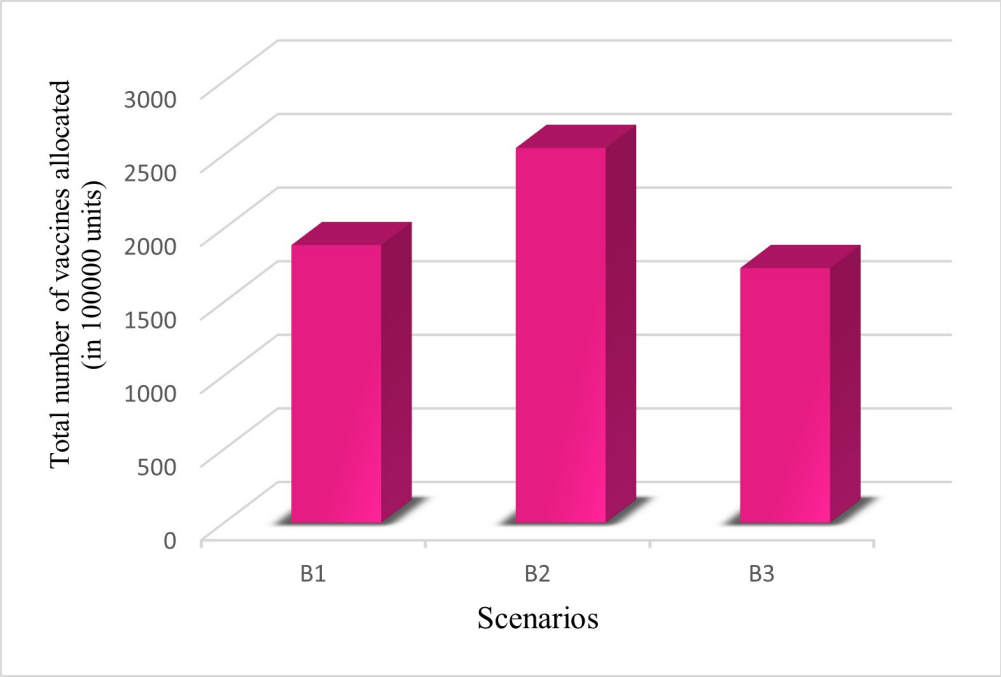

Figure 2.15 Sensitivity analysis under different transmission rate scenarios.

Our model demonstrates remarkable adaptability to key pandemic parameters, a feature pivotal for its application to future vaccination programs. This flexibility encompasses varying scenarios of vaccine effectiveness and vaccine acceptance rates, alongside its responsiveness to cost fluctuations affecting vaccine distribution. Furthermore, the model accounts for changes in disease transmission dynamics, a critical factor in modeling pandemic spread and response strategies. These characteristics— flexibility in vaccine effectiveness and acceptance, economic adaptability, and responsiveness to epidemiological changes —are essential for a modelling framework designed to extend its applicability beyond COVID-19, preparing it for the unpredictable nature of future health pandemics.

In real-world scenarios, as the pandemic continues to evolve, a consistent stream of new data emerges, including updates on vaccine efficacy, changes in

public health behaviors, and the emergence of novel viral variants, the necessity for a dynamic modeling approach becomes clear. A static model might be limited in its ability to address these changes, potentially leading to suboptimal solutions. However, our iterative simulation-optimization framework is designed for adaptability, continuously updating based on real-time data to align with the pandemic's evolving dynamics. This approach not only enhances vaccine demand forecasting but also allows the model to refine strategies in response to the pandemic. Furthermore, this adaptability extends beyond the immediate context of COVID-19, ensuring the model's relevance and effectiveness in managing future pandemics with unknown characteristics. By continuously integrating real-time data and adapting to emerging trends, our model establishes itself as a dynamic and robust tool, bridging the gap between theoretical modeling and practical application. This makes it particularly suited for the complexities and uncertainties inherent in future pandemic management.

2.6 Managerial Implications

The results of this study provide valuable insights for policymakers and managers to optimize vaccine distribution strategies in various ways:

- The extension of Covasim provides valuable support for evidence-based decision-making in pandemic management, accounting for uncertainties in COVID-19 transmission dynamics and disease progression. It enables policymakers to accurately estimate COVID-19 spread, assess susceptible and infected populations, and administer vaccine doses effectively across different regions. This is particularly vital in managing the diverse challenges posed by emerging COVID-19 variants like Alpha, Beta, Delta, and Omicron, where vaccine strategies often evolve from a 2-dose to a multi-dose vaccination program. The extended Covasim model, applicable to different vaccines with multiple doses, equips healthcare managers with the necessary tools to

formulate dynamic strategies, ensuring robust responses to the pandemic's changing landscape.

- Our model is designed to be run bi-weekly, a decision influenced by the dynamic nature of pandemics and vaccination schedules, such as the two-week interval between the first and second doses of the Pfizer vaccine. This bi-weekly update frequency allows us to respond in a timely manner to the changing dynamics of the pandemic, including variations in the number of susceptible individuals, their exposure levels, recovery rates, and the effectiveness of vaccines.

- The adaptability of our model is attributed to both the simulation-optimization framework and the specific features of the VSC model. The simulation-optimization framework provides a dynamic base that allows the model continuously to update with real-time data, aligning closely with the pandemic's evolving dynamics. Our iterative simulation-optimization framework ensures accurate vaccine demand estimation, susceptible and infectious individuals, which then informs the optimization model to make effective supply chain decisions, enabling the model to refine strategies in response to the pandemic. Meanwhile, the VSC model itself is designed with integrated features that enhance flexibility in operational decisions, such as dynamic responses to demand fluctuations. This design aspect ensures that the model can adapt its strategies effectively to meet changing distribution needs, a critical factor for successful vaccine logistics. This adaptability is crucial in ensuring that our VSC model remains an effective solution for vaccine logistics, capable of effectively managing the complexities and uncertainties inherent in global health crises.

- Our model not only adheres to government instructions but also adapts to diverse scenarios like potential future pandemics, VSC fluctuations, or sudden changes in public health strategies. The model's capacity to adapt is enhanced by comprehensive sensitivity analysis, focusing on key factors like vaccine cost, acceptance rates, effectiveness, and transmission rates. This analysis provides insights into the implications of government policies on community immunization and vaccine allocation decisions, thereby supporting decision-makers in their strategic planning. Our findings highlight the critical role of transmission probability in vaccine distribution strategies, emphasizing aggressive allocation in regions with higher transmission risks.

- VSC coordination during crises necessitates collaborative efforts between governments to effectively manage vaccine distribution strategies. Our research findings provide valuable insights for state and federal governments to coordinate vaccine distribution at the state level, minimizing unnecessary distribution and storage, and enabling other states to meet demand requirements. Our results reveal that states with larger populations are more likely to receive higher vaccine allocation proportions, as the model prioritizes vaccination in these regions. Our model offers essential decision-making support, helping policymakers optimize vaccine distribution and storage strategies based on factors like state population and vaccine acceptance rates. These insights can encourage state governments to establish partnerships with their local healthcare facilities and respond proactively to the increasing demand for vaccination in their service regions.

- Incorporating multi-objective functions in vaccine network design provides a powerful tool for addressing various dimensions simultaneously. Our proposed model allows decision-makers and healthcare managers to consider sustainability and cost factors in the VSC network. This enables them to strike a trade-off between these factors and make informed decisions. Given the increasing global concerns related to environmental issues and global warming, particularly in the transportation of cold chain products with high HFC gas emissions, our model can serve as a valuable roadmap for policymakers to assess the level of emissions reductions achievable by implementing greener practices at an increased cost. This information can aid in the development of strategies for reducing environmental impacts while ensuring efficient VSC operations.

2.7 Conclusion and Future Direction

We develop a simulation-optimization model for COVID-19 vaccine distribution. We extend an agent-based model with three vaccination categories for different doses. These categories represent the first, second, and booster shots for different vaccine types. The simulation model estimates the number of infections and disease values, which are then fed into the VSC model. The VSC model considers warehouse locations, state repositories, and vaccine willingness to generate optimal locations and allocation strategies across states and healthcare facilities for future

planning. These results are then used as inputs to estimate the number of infections and susceptible individuals for the same period.

We introduce a sustainable, dynamic VSC model that incorporates inventory control, switching warehouses, and capacity expansion decisions, as well as the environmental impact of GHGs besides CO_2 emissions in transportation. The proposed model is a bi-objective multi-period optimization problem that aims to minimize economic features and environmental impacts in the VSC. We solve the proposed model using the augmented ϵ-constraint approach. We apply our simulation-optimization framework for vaccine location and allocation across all U.S. states.

The proposed model was validated and tested on the cumulative number of COVID-19 infections. Numerical tests in the case study show that the predicted infection results closely match the real outbreak data. Furthermore, the results indicate that there is a delay in observing the effect of vaccination on reducing the number of infections, as it takes time for the vaccination to take effect. In addition, when the vaccination capacity is limited, the model prioritizes the allocation of first doses over second and booster shots for all three vaccine types because a greater number of people can benefit from taking the first dose of the vaccines.

The model recommends locations for the regional warehouses coincide with the actual decisions made by the government in the real-world scenario. The findings related to warehouse locations indicate that the model prioritizes locating a state repository in the state with the shortest distance from the vaccine regional warehouse. Transportation and distance are the main contributors to costs and greenhouse gas emissions associated with VSC. Thus, by reducing the distance that vaccines need to be transported, the proposed model chooses the state repository

closest to the selected regional warehouse. This, in turn, can help to reduce the total costs and the impacts of global warming. Additionally, the model highlights that states with higher population densities are more likely to receive additional vaccines due to the larger number of infected individuals in those areas, as the model gives priority to vaccinating people in these regions.

Our presented model is a preliminary effort in this field. There are several potential research directions that could help to bridge the gap. One of the potential directions could be the inclusion of the perishability factor of vaccines into the model. Another suggestion would be to consider the uncertainty in input parameters in both the Covasim simulation and optimization model. For instance, incorporating uncertainty in the disease transmission rate, which significantly affects most variables related to vaccine doses, and including the uncertain time between taking the doses will be a fascinating future direction. Additionally, the COVID-19 pandemic has highlighted the need to consider the resilience of VSC networks to disruptions. Hence, another future research direction would be to develop a resilient VSC network that increases the likelihood of continuous functionality of VSC in the face of disruptions and the equitable distribution of vaccines. Finally, studying specific vaccination strategies based on different risk groups and prioritizing vaccine allocations to target groups, such as healthcare workers, other essential workers, or patients with comorbidities, can be a crucial future research avenue.

CHAPTER 3

ASSESSING THE VALUE OF HETEROGENEOUS ELASTICITIES FOR INCENTIVE-BASED RESIDENTIAL DEMAND RESPONSE

3.1 Introduction

3.1.1 Background and literature review

The increasing frequency of extreme weather events poses significant challenges to the safe operation of electric power systems worldwide. When the power system's supply capacity approaches its limit, energy demand rises, increasing the risk of system failures and operational costs, and potential financial losses [75]. In 2022, the California Independent System Operator (CAISO) reported a remarkable increase in power demand due to record-high temperatures throughout summer heatwaves. This increase in demand placed considerable stress on the electrical grid, significantly increasing the risk of rotating outages unless consumers reduce their energy consumption to a greater extent [76]. Consequently, the need to balance real-time energy supply and demand has led to increased utilization of demand response (DR) programs. Several studies have emphasized that the heightened uncertainty in electricity generation from renewable sources could potentially destabilize the system if additional demand-side management measures are not implemented [77, 78].

In the smart grid context, DR programs are increasingly being recognized for their capability to mitigate peak loads and lower grid operational costs [79, 80].

DR represents an effective solution to address reliability and efficiency issues in the power grid, involving changes in end-consumers' electricity consumption patterns from their normal routines during peak hours. These programs offer substantial benefits, including cost reduction, energy conservation, and grid stability [13, 81]. It also provides financial benefits for Load Serving Entities (LSE), entities that purchase electricity at wholesale prices and supply it at a fixed rate. When the wholesale price of electricity exceeds the flat rate charged to customers by LSE, it becomes financially beneficial for them to motivate customers to reduce their electricity usage by providing monetary rewards.

The U.S. Department of Energy reports that the residential sector accounts for more than 38% of total electricity consumption in the United States, making it a significant source of flexibility that the system can exploit. [77]. As reported by the U.S. Federal Energy Regulatory Commission, despite 80% of the potential peak load reduction being achieved by large industrial and commercial customers [75], only a small proportion has been realized by the residential sector. Thus, residential demand response holds significant potential to reduce electricity consumption and costs, given the substantial size of the residential sector and its sparse utilization.

DR programs are broadly categorized into price-based demand response (PBDR) and incentive-based demand response (IBDR). PBDR programs charge customers varying electricity prices throughout the day, whereas IBDR programs provide specific financial incentives to customers for reducing their electricity usage at peak hours [82, 83]. Research indicates that IBDR tends to be more effective than PBDR, largely due to the direct 'bonus' benefits perceived by consumers [84].

For instance, IBDR programs have been shown to significantly reduce peak load, up to 93% in some U.S. cases [85].

Several studies have advanced our understanding of IBDR programs through innovative models focused on financial incentives and demand management. The foundational works of Ghosh et al.[86] and Aalami et al. [87] have addressed structural aspects of DR programs, focusing on optimizing operational costs and integrating interruptible/curtailable loads for effective demand management. Furthermore, Zhong et al. [88]) and Li et al. [14] introduced novel consumer engagement strategies, such as the Coupon Incentive-based Demand Response (CIDR) and economic analyses of consumer coupons, encouraging consumer participation in DR programs. Although elasticity plays a crucial role in numerous DR programs, these studies have not delved into the detailed analysis of how the heterogeneous nature of consumer sensitivities to incentives affect the outcomes of these programs. This observation points to a critical gap, the need for focused research on customer-specific elasticity within the IBDR framework.

A crucial aspect of IBDR programs is to accurately model how demand changes with changes in financial incentives, an economic concept known as elasticity [89]. A higher elasticity indicates that demand is more sensitive to changes in price [90]. Elasticity is utilized for load consumption analysis and forecasting, shaping the design of DR programs, particularly for small customers. Elasticity shows the relationship between utilities' financial incentives and customer load changes [43].

To further improve the understanding of residential load profiles and consumer behaviors, Asadinejad et al. [90] investigated the customer demand response behavior and elasticity under IBDR programs, analyzing residential

customers in the U.S. across various appliances and thermostat settings. Their findings indicate that elasticity significantly varies among appliances, with HVAC systems demonstrating higher elasticity due to their substantial energy consumption, emphasizing the need for appliance-specific incentives in DR programs. Similarly, Shi et al. [91] proposed an integrated model that combines technical and social-behavioral factors to enhance IBDR programs, analyzing appliance usage patterns via a large-scale survey of customers in Texas and New York. Moreover, Lu et al. [92] explored the optimal bidding strategy of demand response aggregators by modeling customer responsiveness behaviors under different incentives. Pandey et al. [93] proposed an improved incentive-based DR model to assess their individual and combined effects on the system's economic and technical performance for distribution networks.

3.1.2 Contributions

Despite the increasing implementation of residential DR programs in the U.S., participation levels remain below expectations. This under-performance is closely attributed to the lack of a comprehensive understanding and utilization of individual consumer behavioral patterns. Existing IBDR programs do not take full advantage of the reduction potential: their incentive policies do not incorporate (a) appliance-specific demand elasticity values, and (b) customer-specific demand elasticity values. In other words, incentive pricing is based on an aggregate demand model and is set to take on a same value across all customers and appliance types. This has been a reasonable choice so far due to privacy issues and lack of granular household electricity consumption data. However, with the growing proliferation of smart meters and privacy-preserving technologies, it is time to re-envision how

to better utilize the vast amount of electricity consumption data towards designing more efficient IBDR programs.

In this study, we assess the value of incorporating heterogeneous elasticity values in the optimal operations of LSEs with incentive-based demand response. Three optimization problems with increasing levels of granularity related electricity consumption behavior are introduced; (i) first problem uses a single aggregate elasticity value, (ii) second problem uses appliance-specific elasticity values, and (iii) third problem uses customer and appliance-specific elasticity values to model demand. In each successive model, the LSE is also allowed to choose the incentive reward amounts with matching granularity. Additionally, previous studies on DR [88, 14, 90] have overlooked the critical impact of transmission line losses within the distribution system. Given the implementation of DR programs in distribution systems, it is essential to account for energy losses, especially due to the high resistance-to-inductance ratios typical of low voltage networks. Thus, energy loss is accounted for in our third optimization problem (the first and second problems do not model separate customers, so we cannot include network loss into them). Note that estimating the specific elasticity values is out of the scope of this work but we refer the readers to [90].

Comparing the outputs of the above-mentioned three models allows us to uncover nuanced insights into customer model design in IBDR programs. We believe that these findings are invaluable for grid participants and policymakers in creating more accurate and effective models for residential IBDR. The main contributions of this research are as follows:

- We model the optimal decision making process of an LSE by formulating it as optimization problems with varying levels of granularity in consumer elasticity. The comparison of the three different models reveals that the

economic value of implementing an IBDR pricing scheme that is appliance-specific is significant. On the other hand, the economic value of further adding customer-specific granularity into the incentive pricing scheme is not as significant.

- The proposed optimization problems model self-owned generators and storage devices of the LSE and describe the dynamics of the electric storage devices. Furthermore, the third optimization problem (which has the highest granularity) models a realistic grid setup by incorporating transmission line losses through branch power flow equations. Through detailed modeling of the electric grid's dynamics and operational constraints, we are able to analyze the intricate interplay between different grid components (e.g., locational marginal price versus storage charging status), which we can then use to enhance the operation of IBDR programs.

3.2 Problem Formulation

In Figure 4.1, we explain the hierarchical architecture of the incentive-based demand response as applied in the current work, featuring key components including ISO, LSEs, customers, and appliances. For LSEs, the ISO determines the price, known as the Locational Marginal Price (LMP). In the proposed model, the LSE plays a key role in managing electricity demand. At each time step, it sets an incentive price, which is then broadcast to the customers. Customers receive this incentive pricing information and autonomously decide how to adjust their appliance usage. The compensation each customer receives is a function of the incentive price and their subsequent reduction in appliance-specific load.

The LMP represents the economic value of electricity across different regions, accounting for the costs associated with losses and congestion under current operational conditions. It becomes financially consequential for LSEs when the LMP exceeds the flat rate charged to customers as it necessitates LSEs to purchase electricity at prices higher than the flat rates they offer to end-users, resulting in

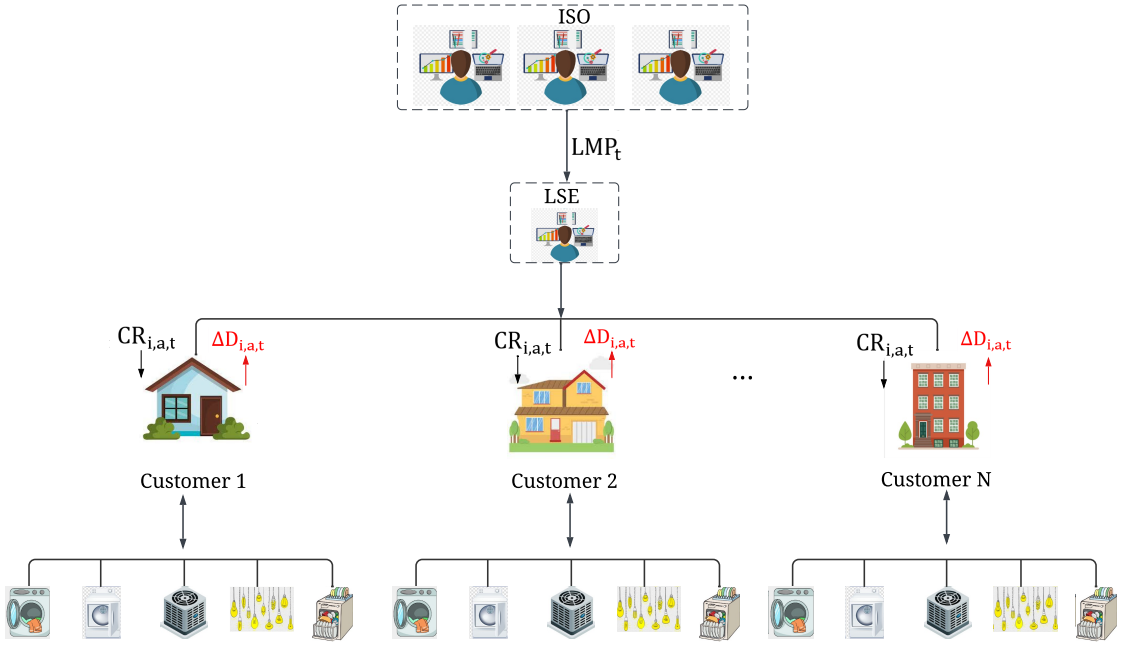

Figure 3.1 Hierarchical architecture of incentive-based demand response for the current work.

direct economic losses. This serves as a catalyst for LSEs to implement demand reduction strategies, which not only offset their economic losses but also encourages efficient energy consumption, especially during peak demand periods when the system operates close to the stability margin.

In this work, we consider an LSE that operates an integrated system including self-owned generators and storage facilities. The LSE either purchases (via market by paying LMP), discharges (from storage devices), or generates electric power and injects it through the distribution feeder in order to serve its customers. The network is modeled as a distribution network (tree network structure) with AC nonlinear power flow equations and line losses. Given forecast values for LMP and estimates of the elasticity values, the LSE solves a multi-period optimization problem through which it identifies the optimal series of incentive pricing for IBDR and also the optimal operational decisions. The incentive price

for IBDR is a crucial component of the LSE's objective function, aligning the management of electricity demand with economic efficiency and the behavioral patterns of the customers.

3.2.1 Model formulation

In our research, we present three distinct models, each with varying degrees of complexity and specificity. We use indices $i, j, k \in \mathcal{N}$ to denote network nodes, where each node acts as an aggregation of customers served by that node. We will use the word node and customer interchangeably (i.e., node i is equivalent to customer i). The nodes are connected via transmission lines, belonging to set $\mathcal{E}$. Each node (customer) is associated with multiple appliances, indexed by $a \in \mathcal{A}$. The LSE owns a set of generators $g \in \mathcal{G}$ and storage units $s \in \mathcal{S}$, each with its specific characteristics and constraints. Time periods are indexed by $t \in \mathcal{T}$.

Model 1 lays the foundation by utilizing an aggregate elasticity value ($\boldsymbol{\epsilon}$). This model provides a broad, collective perspective on total demand but lacks the details of individual appliance or consumer-specific behaviors.

Model 2 enhances our analysis by integrating appliance-specific elasticity ($\boldsymbol{\epsilon}_j$). It offers a more detailed view by accounting for the demand for each appliance individually. In this model, the focus shifts to understanding how the variation in elasticity values across different appliances impacts the optimal incentive pricing for IBDR. Model 3, the most detailed model, incorporates both customer and appliance-specific elasticity($\boldsymbol{\epsilon}_{i,j}$). This model enables us to formulate demand reduction with precision for each customer-appliance combination, offering critical insights for load aggregators to optimize incentive pricing and reduce costs effectively. While all three models offer valuable perspectives, our dissertation will

Table 3.1 Parameters

Symbol	Description
$\boldsymbol{LMP}_t$	Locational marginal price at time t
$\boldsymbol{CF}$	Fixed flat rate charged to customers
$\boldsymbol{D}^0_{i,a,t}$	Base demand for customer i, appliance a, time t
$\boldsymbol{C}_g$	Generation cost coefficient for generator g
$\boldsymbol{C}^c_s$	Charging cost coefficient for storage unit s
$\boldsymbol{C}^d_s$	Discharging cost coefficient for storage s
$\boldsymbol{CR}^{max/min}$	Max/min reward value
$\boldsymbol{E}^{max/min}_s$	Max/min energy level for storage s
$\boldsymbol{X}^{max}_g$	Max capacity for generator g
$\boldsymbol{P}^{c,\max}_s$	Max charging power level for storage s
$\boldsymbol{P}^{d,\max}_s$	Max discharging power level for storage s
$\boldsymbol{\eta}^c_s$	Charging efficiency rate for storage s
$\boldsymbol{\eta}^d_s$	Discharging efficiency rate for storage s
$\boldsymbol{\epsilon}, \boldsymbol{\epsilon}_a, \boldsymbol{\epsilon}_{i,a}$	Elasticity (varying levels of specificity)
$\boldsymbol{\phi}, \boldsymbol{\phi}_a, \boldsymbol{\phi}_{i,a}$	Reduction ceiling (varying levels of specificity)
$\boldsymbol{r}_{i,j}$	Resistance of line connecting node i and j
$\boldsymbol{x}_{i,j}$	Reactance of line connecting node i and j

focus on Models 2 and 3, as they provide a more detailed and granular analysis of electricity demand crucial for effective load management. They also enable us to understand the impact of modeling appliance and consumer-specific elasticity, uncovering nuanced patterns and insights. The parameters and decision variables can be found in Tables 3.1 and 3.2.

3.2.2 Power flow and storage constraints

The resistance to reactance ratios in distribution systems are large compared to that of transmission systems, which lead to significant line losses. Therefore, in our study, we incorporate power flow constraints and line losses into the DR program

Table 3.2 Decision Variables

Symbol	Description
D_t	Demand at time t
$D_{i,t}$	Demand for customer i, time t
$D_{i,a,t}$	Demand for customer i, appliance a, time t
$\Delta D_{i,a,t}$	Demand reduction for customer i, appliance a, time t
$CR_{i,a,t}$	Incentive reward for customer i, appliance a, time t
Y_t	Amount of purchased electricity at time t
$X_{g,t}$	Generated electricity for generator g, time t
$P^c_{s,t}$	Charging power level for storage s, time t
$P^d_{s,t}$	Discharging power level for storage s, time t
$P_{s,t}$	Net power level for storage s, time t
$E_{s,t}$	Stored energy level for storage s, time t
$P_{i,j,t}$	Active power from node i to node j at time t
$Q_{i,j,t}$	Reactive power from node i to node j at time t
$I_{i,j,t}$	Complex current from node i to node j at time t
$D^{img}_{i,t}$	Reactive demand on node i at time t
$V_{i,t}$	Complex voltage on node i at time t
loss_t	Total network loss at time t

for residential load management using the branch flow model [94, 95, 96]. Unlike traditional bus injection models that focus on nodal variables such as bus current and power injections [97], the branch flow model emphasizes the currents and power flows on individual branches [96, 98]. The branch flow model's emphasis on branch-specific dynamics allows for a more convenient modeling of power flow and loss within radial distribution networks [96].

The power flow equations are presented in Equations (3.1) through (3.6). Equation (3.1) defines the relationship between voltage, current and apparent power. It is important to note that this equation represents a convex relaxation

of the original equality constraint. As detailed in [94, 95], this relaxation is shown to be exact under certain conditions. Equations (3.2) and (3.3) represent the real power balance and the reactive power balance, respectively. The Voltage difference across the grid is expressed in Equation (3.4). The input feeder is modeled in equation (3.5). Equation (3.6) quantifies the total losses within the distribution grid served by the LSE.

$$\frac{P_{i,j,t}^2 + Q_{i,j,t}^2}{|V_{i,t}|^2} \leq |I_{i,j,t}|^2 \tag{3.1}$$

$$P_{i,j,t} = \sum_{k:(j,k)\in\mathcal{E}} P_{j,k,t} + \boldsymbol{r}_{i,j}|I_{i,j,t}|^2 + D_{j,t} \tag{3.2}$$

$$Q_{i,j,t} = \sum_{k:(j,k)\in\mathcal{E}} Q_{j,k,t} + \boldsymbol{x}_{i,j}|I_{i,j,t}|^2 + D_{j,t}^{img} \tag{3.3}$$

$$\begin{aligned} |V_{i,t}|^2 - |V_{j,t}|^2 &= 2(\boldsymbol{r}_{i,j}P_{i,j,t} + \boldsymbol{x}_{i,j}Q_{i,j,t}) \\ &\quad - (\boldsymbol{r}_{i,j}^2 + \boldsymbol{x}_{i,j}^2)|I_{i,j,t}|^2 \end{aligned} \tag{3.4}$$

$$\begin{aligned} \sum_{g\in\mathcal{G}} X_{g,t} + \sum_{s\in\mathcal{S}} P_{s,t}^d + Y_t - \sum_{s\in\mathcal{S}} P_{s,t}^c \\ - D_{0,t} = \sum_{i:(0,i)\in\mathcal{E}} P_{0,i,t} \end{aligned} \tag{3.5}$$

$$loss_t = \sum_{i\in\mathcal{I}} \sum_{j\in\mathcal{J}} \boldsymbol{r}_{i,j}|I_{i,j,t}|^2 \tag{3.6}$$

Incorporating loss into DR programs can significantly enhance distribution system efficiency by optimizing network performance and reducing overall energy costs [99, 100]. High losses indicate that a significant portion of the generated power is not reaching the end-users, leading to wasted energy during transmission. Failure to capture loss in IBDR models will not only underestimate the amount of power that needs to be acquired at each time period, but will also lead to sub-optimal incentive pricing schemes, thereby undermining the effectiveness of IBDR programs.

As distributed energy storage and generator devices are integral to modern power systems [101], we also integrate these components into our models. In doing so, our model gains a heightened capability to optimize energy distribution and effectively manage DR, leading to more robust and adaptable strategies in residential load management. The following equations describe the constraints related to LSE-owned storage and generators. Equation (3.7) embeds the time-dependent transition in stored energy level. Equation (3.8) models the storage charging and discharging with their respective efficiency rates. Equation (3.9) imposes limits on energy storage. Equations (3.10) and (3.11) imply the bounds on discharging and charging power, respectively. The generation limit is set in Equation (3.12).

$$E_{s,t} = E_{s,t-1} + P_{s,t} \tag{3.7}$$

$$P_{s,t} = (\boldsymbol{\eta}_s^c P_{s,t}^c - \frac{1}{\boldsymbol{\eta}_s^d} P_{s,t}^d) \tag{3.8}$$

$$\boldsymbol{E}_s^{min} \leq E_{s,t} \leq \boldsymbol{E}_s^{max} \tag{3.9}$$

$$P_{s,t}^d \leq \boldsymbol{P}_s^{d,max} \tag{3.10}$$

$$P_{s,t}^c \leq \boldsymbol{P}_s^{c,max} \tag{3.11}$$

$$X_{g,t} \leq \boldsymbol{X}_g^{max} \tag{3.12}$$

3.2.3 Model 1: aggregate elasticity

We begin by presenting Model 1, which is the simplest but lays the foundation for the following models. The LSE aims to minimize the net cost (3.13) comprising terms associated with purchasing cost, fixed rate received from consumers, incentive reward payments, self-generation costs, and storage operation costs.

Equations (3.14)-(3.15) ensure that the realized electricity demand is the baseline demand minus demand reduction, which relates to the aggregate elasticity,

$\boldsymbol{\epsilon}$. Equation (3.16) imposes the demand reduction limit by using a predetermined factor $\boldsymbol{\phi}$. In practice, this factor is determined as the point from which further reduction is unlikely to happen due to essential usages. Equation (3.17) provides a range of incentive values that the LSE can select from and (3.18) states that the total supply of electricity should be equal to the demand across all times. Finally, we have the storage/generator constraints and the non-negativity constraints on all the decision variables; the latter omitted for brevity.

$$\min \sum_{t=1}^{T} \Bigg[\boldsymbol{LMP}_t \cdot Y_t - \boldsymbol{CF} \cdot D_t + CR_t \cdot \Delta D_t + \sum_{g \in \mathcal{G}} \boldsymbol{C}_g X_{g,t} + \sum_{s \in \mathcal{S}} (\boldsymbol{C}^d_s P^d_{s,t} + \boldsymbol{C}^c_s P^c_{s,t}) \Bigg] \tag{3.13}$$

$$\text{s.t.} \quad D_t = D^0_t - \Delta D_t \tag{3.14}$$

$$\Delta D_t = \boldsymbol{\epsilon} (\frac{CR_t}{\boldsymbol{CF}}) \boldsymbol{D^0_t} \tag{3.15}$$

$$\Delta D_t \leq \boldsymbol{\phi} \boldsymbol{D^0_t} \tag{3.16}$$

$$\boldsymbol{CR}^{min} \leq CR_t \leq \boldsymbol{CR}^{max} \tag{3.17}$$

$$\sum_{g \in \mathcal{G}} X_{g,t} + \sum_{s \in \mathcal{S}} P^d_{s,t} + Y_t = D_t + \sum_{s \in \mathcal{S}} P^c_{s,t} \tag{3.18}$$

Equations (3.7)-(3.12)

3.2.4 Model 2: appliance-specific elasticity

Previous studies such as [90] have shown that the elasticity values can vary significantly across different appliance types. Therefore, in what follows, we increase the fidelity of the IBDR model by incorporating appliance-specific elasticity values. In accordance to this change, equations (3.21)-(3.24) are appliance-specific counterparts of equations (3.14)-(3.17) in Model 1. Equation (3.20) simply states that the demand at any given time is the summation of all

the appliance-specific demands. As before, we omit the non-negativity constraints in our presentation for brevity. Note that the LSE now has the option to choose different incentive rewards for different appliances.

$$\min \sum_{t=1}^{T} \Bigg[\boldsymbol{LMP}_t \cdot Y_t - \boldsymbol{CF} \cdot D_t + \sum_{a \in \mathcal{A}} CR_{a,t} \Delta D_{a,t} + \sum_{g \in \mathcal{G}} \boldsymbol{C}_g X_{g,t} + \sum_{s \in \mathcal{S}} (\boldsymbol{C}_s^d P_{s,t}^d + \boldsymbol{C}_s^c P_{s,t}^c) \Bigg] \tag{3.19}$$

$$\text{s.t.} \quad D_t = \sum_{a \in \mathcal{A}} D_{a,t} \tag{3.20}$$

$$D_{a,t} = \boldsymbol{D}_{\boldsymbol{a,t}}^{\boldsymbol{0}} - \Delta D_{a,t} \tag{3.21}$$

$$\Delta D_{a,t} \leq \boldsymbol{\phi}_a \boldsymbol{D}_{\boldsymbol{a,t}}^{\boldsymbol{0}} \tag{3.22}$$

$$\Delta D_{a,t} = \boldsymbol{\epsilon}_a \left(\frac{CR_{a,t}}{\boldsymbol{CF}} \right) \boldsymbol{D}_{\boldsymbol{a,t}}^{\boldsymbol{0}} \tag{3.23}$$

$$\boldsymbol{CR}^{min} \leq CR_{a,t} \leq \boldsymbol{CR}^{max} \tag{3.24}$$

Equations (3.7)-(3.12), (3.18)

3.2.5 Model 3: customer and appliance-specific elasticity

In Model 3, we increase the fidelity of the IBDR model one step further by incorporating customer and appliance-specific elasticity values. In accordance to this change, Equations (3.27)-(3.30) are customer-appliance-specific counterparts of Equations (3.14)-(3.17) in Model 1. Equation (3.26) simply states that the demand at any given time is the summation of all the customer-appliance-specific demands. For Model 3, we not only include the storage/generator constraints but also capture the line losses via the power flow equations of the branch flow model, (3.1)-(3.6). Again, non-negativity constraints are omitted for brevity. Note that the LSE now has the option to choose different incentive rewards for different customers and appliances.

$$\min \sum_{t=1}^{T} \Bigg[\boldsymbol{LMP}_t \cdot Y_t - \boldsymbol{CF} \cdot D_t + \sum_{i \in \mathcal{N}} \sum_{a \in \mathcal{A}} CR_{i,a,t} \Delta D_{i,a,t} + \sum_{g \in \mathcal{G}} \boldsymbol{C}_g X_{g,t} + \sum_{s \in \mathcal{S}} (\boldsymbol{C}_s^d P_{s,t}^d + \boldsymbol{C}_s^c P_{s,t}^c) \Bigg] \tag{3.25}$$

$$D_t = \sum_{i \in \mathcal{N}} \sum_{a \in \mathcal{A}} D_{i,a,t} \tag{3.26}$$

$$D_{i,a,t} = \boldsymbol{D}_{\boldsymbol{i,a,t}}^{\boldsymbol{0}} - \Delta D_{i,a,t} \tag{3.27}$$

$$\Delta D_{i,a,t} \leq \boldsymbol{\phi}_{i,a} \boldsymbol{D}_{\boldsymbol{i,a,t}}^{\boldsymbol{0}} \tag{3.28}$$

$$\Delta D_{i,a,t} = \boldsymbol{\epsilon}_{i,a} \left(\frac{CR_{i,a,t}}{\boldsymbol{CF}} \right) \boldsymbol{D}_{\boldsymbol{i,a,t}}^{\boldsymbol{0}} \tag{3.29}$$

$$\boldsymbol{CR}^{min} \leq CR_{i,a,t} \leq \boldsymbol{CR}^{max} \tag{3.30}$$

$$\sum_{g \in \mathcal{G}} X_{g,t} + \sum_{s \in \mathcal{S}} P_{s,t}^d + Y_t \geq D_t + loss_t + \sum_{s \in \mathcal{S}} P_{s,t}^c \tag{3.31}$$

Equations (3.1)-(3.12)

3.3 Results

In this section, we implement the proposed models to a realistic test case and examine the impact of model fidelity (specific elasticity values, line losses) on IBDR programs. Subsection 3.3.1 describes the construct of the test case used for applying the proposed IBDR models. Section 3.3.2 offers comparative analyses of the three models, employing real-world residential data to illustrate their efficacy and applicability.

3.3.1 Description of test case

In this test case, we consider a IBDR scenario in Essex County, New Jersey. The LMP data is collected from the PJM website [102]. The fixed rate ($\boldsymbol{CF}$) charged from the LSE to customers is set at \$120/MWh. The generation cost coefficient

is established to be \$90/MWh. Regarding storage parameters, the initial stored energy level is set to 4 MWh, with minimum and maximum storage levels of 0 MWh and 12 MWh, respectively. Charging and discharging efficiency rates are 0.9, and the cost coefficients for both charging and discharging are standardized at \$0.1/MWh, bench-marked based on the work of [101].The $\boldsymbol{P}_s^{c,\max}$ and $\boldsymbol{P}_s^{d,\max}$ are set to 4 MW, while $\boldsymbol{X}_g^{max}$ is 1 MWh.The maximum and minimum values for the incentive reward $\boldsymbol{CR}^{max/min}$ are \$50/MWh and \$0/MWh, respectively. The values for $\boldsymbol{\phi}_a$ were chosen to be 0.8, 0.8, 0.8, 0.7 and 0.5 for dishwasher, dryer, washer, lighting, HVAC, respectively. The value for $\boldsymbol{\phi}$ is computed as the weighted average of $\boldsymbol{\phi}_a$, where the weights are determined by the relative demand of each appliance. Lastly, $\boldsymbol{\phi}_{i,a}$ values are randomly sampled from normal distributions with mean $\boldsymbol{\phi}_a$ and standard deviation 0.01.

We considered five different residential appliances: (1) Heating, Ventilation, and Air Conditioning (HVAC), (2) lighting, (3) dishwasher, (4) washer, and (5) dryer. The elasticity values are derived from the study conducted by [90] and listed in Table 3.3. We can observe that lighting exhibits the highest elasticity, with a value of 0.42. This indicates consumers are more responsive to incentives when it comes to energy savings from lighting. In contrast, the HVAC system displays the lowest elasticity value at 0.11, suggesting a reluctance among consumers to modify their heating or cooling usage in response to incentives. The elasticity values for other appliances, such as dishwashers, washers, and dryers, show variability, falling between these two extremes. The analysis underscores the necessity for DR programs to be finely attuned to the distinct usage patterns and preferences of consumers across different appliances. To generate customer-appliance-specific

Table 3.3 Appliance-specific Elasticity Values

Appliance	**Elasticity**
Dishwasher	0.13
Washer	0.27
Dryer	0.33
Lighting	0.42
HVAC	0.11

elasticity values, $\boldsymbol{\epsilon}_{i,a}$, we randomly sampled from normal distributions with mean $\boldsymbol{\epsilon}_a$ and standard deviation 0.02.

To generate a baseline demand data, we utilized the time-series end-use load profiles provided by the National Renewable Energy Laboratory (NREL) [13]. This dataset offers detailed insights into energy consumption patterns across various residential and commercial building types in the United States. Within this dataset, the data is segmented by building type (single-family homes, offices, and restaurants), and further categorized by end-use (heating, cooling, lighting, etc.), in 15-minute intervals. The test case used in this research was generated by overlaying demand data from 33 single-family detached buildings onto the IEEE 33-bus system (which provide the resistance and reactance values of transmission lines).

The models are evaluated over a planning horizon of one month, from January 1, 2018, to February 1, 2018, including 743 time periods. Computations were conducted on a desktop computer equipped with an Intel i7 CPU and 64.0 GB of memory, using Python 3.6.8 in the Visual Studio Code environment.

3.3.2 Comprehensive study of the proposed models

In this section, we present the findings from our case study by running three distinct models, each incorporating varying elasticity parameters to assess their impact on customer behavior.

We begin with an output from Model 3, Figure 3.2, which offers a comprehensive view of the overall dynamics between LMP, demand, electricity market purchases, and losses over planning time. For clarity, this figure focuses on the first 36 time periods. It is observed that loss accounts for a significant portion of the total energy, which the LSE has to account for in addition to the actual demand. As depicted, there are instances where the amount of market purchase exceeds the actual demand plus loss. This suggests that in certain periods, additional electricity is being purchased, potentially for storage to accommodate future demand. This pattern highlights the complex decisions involved in electricity market operations, where key decisions are influenced by a variety of factors including anticipated future prices and needs, and network losses.

Figure 3.3 illustrates the overall demand and its reduction, with the orange bars highlighting the extent of demand reduction achieved. The summation of the blue bar and orange bar constitute the baseline demand. Figure 3.4 segments the total demand reduction by appliance types. It is noted that the demand reduction ratio is quantified as the demand reduction divided by the baseline demand for each appliance type. From these analyses, it becomes evident that demand reduction is most significant for lighting, attributed to customers' higher willingness to reduce its usage in response to incentives. Conversely, the dishwasher and HVAC exhibit the smallest reduction due to their lowest elasticity values.

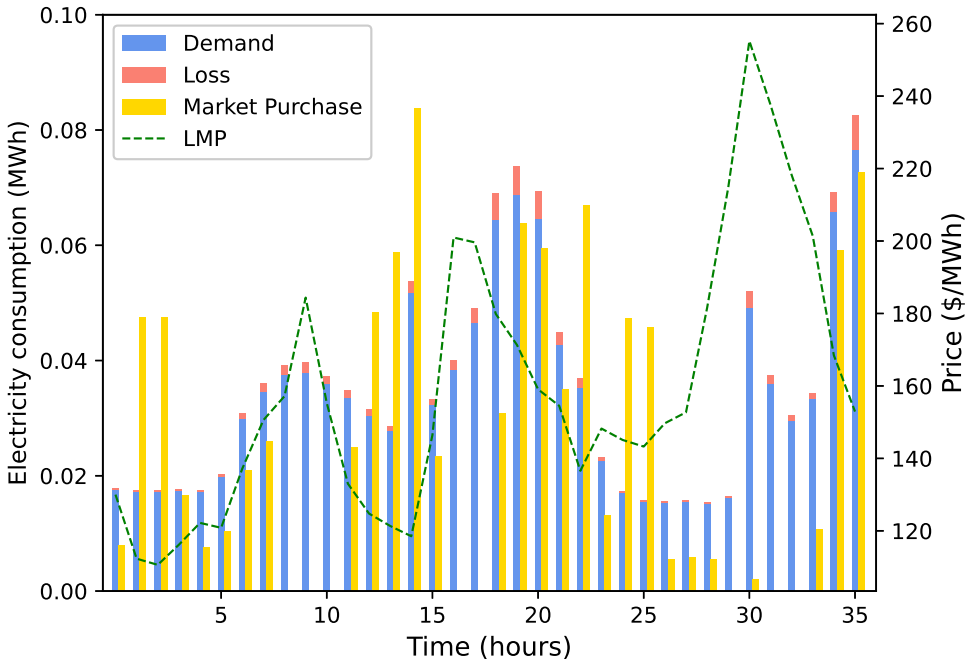

Figure 3.2 Analysis of LMP, demand, and market purchases against loss. Demand, loss, and market purchases are measured in MWh on the left y-axis. The LMP is represented by a green dotted line, measured in $/MWh on the right y-axis.

Figure 3.5 presents a detailed analysis of appliance-specific reward levels. This analysis, when compared with the findings from Figure 3.3, reveals important insights into the allocation of incentives. Although the realized demand reduction ratio is most significant for lighting, as highlighted in Figure 3.3, Figure 3.5 reveals that the total incentives paid out to customers to reduce HVAC usage is comparable to that of lighting. This is attributed to the high baseline demand for HVAC and its associated low elasticity value. In other words, it is much more costly to reduce 1MWh of HVAC usage when compared to 1MWh of lighting usage. These findings highlight the cost savings potential of implementing IBDR programs with appliance-specific incentives.

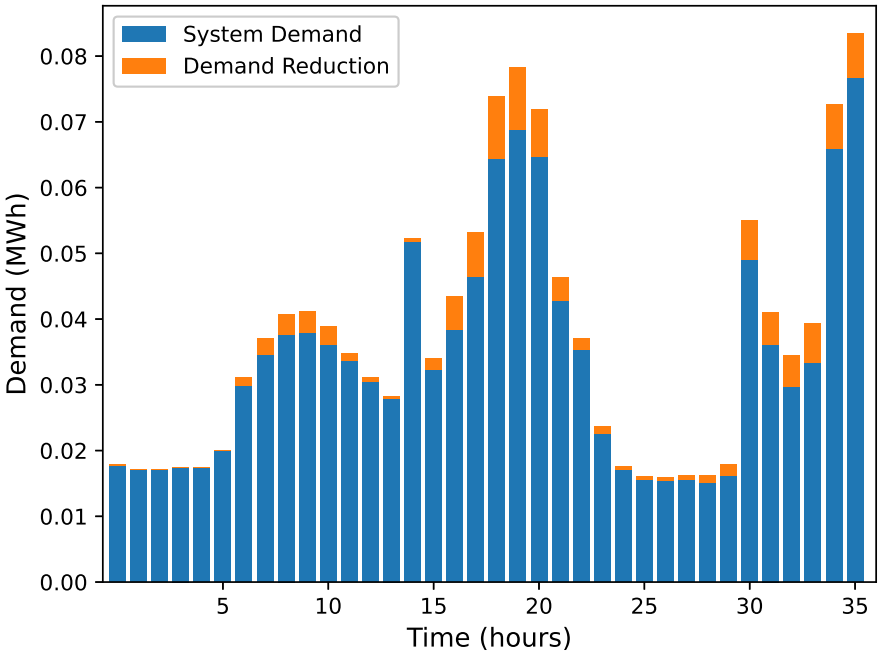

Figure 3.3 Analysis of total demand and its reduction.

Figure 3.6 provides a comprehensive breakdown of the various cost components within the objective function. Notably, the purchasing cost stands out as being significantly higher in comparison to the other costs. In scenarios where the selling revenue exceeds the purchasing cost plus operating costs, we observe a positive profit differential. This distinction underscores the importance of strategic purchasing and selling decisions within the market to optimize financial outcomes. On the other hand, the charging and discharging costs are found to be negligible. The incentive reward costs are notable but not overwhelming, which shows that the LSE is efficiently driving demand reduction with relatively small additional costs.

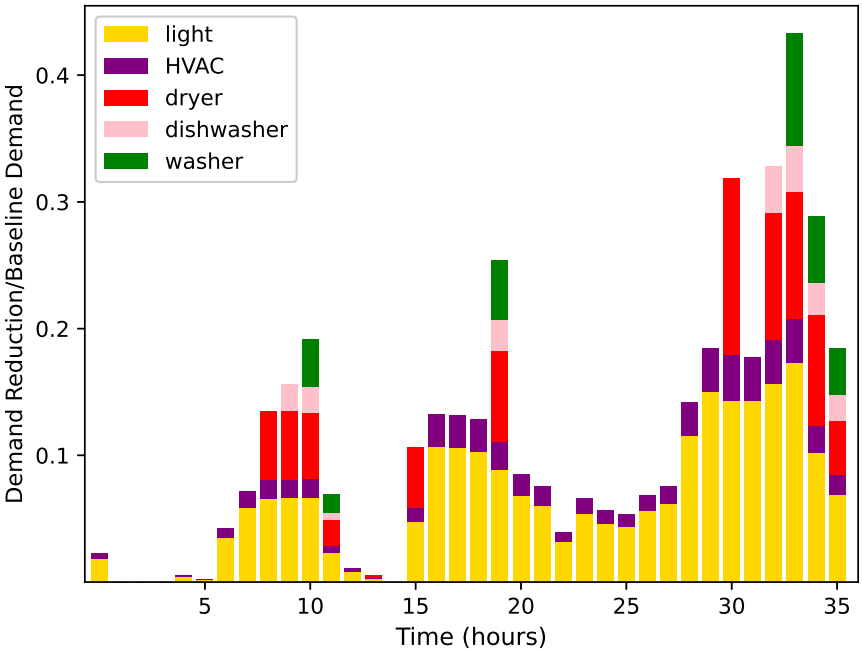

Figure 3.4 Realized demand reduction ratio by appliance type.

Table 3.4 Cost Function Values Across Models

Models	**Value**
Model 1 (fixed elasticity)	1484.7
Model 2 (appliance elasticity)	1408.9
Model 3 (consumer & appliance elasticity)	1404.5

To illustrate the impact of granular elasticity values on DR program outcomes, we present the economic efficiency of the proposed models through a comparative analysis. Table 3.4 provides a comparison of the optimal objective values achieved by each model.

From Table 3.4, we observe a significant reduction in the cost objective value, transitioning from Model 1 to Model 3. Specifically, transitioning from Model 1 to Model 2 yields an improvement in economic efficiency of approximately

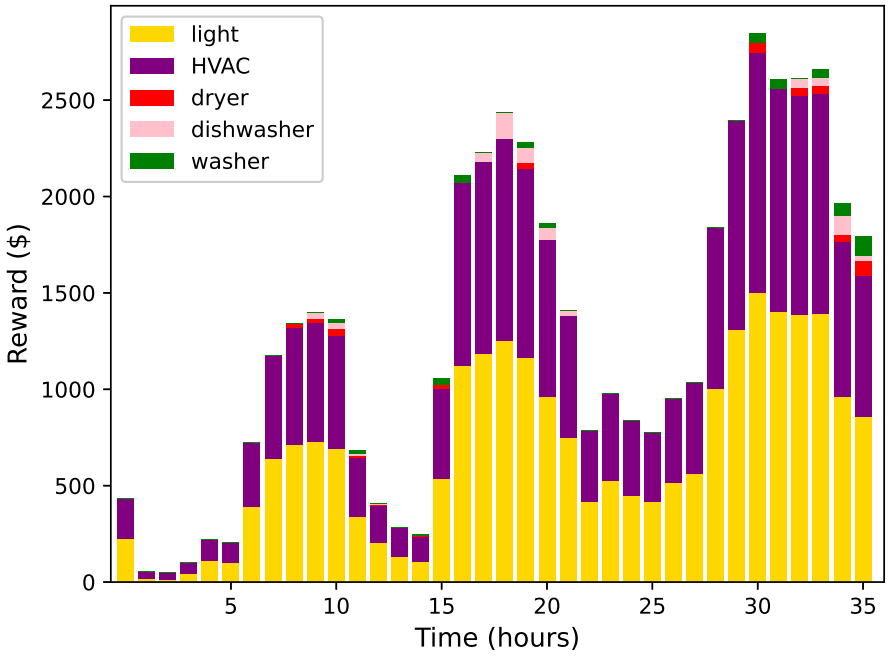

Figure 3.5 Total incentive reward amounts paid out to customers by appliance type.

5.11%, indicating a substantial enhancement through the implementation of appliance-specific elasticity. Further refinement in Model 3, which incorporates both customer-specific and appliance-specific elasticity, results in a modest but noteworthy improvement of approximately 0.31% over Model 2. The significant benefit from Model 1 to Model 2 highlights the initial effectiveness of appliance-specific customizations, whereas the smaller improvement from Model 2 to Model 3 indicates diminishing returns from more detailed, customer-specific elasticity.

To further elucidate the comparative cost-benefit implications for LSE across the different models studied, Figure 3.7 provides a detailed visual representation. This figure aims to clarify the economic outcomes of implementing each model,

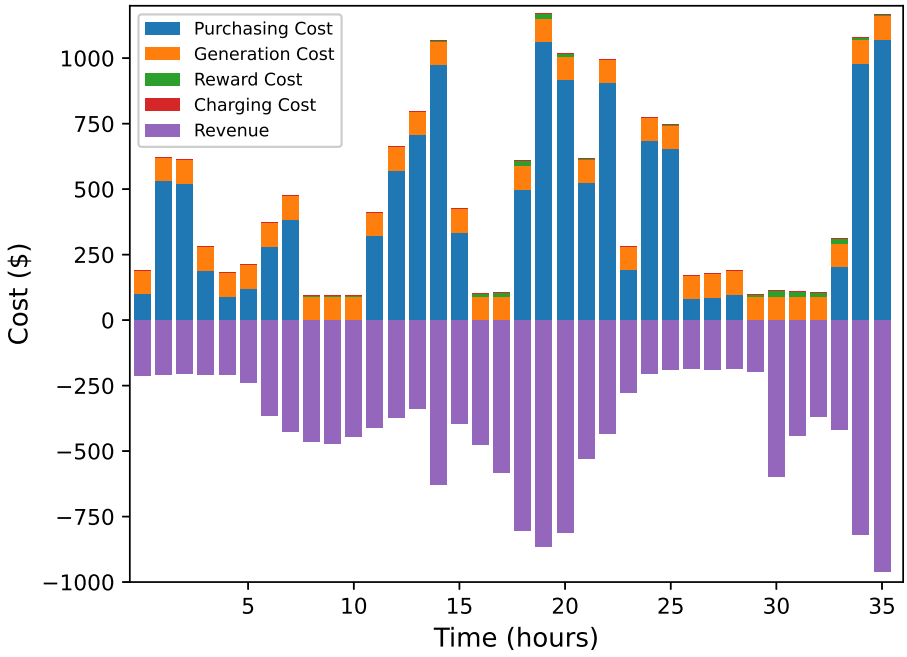

Figure 3.6 Breakdown of cost components within the objective.

highlighting the differences in cost components such as purchasing costs, generation costs, revenue, and the total costs associated with each model.

Analysis of Figure 3.7 reveals that the purchasing cost is higher in Model 1 compared to Models 2 and 3, suggesting that the introduction of appliance-specific and customer-appliance-specific elasticity can lead to significant savings in energy procurement costs. Despite these variations, revenue appears relatively consistent across all models. More importantly, Models 2 and 3 are observed to incur lower total costs compared to Model 1, illustrating the economic benefits for the LSE by leveraging granular elasticity values. This approach not only enhances energy savings but also improves the financial performance of the LSE.

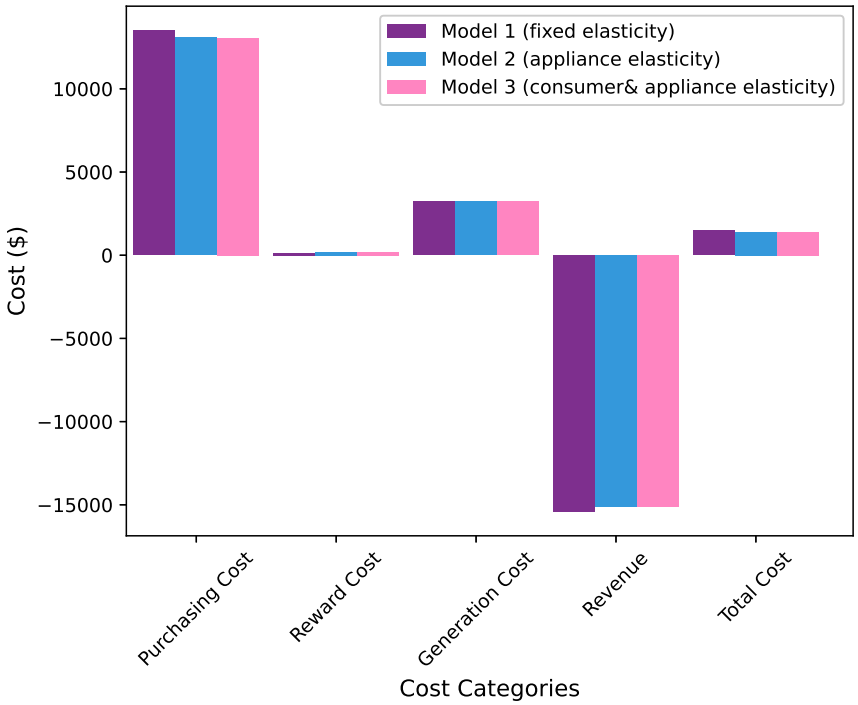

Figure 3.7 Analysis of cost components across models.

3.4 Conclusion

This paper presents a comparative analysis of three distinct models, each incorporating nuanced values of electricity elasticity. Model 1 employs fixed elasticity as a baseline, Model 2 introduces appliance-based elasticity to reflect the role of devices in residential life, and Model 3 extends this by including both appliance and consumer-specific elasticity, emphasizing the importance of understanding individual behaviors in DR programs. Moreover, a realistic grid setup is modeled by incorporating transmission line losses through branch power flow equations.

Our findings advocate the need and value for utilizing granular elasticity information in operating IBDR programs to achieve maximal economic efficiency

by exploiting the heterogeneous responsiveness of customers regarding different appliances. Models 2 and 3 demonstrate considerable economic and operational benefits over model 1, highlighting the advantages of nuanced models for LSEs.

Future Work: Given the diversity in consumer consumption habits, accurately predicting users' responses is challenging, which can lead to increased total costs when user response behaviors are mischaracterized. IBDR programs often require complete consumer information; however, acquiring complete data can be difficult. Reinforcement Learning (RL) is identified as a promising approach to overcome the limitations of incomplete information[103, 104]. Future research directions include employing RL to better understand and predict consumer behaviors more effectively, aiming to optimize dynamic pricing strategies and energy consumption schedules. This direction seeks to minimize costs for service providers like LSEs while improving the efficacy of DR programs.

CHAPTER 4

A MULTI-AGENT REINFORCEMENT LEARNING FRAMEWORK FOR DYNAMIC PRICING IN INCENTIVE-BASED DEMAND RESPONSE PROGRAMS

4.1 Introduction

In the evolving landscape of energy management, demand response (DR) programs have become pivotal for balancing electricity supply and demand, especially during peak load periods. Modern information and communication technologies within smart grid systems have significantly supported the efficacy of DR strategies, establishing them as a fundamental component for enhancing grid reliability and mitigating energy costs [105, 106]. The US Department of Energy defines DR as programs that influence electricity consumption through dynamic pricing or incentives during high market prices [107]. The integration of smart buildings and intelligent infrastructure highlights DR's capability to optimize energy consumption and effectively manage load, contributing to a more resilient and sustainable energy system.

The literature identified two categories of DR programs: price-based and incentive-based [108]. Price-based DR (PBDR) programs encourage consumers to adjust their energy usage according to fluctuating electricity prices. Incentive-based DR (IBDR) offers consumers financial rewards or penalties to promote reductions in energy consumption during peak demand periods [109]. While

incentive-based programs foster positive and long-term consumer engagement through voluntary participation, price-based programs, which penalize non-compliance, may lead to more transient responses [110]. Although incentive-based strategies have shown clear benefits in the industrial sector, they are less utilized in the residential sector [111], which accounts for a significant portion of total energy demand—approximately 40% [90]. Thus, this study aims to explore the potential of IBDR in the residential sector to contribute to a more reliable and continuous response.

Substantial research in DR has traditionally relied on deterministic models, often employing predetermined pricing mechanisms such as Time-of-Use (TOU) [112] and day-ahead pricing [113], or linear pricing strategies [114]. These models typically assume a static framework and fail to accommodate the flexibility and unpredictable fluctuations required in dynamic electricity market environments. Additionally, model-based approaches to implementing IBDR programs require detailed information about individual participants, raising concerns about privacy and data availability [115]. Moreover, these approaches typically use traditional optimization techniques like linear [116] and dynamic programming [6], which are not suited for real-time computations involving large-scale participant groups.

While utility companies aim to estimate the impact of retail pricing strategies on consumer behavior over time, current models typically focus only on immediate load responses, ignoring subsequent interactions and longer-term effects. Furthermore, service providers in practical smart grid systems face substantial challenges in obtaining precise customer-side information including current load demand levels and the customers' willingness to change their electricity usage based on varying retail prices [117]. Predicting the long-term

effects of current pricing strategies on future customer behavior remains another considerable challenge. This myopic view neglects the inherent variability and uncertainty of energy demand, particularly in environments influenced by human behavior and other unpredictable factors. Consequently, the lack of precision in understanding and predicting consumer behavior continues to pose significant challenges in designing effective dynamic pricing strategies for smart grids. This underscores the need to develop methodologies that effectively manage IBDR under unknown market conditions, accommodating immediate and future impacts on the grid and consumer behavior.

Reinforcement Learning (RL) has emerged as a highly effective method for decision-making in IBDR programs, leveraging its model-free approach that requires no prior knowledge about the program structure or participant dynamics [104, 118, 117]. This versatility allows RL to manage multiple agents, enhancing scalability and enabling real-time control applications [104]. Moreover, RL's capability to model DR control programs as sequential decision-making problems makes it particularly suited for developing dynamic pricing strategies in DR. RL has been increasingly utilized in the residential sector for DR, primarily focusing on home energy management within individual households. For example, Wen et al. [119] employed RL techniques like Q-learning with eligibility traces to optimize the timing of appliance operations and reduce energy costs by learning user preferences and behaviors. Another innovative study develops Deep Q-Network (DQN) to schedule household appliance loads, creatively using Atari game Tetris environment, where flexible blocks represent the loads [120].

Recent advancements in dynamic pricing for DR programs have mainly incorporated online RL techniques to enhance decision-making processes. Kim

et al. [117] propose an online RL-based dynamic pricing and energy consumption scheduling algorithm for microgrids, enabling service providers and consumers to learn strategies that minimize costs and optimize energy distribution. Similarly, Ghasemkhani et al. [121] apply online RL to dynamically adjust pricing strategies in DR programs, effectively learning users' unpredictable response functions and achieving near-optimal load reduction without assuming fixed response models. Lu et al. [107] presents a daily iterative dynamic pricing DR algorithm utilizing online RL to optimize both service provider profits and consumer costs in a hierarchical electricity market.

Although online RL offers significant advantages for dynamic decision-making in DR programs, it comes with notable limitations. The method requires prolonged interaction with consumers, which can lead to extended periods of learning due to RL's inherently slow convergence [103]. This prolonged learning process may extend over months or years to develop effective policy. Furthermore, the exploration aspect of online RL necessitates engaging with new and potentially risky scenarios, which can introduce safety and system reliability concerns [103, 107]. These challenges highlight the potential limitations of using online RL in practical DR implementations, where time efficiency and system safety are crucial.

Addressing the challenges associated with online RL, this paper explores the potential of entirely offline RL methods, which leverage pre-existing datasets to formulate effective and safe DR policies. While the applications of offline RL in dynamic pricing for DR programs remain relatively underexplored, some studies ventured into exploring its potential. For example, Jang et al. [122] utilize offline RL to reduce energy consumption in office buildings through dynamic

pricing. This study integrates offline pre-training with online RL to accelerate the convergence process, effectively reducing both energy and data costs. In another study, Xu et al. [103] introduce a fully offline RL method to design dynamic pricing DR programs, utilizing data from smart meters without the need for real-world consumer interactions. They employ a data augmentation method and Deep Q-network (DQN) algorithms within an MDP framework to develop high-performance DR pricing policies.

Multi-Agent RL (MARL) is increasingly applied to manage load scheduling across multiple households, optimizing the balance between energy supply and demand. Lu et al. [123] introduce a real-time, incentive-based DR algorithm that aids service providers in purchasing energy flexibility from residential customers, utilizing DNNs to predict market prices and demand uncertainties. This is followed by RL to dynamically adjust incentive rates, ensuring profitability for both service providers and customers. Similarly, other studies like [124, 125] enhance IBDR programs using deep learning and RL. Wen et al. [124] focus on addressing future uncertainties by forecasting day-ahead wholesale electricity prices, power load, and photovoltaic power output, while Xu et al. [125] refine incentive rate calculations to better reflect real-time customer demand fluctuations. Both studies contribute significantly to increased profitability and grid stability.

Recently, Tilburg et al. [104] introduce a decentralized MARL method for an IBDR program aimed at reducing aggregator costs by offering financial incentives to residential consumers. They consider one agent representing the aggregator and multiple residential agents. In this work [104], the target demand reduction is set by the DSO, with residential participants responding to the incentives. The participant agents use a Disjunctively Constrained Knapsack Problem (DCKP)

optimization to respond to incentives by shifting or curtailing household appliances to achieve the desired demand reduction while ensuring user satisfaction. In contrast, our approach leverages a MARL framework that dynamically estimates real-time demand for each household using a sigmoid function simulator to address the limitations of the DCKP method. This method incentivizes consumers differently based on their specific appliances and consumption patterns at various times, offering a more granular and adaptive response. Furthermore, our model does not predetermine reduction levels, so both the aggregator and consumers can learn and adjust automatically through the RL framework to achieve optimal energy reduction.

4.2 Problem Formulation and System Model

In this section, we present the hierarchical architecture of the IBDR system employed in this study, highlighting its key components: the Independent System Operator (ISO), Load Serving Entities (LSEs), customers, and their appliances. The ISO sets the Locational Marginal Price (LMP), representing the economic value of electricity across different regions by accounting for costs associated with losses and congestion under current operational conditions. For LSEs, the challenge arises when the LMP exceeds the flat rate charged to customers, compelling them to purchase electricity at higher prices than they offer to end-users, leading to direct economic losses. This necessitates the implementation of demand reduction strategies to mitigate these losses and promote efficient energy consumption, particularly during peak demand periods when the system is at risk of instability.

Figure 4.1 shows the architecture of the proposed DR approach. Our approach features a MARL approach, incorporating multiple Residential Agents (RAs). At each time step, the aggregator sets an incentive price based on step-ahead predictions of participant electricity demands, LMP, and participants' responses to the incentives. This incentive price is then broadcast to the RAs, who adjust their appliance consumption accordingly. The RAs learn to respond to incentives by shifting or curtailing the use of household appliances (e.g., washers, dishwashers, dryers, lighting, and HVAC). The compensation received by each RA is a function of the incentive price and their subsequent reduction in appliance-specific load. The real-time RAs' consumption (real demand) is estimated through an internal simulator that separately manages curtailable and non-curtailable appliances. This approach promotes a more flexible, real-time automated system, maintaining capacity limits and enhancing overall grid reliability and efficiency.

The proposed model employs a Markov Decision Process (MDP) framework to address the problem of dynamic pricing in the IBDR system. The MDP framework is suitable for sequential decision-making in stochastic environments, defined by states, actions, transition probabilities, and rewards [126]. In our model, the state space S_t includes consumer states and environmental variables such as LMP, current demand D_t, and stored energy level $E_{s,t}$. The action space A consists of various incentive pricing signals for each RA as $a_i = \{CR_t^i\}$. Transition probabilities P define the likelihood of moving from one state to another based on the chosen actions. The reward function r_i is derived from the equation $r_i = LMP_t \times Y_t - CF \times D_t + CR_t^i \times \Delta D_t$, where Y_t represents the amount of purchased electricity. This reward function evaluates the immediate payoff from

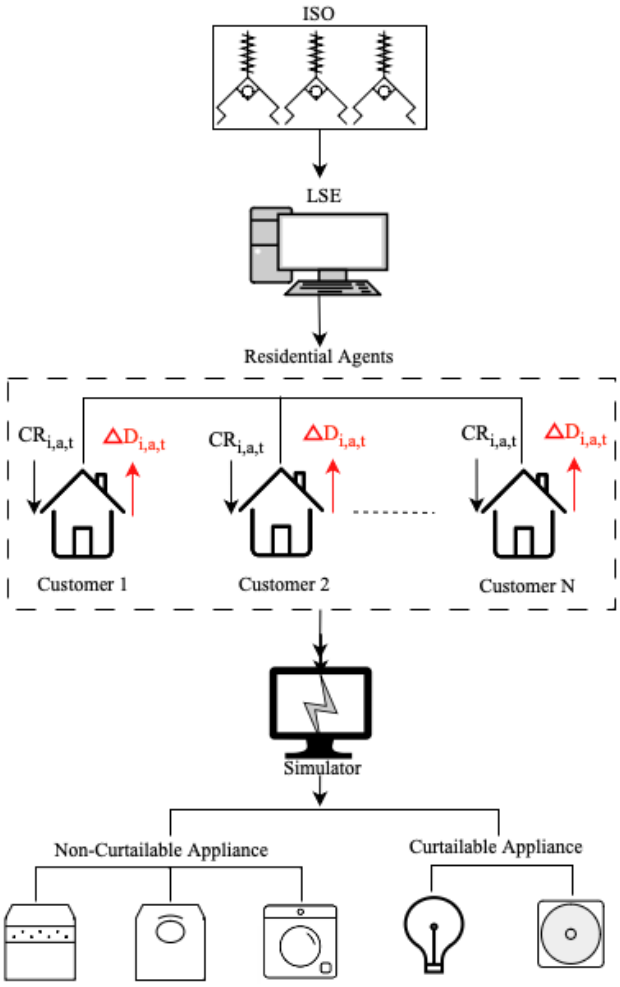

Figure 4.1 Hierarchical architecture of incentive-based demand response.

transitioning between states, focusing on both immediate and cumulative future rewards. The cumulative reward $\hat{r}$ is calculated as the sum of individual rewards from all RA agents, $\hat{r} = \sum_{i=1}^{N} r_i$. At each time step t, the RL agents observe the current state $S_t = \{LMP_t, D_t, E_{s,t}\}$, select an action a_i, receive a reward r_i, and transition to a new state, thereby learning to optimize their actions to maximize the cumulative discounted return. The MDP framework for this study is shown in Figure 4.2.

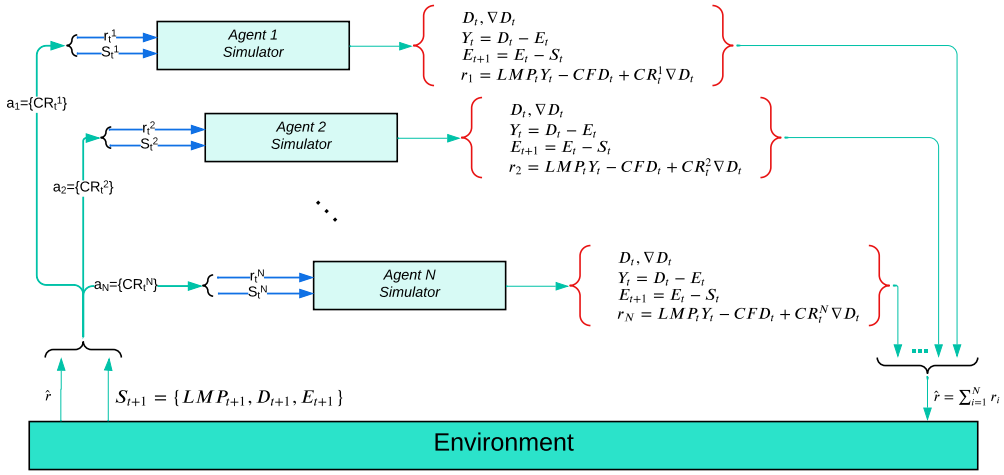

Figure 4.2 MDP framework in this study.

Our model uses a MARL framework, where each RA autonomously learns to adjust its energy consumption based on incentive signals. Unlike traditional deterministic methods, the proposed framework dynamically estimates real-time demand for each household using a sigmoid function simulator to address uncertainties and varying consumer behaviors. This allows the agents to continuously learn and optimize their strategies through RL, balancing immediate and future rewards to maximize overall efficiency.

We utilize a sigmoid function simulator to estimate real-time electricity demand for each appliance within every household during each time period. Appliances in each household are categorized into two subsets: curtailable appliances CA and non-curtailable appliances NAC, with $D_t = \sum_i (CA \cup NCA)_i$. Accordingly, two distinct simulators are deployed to manage the demand estimation processes for these subsets. The sigmoid function is particularly chosen for its ability to model the randomness in customer behavior, providing a realistic

depiction of activation and deactivation thresholds. This allows for a more accurate and dynamic response to varying energy consumption patterns and incentive schemes.

- **Non-Curtailable appliances (NCA):** These appliances require uninterrupted operation once they start. Their operation cannot be shifted in time or curtailed in power [127, 104]. Examples include washers, dishwashers, and dryers, which must complete their cycles without interruption. To estimate the real energy consumption for NC appliances, we use Equation (4.1):

$$P_{i,a,t}^{\text{NCA}} = \frac{1}{1 + e^{-\alpha_{i,a}(\text{prior}_{i,a} - \beta_{i,a} - \phi \frac{\text{Cr}_{i,a,t}}{\text{Cr}_{\text{mean}}})}} \tag{4.1}$$

  where $P_{i,a,t}^{\text{NCA}}$ represents the probability of using NCA for consumer i at time t. The parameter $\alpha_{i,a}$ controls how fast the probability transitions from zero to full probability of using the appliance. The variable $\text{prior}_{i,a}$ indicates the number of hours since the appliance was last used, while $\beta_{i,a}$ is the number of hours since the last use that gives a 0.5 probability of using the appliance. The constant ϕ scales the impact of the reward $\text{Cr}_{i,a,t}$ offered to consumer i for appliance a at time t. Finally, Cr_{mean} is the mean reward over a specified horizon. This formula calculates the probability that a consumer will use their NC appliances based on the time elapsed since the last use and the reward offered for not using it, allowing for estimating real-time energy consumption in a dynamic and probabilistic manner.

- **Curtailable appliances (CA):** These appliances allow for flexible power consumption and can be managed either by shifting their operation time or by reducing their power consumption [127, 128]. For example, lighting can be dimmed, and HVAC setpoints can be adjusted to lower power usage without immediately disrupting their functionality. Their real energy consumption is estimated using Equation (4.2):

$$P_{i,a,t}^{\text{CA}} = \frac{\beta_{i,a}}{1 + e^{(\phi \frac{\text{Cr}_{i,a,t}}{\text{CF}} - \alpha_{i,a})}} \tag{4.2}$$

  where $P_{i,a,t}^{\text{CA}}$ represents the probability of using CA like lighting and HVAC systems for consumer i at time t. The CF denotes the fixed flat rate charged to customers. This formula calculates the likelihood of adjusting power consumption for curtailable appliances, considering the reward incentive and fixed rate, enabling effective and responsive energy usage adjustments.

4.3 Reinforcement Learning-Based DR Algorithm

The proposed MARL for IBDR (MARL-IBDR) framework leverages the interaction of multiple agents, each with distinct reward functions, to manage residential energy consumption. In this framework, RAs focus on minimizing their own costs by responding to incentive pricing signals, while the cumulative reward $\hat{r}$ is optimized to reflect overall energy efficiency. This interaction creates a dynamic and non-stationary environment, as the optimal strategies of the agents continuously evolve in response to each other's actions. Unlike traditional single-agent RL approaches, which assume a static environment, MARL must address the complexities arising from these evolving interactions. Despite these complexities, simultaneous learning within MARL-IBDR introduces non-stationary problems, which challenge many theoretical guarantees of single-agent RL, such as convergence [129, 104]. However, the simultaneous learning approach is beneficial due to its simplicity and effectiveness in handling multi-agent environments, making it a practical choice for complex real-world applications [130, 131].

To balance exploration and exploitation, the MARL-iDR framework employs an ϵ-greedy strategy with decay. Initially, agents select actions randomly with a high probability (ϵ), which decreases over time, allowing for extensive exploration during the early stages of training and more focused policy refinement later [132]. This method ensures that the agents thoroughly explore the action space before converging on an optimal strategy.

Deep Q-Networks (DQNs) are utilized to handle the large and continuous state spaces typical in residential energy management scenarios. DQNs are a

state-of-the-art RL approach that uses neural networks to approximate the Q-values of state-action pairs [126, 133]. This approach enables the efficient handling of high-dimensional input spaces, making it suitable for complex environments. One of the critical features of DQNs is the use of a separate target network, which helps stabilize training by providing consistent target values for the Q-learning updates. Additionally, DQNs employ experience replay, a technique where the agent stores past experiences in a replay buffer and randomly samples from this buffer to train the network [134, 133]. This process breaks the temporal correlations between consecutive experiences, reducing the risk of the network overfitting to recent events and improving overall learning stability. These features collectively enhance the robustness and performance of DQNs in managing the complexities of residential energy demand response.

The training procedure for the MARL-IBDR framework involves initializing policy and target networks for each agent and training these networks over multiple episodes, where each episode represents a single day divided into several time steps. At each time step, the RAs first observe the state of their appliances and compute control actions based on the ϵ-greedy policy. The aggregator then predicts the overall demand and sets incentive prices. The RAs receive these incentive rates set by the aggregator and adjust their appliance consumption accordingly. Each agent's actions and corresponding rewards are stored in the replay buffer, and the networks are trained by sampling experiences from this buffer. This iterative process continues, with rewards being calculated for RAs, and policies being refined over time. The policy for each agent is determined using the following formula:

$$\pi(s) = \arg\max_{a} Q(s, a \mid \theta) \tag{4.3}$$

CHAPTER 5

APPENDICES

The appendix provides detailed descriptions of the Covasim parameters used in the study and includes detailed model validation results. It serves as a reference for understanding the key variables and their descriptions, as well as showcasing the accuracy of the model through comparison with real outbreak data.

5.1 Covasim Parameters

The Tabel 5.1 outlines the key parameters utilized in the Covasim model, which are critical for simulating disease transmission and vaccination dynamics.

5.2 Model Validation Results

Figures 5.1 to 5.7 illustrate the results of model validation against the real outbreak data for all the states in the US.

Table 5.1 Description of Covasim Parameters

Parameter	Description
λ_{wt}	Disease transmission rate from S_{wt} to I_{wt} in state w at time t
α_a^1	Proportion of individuals who get immunization by the first shot of vaccine type a
α_a^2	Proportion of individuals who get immunization by the second shot of vaccine type a
α_a^3	Proportion of individuals who get immunization by the third shot of vaccine type a
π_w	The initial number of susceptible individuals in state w, inputted from the agent-based simulation model
ω_w	The initial number of infections in state w, inputted from the agent-based simulation model
θ_{aw}	The initial number of individuals who have received the first-dose type $a \in \{1, 2\}$ vaccine shot in state w
ϑ_{aw}	The initial number of individuals who have received the second-dose type $a \in \{1, 2\}$ vaccine shot in state w
ϕ_{aw}	The initial number of individuals who have received the third-dose type $a \in \{1, 2\}$ vaccine shot in state w
σ_{aw}	The initial number of individuals who have received the first-dose type $a \in \{3\}$ vaccine shot in state w
η_{aw}	The initial number of individuals who have received the second-dose type $a \in \{3\}$ vaccine shot in state w
β_{aw}^1	The vaccine acceptance rate of the first shot for each vaccine type a in state w
β_{aw}^2	The vaccine acceptance rate of the second shot for each vaccine type a in state w
β_{aw}^3	The vaccine acceptance rate of the third shot for each vaccine type a in state w

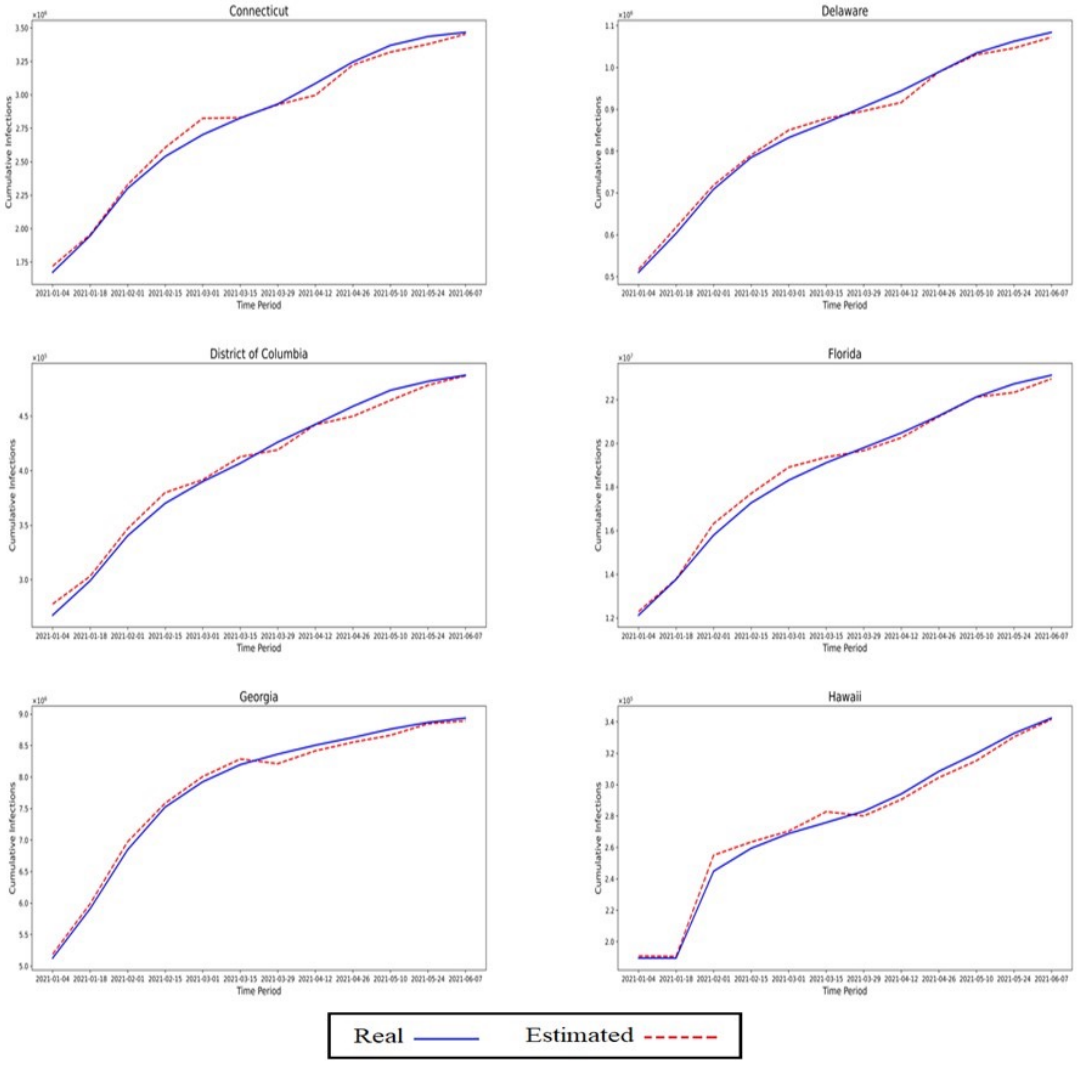

Figure 5.1 Model validation against real outbreak data in the US.

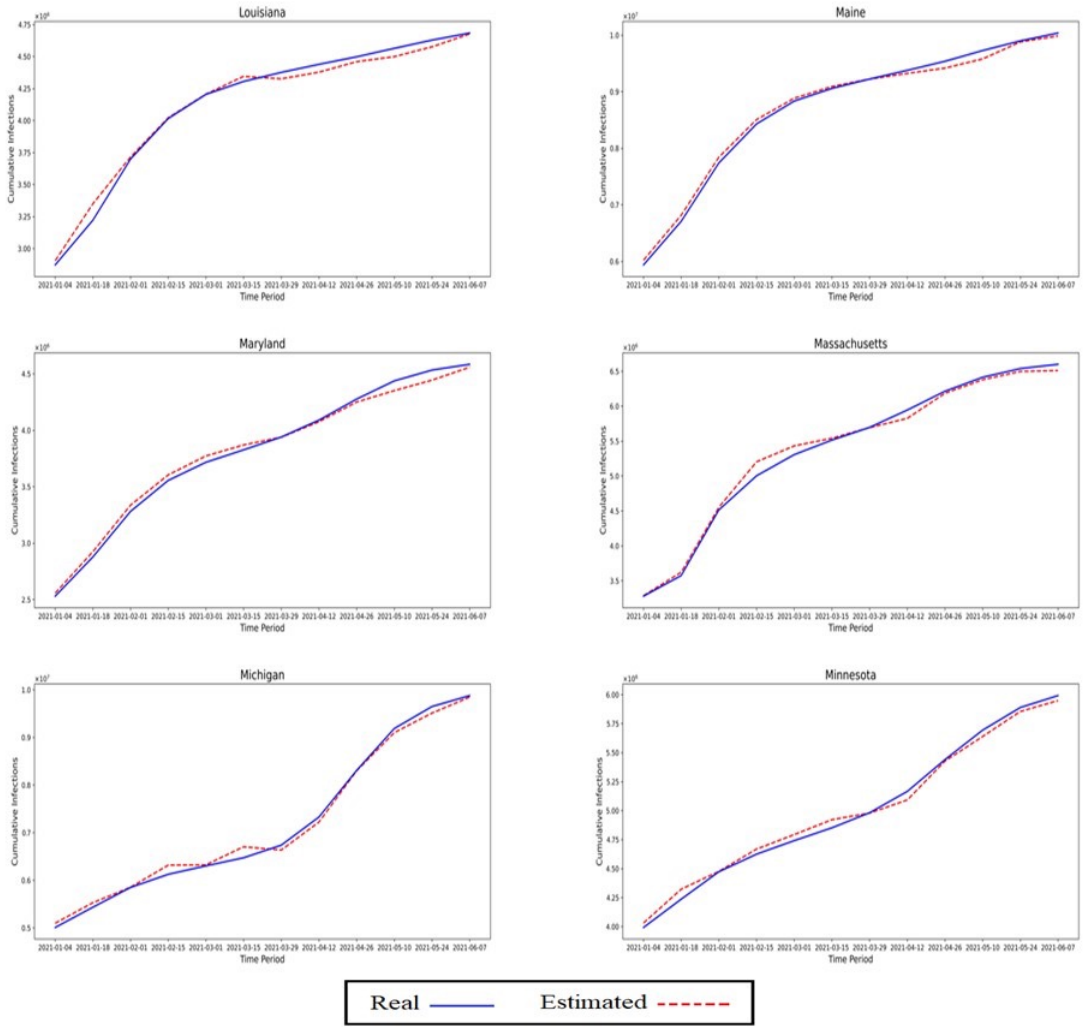

Figure 5.2 Model validation against real outbreak data in the US - continued.

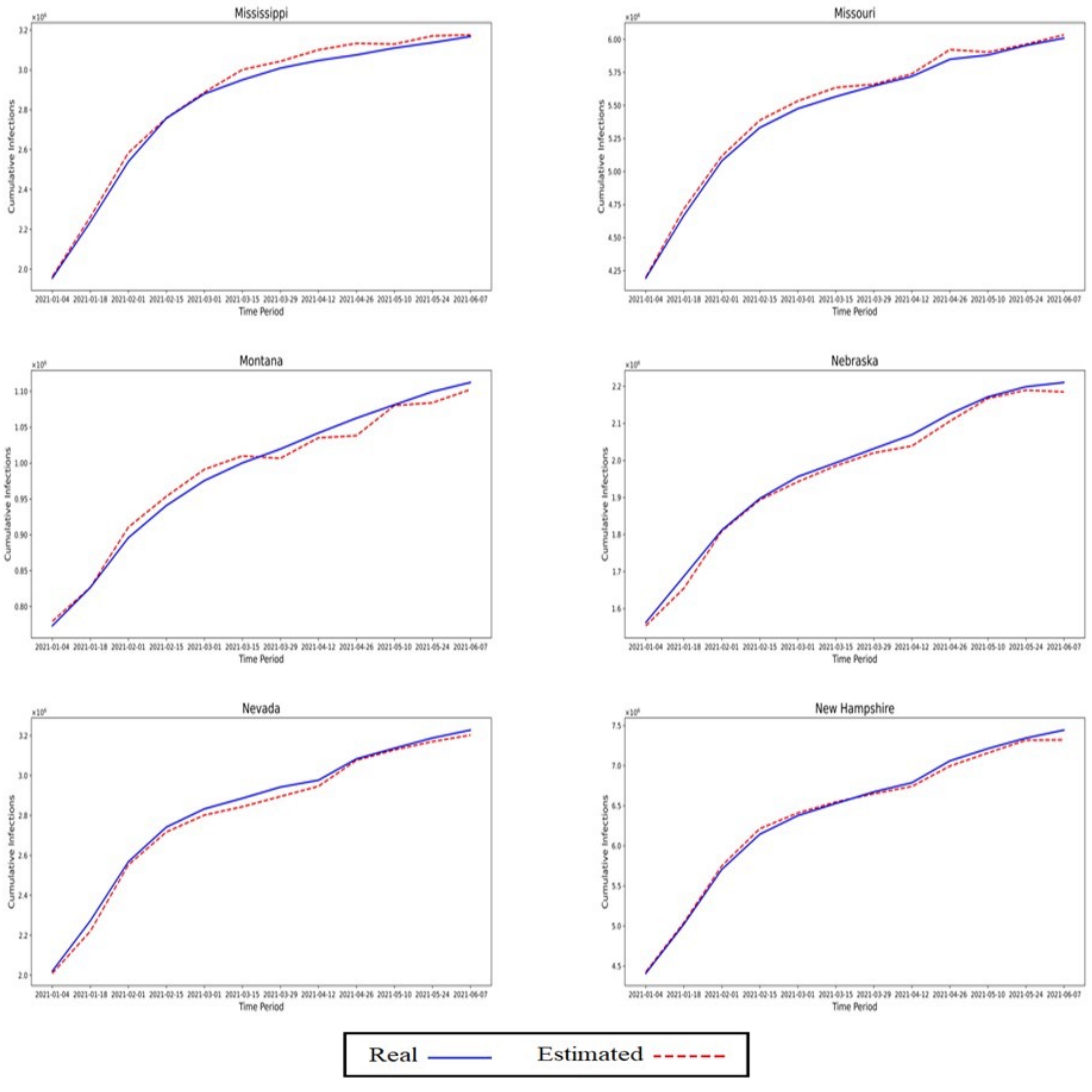

Figure 5.3 Model validation against real outbreak data in the US - continued.

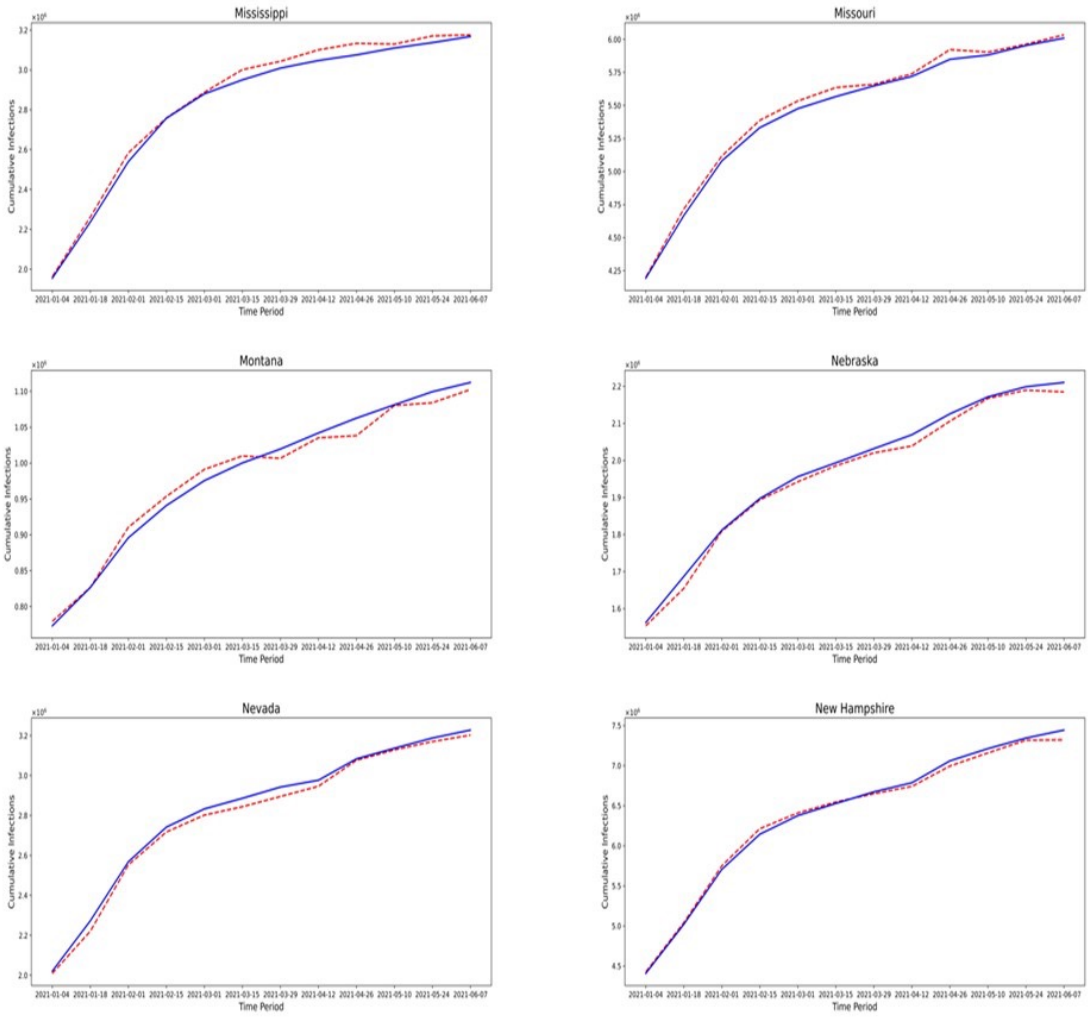

Figure 5.4 Model validation against real outbreak data in the US - continued.

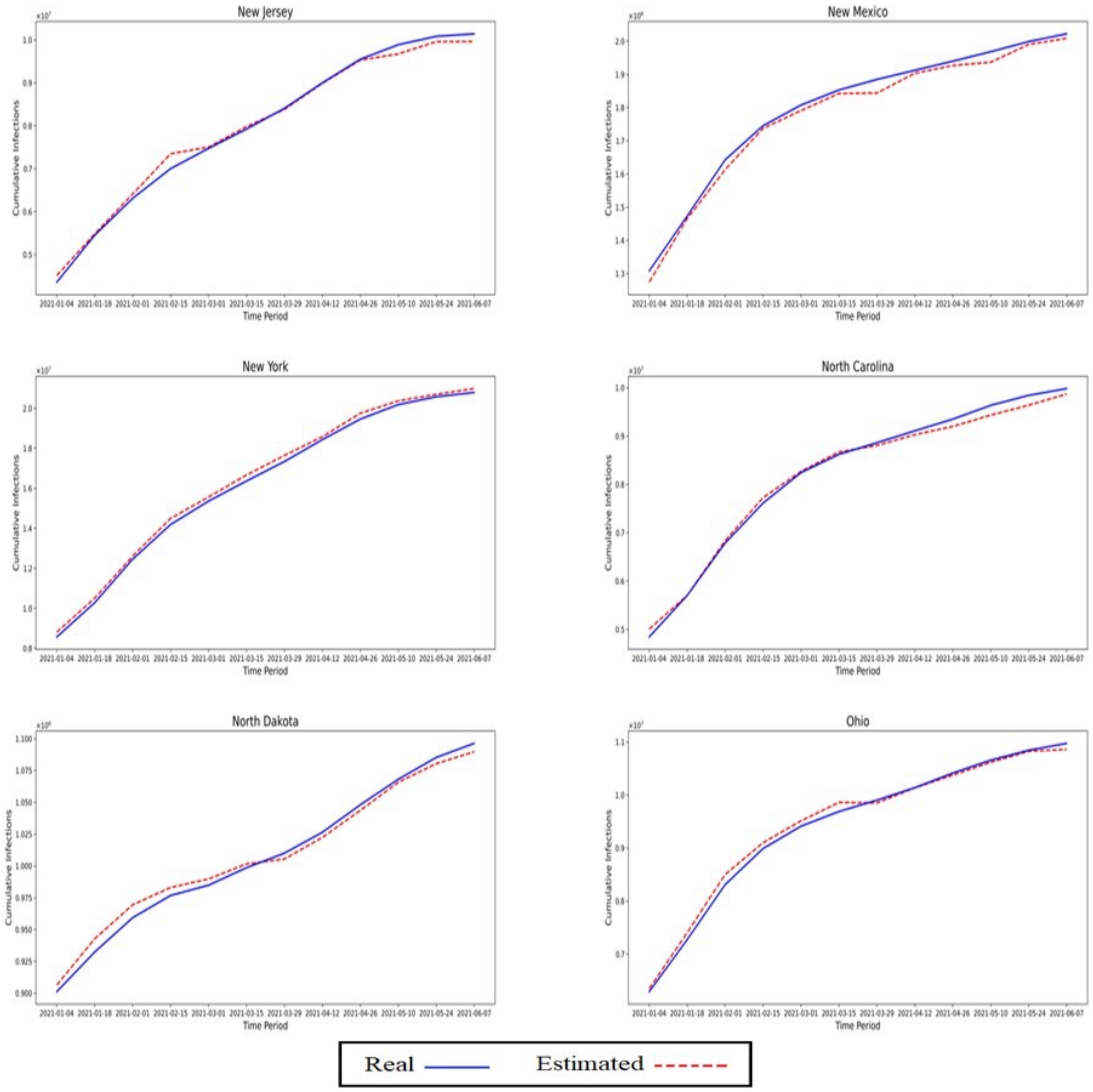

Figure 5.5 Model validation against real outbreak data in the US - continued.

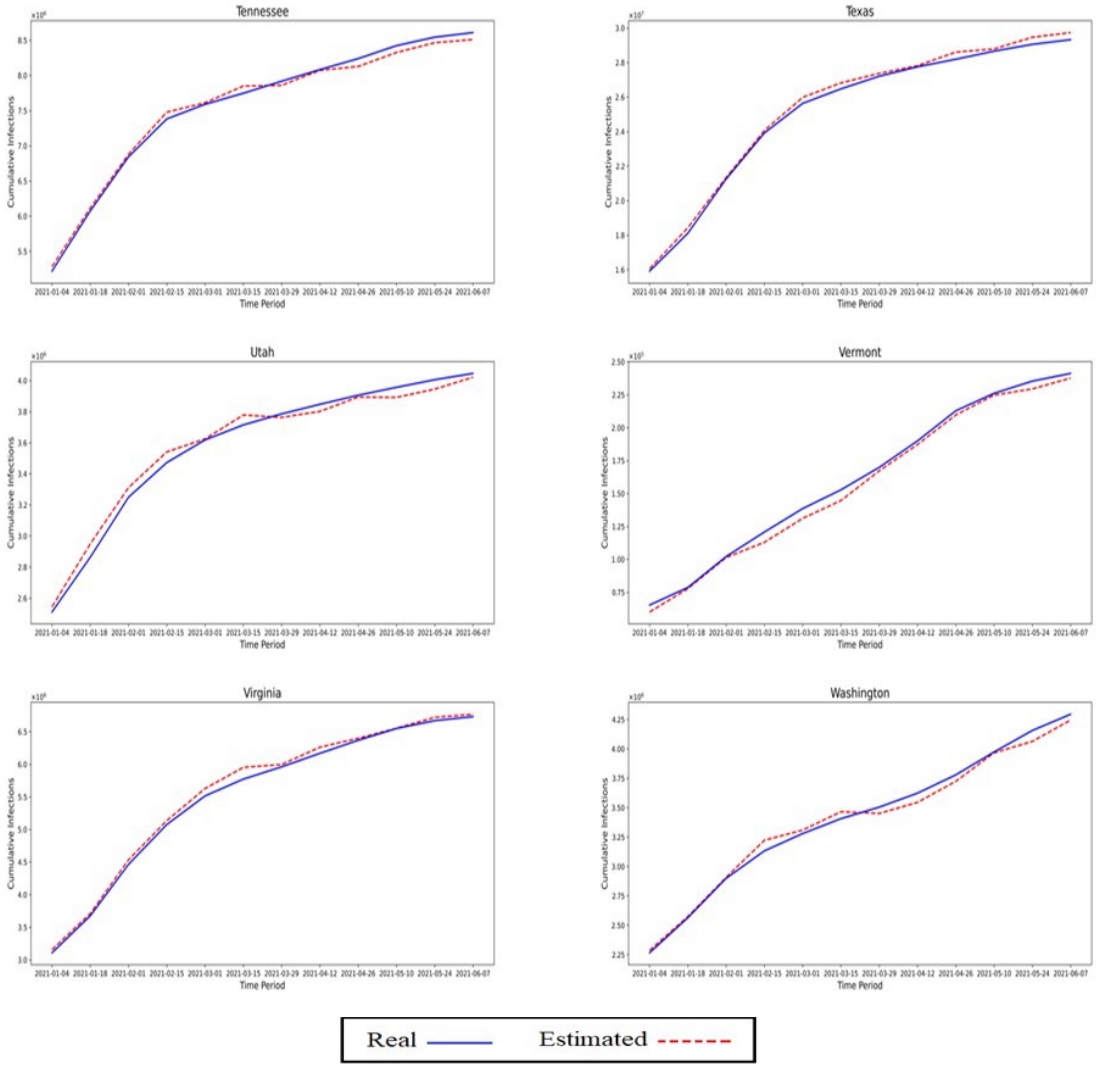

Figure 5.6 Model validation against real outbreak data in the US.

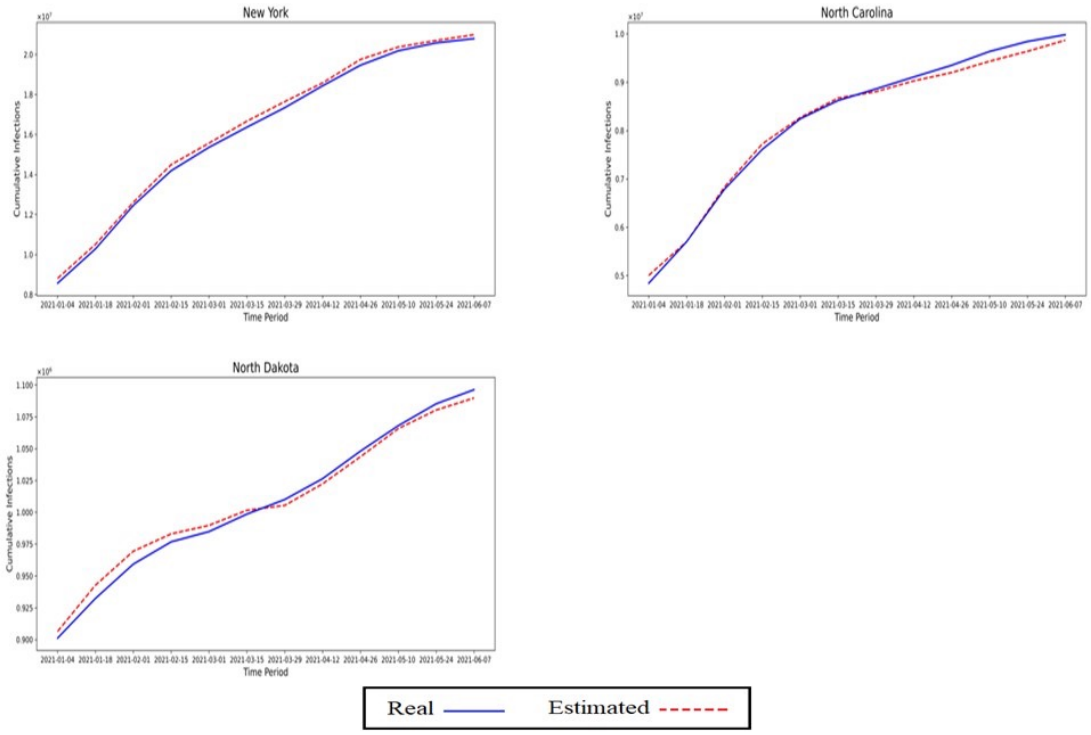

Figure 5.7 Model validation against real outbreak data in the US.

REFERENCES

[1] C.-Y. Cheng, T.-L. Chen, and Y.-Y. Chen, "An analysis of the structural complexity of supply chain networks," *Applied Mathematical Modelling*, vol. 38, no. 9-10, pp. 2328–2344, 2014.

[2] B. K. Lee, R. Zhou, R. de Souza, and J. Park, "Data-driven risk measurement of firm-to-firm relationships in a supply chain," *International Journal of Production Economics*, vol. 180, pp. 148–157, 2016.

[3] Q. Long, "Data-driven decision making for supply chain networks with agent-based computational experiment," *Knowledge-Based Systems*, vol. 141, pp. 55–66, 2018.

[4] C. M. Bishop and N. M. Nasrabadi, *Pattern recognition and machine learning*. Springer, 2006, vol. 4, no. 4.

[5] F. Wahid and D. Kim, "A prediction approach for demand analysis of energy consumption using k-nearest neighbor in residential buildings," *International Journal of Smart Home*, vol. 10, no. 2, pp. 97–108, 2016.

[6] F. Zhang, C. Deb, S. E. Lee, J. Yang, and K. W. Shah, "Time series forecasting for building energy consumption using weighted support vector regression with differential evolution optimization technique," *Energy and Buildings*, vol. 126, pp. 94–103, 2016.

[7] C. Fan, F. Xiao, and S. Wang, "Development of prediction models for next-day building energy consumption and peak power demand using data mining techniques," *Applied Energy*, vol. 127, pp. 1–10, 2014.

[8] Y. B. De Bruin, A.-S. Lequarre, J. McCourt, P. Clevestig, F. Pigazzani, M. Z. Jeddi, C. Colosio, and M. Goulart, "Initial impacts of global risk mitigation measures taken during the combatting of the COVID-19 pandemic," *Safety Science*, vol. 128, p. 104773, 2020.

[9] T. Hale, N. Angrist, R. Goldszmidt, B. Kira, A. Petherick, T. Phillips, S. Webster, E. Cameron-Blake, L. Hallas, and S. Majumdar, "A global panel database of pandemic policies (Oxford COVID-19 Government Response Tracker)," *Nature Human Behaviour*, vol. 5, no. 4, pp. 529–538, 2021.

[10] J. Verschuur, E. E. Koks, and J. W. Hall, "Observed impacts of the COVID-19 pandemic on global trade," *Nature Human Behaviour*, vol. 5, no. 3, pp. 305–307, 2021.

[11] D. L. Heymann and N. Shindo, "COVID-19: what is next for public health?" *The Lancet*, vol. 395, no. 10224, pp. 542–545, 2020.

[12] R. M. Viner, S. J. Russell, H. Croker, J. Packer, J. Ward, C. Stansfield, O. Mytton, C. Bonell, and R. Booy, "School closure and management practices during coronavirus outbreaks including covid-19: a rapid systematic review," *The Lancet Child & Adolescent Health*, vol. 4, no. 5, pp. 397–404, 2020.

[13] National Renewable Energy Laboratory (NREL), "Green the grid, green the grid: the role of storage and demand response," 2015, Accessed: 2023-09-15. [Online]. Available: https://www.nrel.gov/docs/fy15osti/63041.pdf

[14] Z. Li, S. Wang, X. Zheng, F. De Leon, and T. Hong, "Dynamic demand response using customer coupons considering multiple load aggregators to simultaneously achieve efficiency and fairness," *IEEE Transactions on Smart Grid*, vol. 9, no. 4, pp. 3112–3121, 2016.

[15] H. Xu, H. Sun, D. Nikovski, S. Kitamura, K. Mori, and H. Hashimoto, "Deep reinforcement learning for joint bidding and pricing of load serving entity," *IEEE Transactions on Smart Grid*, vol. 10, no. 6, pp. 6366–6375, 2019.

[16] S. Eikenberry, M. Mancuso, E. Iboi, T. Phan, K. Eikenberry, Y. Kuang, E. Kostelich, and A. Gumel, "To mask or not to mask: modeling the potential for face mask use by the general public to curtail the COVID-19 pandemic," *Infectious Disease Modelling*, vol. 5, pp. 293–308, 2020.

[17] K. Zhang, T. Vilches, M. Tariq, A. Galvani, and S. Moghadas, "The impact of mask-wearing and shelter-in-place on COVID-19 outbreaks in the United States," *The International Journal of Infectious Diseases*, vol. 101, pp. 334–341, 2020.

[18] A. Mullard, "COVID-19 vaccine development pipeline gears up," *The Lancet*, vol. 395, no. 10239, pp. 1751–1752, 2020.

[19] H. Jahani, A. Chaleshtori, S. Khaksar, A. Aghaie, and J.-B. Sheu, "COVID-19 vaccine distribution planning using a congested queuing system—A real case from Australia," *Transportation Research Part E: Logistics and Transport. Review*, vol. 163, p. 102749, 2022.

[20] "Coronavirus Disease (COVID-19): Vaccines," https://www.who.int/news-room/questions-and-answers/item/coronavirus-disease-(covid-19)-vaccines, accessed on 20 November 2022.

[21] American Council on Science and Health, "COVID-19 Ethics: How Do We Prioritize The Vaccination Order?" https://www.acsh.org/news/2021/01/06/covid-19-ethics-how-do-we-prioritize-vaccination-order-15253, 2021, accessed on 25 October 2022.

[22] T. Kundu, J.-B. Sheu, and H.-T. Kuo, "Emergency logistics management—review and propositions for future research," *Transportation Research Part E: Logistics and Transport. Review*, vol. 164, p. 102789, 2022.

[23] C. Kerr, R. Stuart, D. Mistry, R. Abeysuriya, K. Rosenfeld, G. Hart, R. Nú˜nez, J. Cohen, P. Selvaraj, and B. Hagedorn, "Covasim: an agent-based model of COVID-19 dynamics and interventions," *PLoS Computational Biology*, vol. 17, no. 7, p. e1009149, 2021.

[24] Q. Luo, R. Weightman, S. T. McQuade, M. Díaz, E. Tr´elat, and W. Barbour, "Optimization of vaccination for COVID-19 in the midst of a pandemic," *arXiv preprint arXiv:2203.09502*, 2022.

[25] Q. Li and Y. Huang, "Optimizing global COVID-19 vaccine allocation: an agent-based computational model of 148 countries," *PLoS Computational Biology*, vol. 18, no. 9, p. e1010463, 2022.

[26] M. Shamil, F. Farheen, N. Ibtehaz, I. Khan, and M. Rahman, "An agent-based modeling of covid-19: validation, analysis, and recommendations," *Cognitive Computation*, pp. 1–12, 2021.

[27] S. Müller, M. Balmer, W. Charlton, R. Ewert, A. Neumann, C. Rakow, T. Schlenther, and K. Nagel, "Predicting the effects of COVID-19 related interventions in urban settings by combining activity-based modelling, agent-based simulation, and mobile phone data," *PLoS One*, vol. 16, no. 10, 2021.

[28] J. Li and P. Giabbanelli, "Returning to a normal life via COVID-19 vaccines in the United States: a large-scale agent-based simulation study," *JMIR Medical Informatics*, vol. 9, no. 4, p. e27419, 2021.

[29] B. Jahn, G. Sroczynski, M. Bicher, C. Rippinger, N. Mühlberger, J. Santamaria, C. Urach, M. Schomaker, I. Stojkov, and D. Schmid, "Targeted covid-19 vaccination (tav-covid) considering limited vaccination capacities—an agent-based modeling evaluation," *Vaccines*, vol. 9, no. 5, p. 434, 2021.

[30] E. J. Emanuel, G. Persad, R. Upshur, B. Thome, M. Parker, A. Glickman, C. Zhang, C. Boyle, M. Smith, and J. P. Phillips, "Fair allocation of scarce medical resources in the time of covid-19," *New England Journal of Medicine*, 2020.

[31] S. Ahadian, M. Pishvaee, and H. Jahani, "Reorganization of a medical service network to manage pandemic waves: a real case study," *Operational Research for Health Care*, vol. 39, p. 100410, 2023.

[32] M. Alizadeh, M. Pishvaee, H. Jahani, M. Paydar, and A. Makui, "Viable healthcare supply chain network design for a pandemic," *Annals of Operations Research*, vol. 328, no. 1, pp. 35–73, 2023.

[33] L. Duijzer, W. van Jaarsveld, J. Wallinga, and R. Dekker, "Dose-optimal vaccine allocation over multiple populations," *Production and Operations Management*, vol. 27, no. 1, pp. 143–159, 2018.

[34] V. Manupati, T. Schoenherr, N. Subramanian, M. Ramkumar, B. Soni, and S. Panigrahi, "A multi-echelon dynamic cold chain for managing vaccine distribution," *Transportation Research Part E: Logistics and Transportation Review*, vol. 156, p. 102542, 2021.

[35] M. Fadaki, A. Abareshi, S. Far, and P. Lee, "Multi-period vaccine allocation model in a pandemic: a case study of COVID-19 in Australia," *Transportation Research Part E: Logistics and Transport. Review*, vol. 161, p. 102689, 2022.

[36] R. Ochoa-Barrag´an, A. del Carmen Munguía-L´opez, and J. Ponce-Ortega, "Strategic planning for the optimal distribution of COVID-19 vaccines," *Socio-Economic Planning Sciences*, vol. 87, p. 101559, 2023.

[37] H. Bandi and D. Bertsimas, "Optimizing influenza vaccine composition: from predictions to prescriptions," *Machine Learning for Healthcare Conference*, pp. 121–142, 2020.

[38] S.-H. Cho, "The optimal composition of influenza vaccines subject to random production yields," *Manufacturing & Service Operations Management*, vol. 12, no. 2, pp. 256–277, 2010.

[39] L. Kornish and R. Keeney, "Repeated commit-or-defer decisions with a deadline: the influenza vaccine composition," *Operations Research*, vol. 56, no. 3, pp. 527–541, 2008.

[40] K. Arifoglu, S. Deo, and S. Iravani, "Consumption externality and yield uncertainty in the influenza vaccine supply chain: interventions in demand and supply sides," *Management Science*, vol. 58, no. 6, pp. 1072–1091, 2012.

[41] A. Federgruen and N. Yang, "Competition under generalized attraction models: applications to quality competition under yield uncertainty," *Management Science*, vol. 55, no. 12, pp. 2028–2043, 2009.

[42] H. Mamani, S. Chick, and D. Simchi-Levi, "A game-theoretic model of international influenza vaccination coordination," *Management Science*, vol. 59, no. 7, pp. 1650–1670, 2013.

[43] C.-L. Su and D. Kirschen, "Quantifying the effect of demand response on electricity markets," *IEEE Transactions on Power Systems*, vol. 24, no. 3, pp. 1199–1207, 2009.

[44] S. Jacobson, E. Sewell, R. Proano, and J. Jokela, "Stockpile levels for pediatric vaccines: how much is enough?" *Vaccine*, vol. 24, no. 17, pp. 3530–3537, 2006.

[45] T. Dai, S.-H. Cho, and F. Zhang, "Contracting for on-time delivery in the us influenza vaccine supply chain," *Manufacturing & Service Operations Management*, vol. 18, no. 3, pp. 332–346, 2016.

[46] M. Golan, B. Trump, J. Cegan, and I. Linkov, "The Vaccine Supply Chain: a Call for Resilience Analytics to Support COVID-19 Vaccine Production and Distribution," in *COVID-19: Systemic Risk and Resilience*. Springer, 2021, pp. 389–437.

[47] K. Bubar, K. Reinholt, S. Kissler, M. Lipsitch, S. Cobey, Y. Grad, and D. Larremore, "Model-informed COVID-19 vaccine prioritization strategies by age and serostatus," *Science*, vol. 371, no. 6532, pp. 916–921, 2021.

[48] A. Babus, S. Das, and S. Lee, "The optimal allocation of covid-19 vaccines," *Economics Letters*, vol. 224, p. 111008, 2023.

[49] B. Vahdani, M. Mohammadi, S. Thevenin, M. Gendreau, A. Dolgui, and P. Meyer, "Fair-split distribution of multi-dose vaccines with prioritized age groups and dynamic demand: the case study of COVID-19," *European Journal of Operational Research*, vol. 310, no. 3, pp. 1249–1272, 2023.

[50] P. Jarumaneeroj, P. Dusadeerungsikul, T. Chotivanich, T. Nopsopon, and K. Pongpirul, "An epidemiology-based model for the operational allocation of COVID-19 vaccines: a case study of Thailand," *Computers Industrial Engineering*, vol. 167, p. 108031, 2022.

[51] D. Bertsimas, V. Digalakis, A. Jacquillat, M. Li, and A. Previero, "Where to locate COVID-19 mass vaccination facilities?" *Naval Research Logistics*, vol. 69, no. 2, pp. 179–200, 2022.

[52] J. Zhang, D. Long, and Y. Li, "A reliable emergency logistics network for COVID-19 considering the uncertain time-varying demands," *Transportation Research Part E: Logistics and Transportation Review*, vol. 172, p. 103087, 2023.

[53] B. Basciftci, X. Yu, and S. Shen, "Resource distribution under spatiotemporal uncertainty of disease spread: stochastic versus robust approaches," *Computers Operations Research*, vol. 149, 2023.

[54] X. Yin, S. Bushaj, Y. Yuan, and E. Büyüktahakın, "COVID-19: An Agent-Based Simulation-Optimization Approach to Vaccine Center Location Vaccine Allocation Problem," *Under revision for IISE Transactions*, 2023.

[55] H. Jahani, B. Abbasi, and S. Talluri, "Supply chain network redesign: a technical note on optimising financial performance," *Decision Sciences*, vol. 50, no. 6, pp. 1319–1353, 2019.

[56] A. Saif and S. Elhedhli, "Cold supply chain design with environmental considerations: a simulation-optimization approach," *European Journal of Operational Research*, vol. 251, no. 1, pp. 274–287, 2016.

[57] W. Wilhelm, X. Han, and C. Lee, "Computational comparison of two formulations for dynamic supply chain reconfiguration with capacity expansion and contraction," *Computers Operations Research*, vol. 40, no. 10, pp. 2340–2356, 2013.

[58] B. Pimentel, G. Mateus, and F. Almeida, "Stochastic capacity planning and dynamic network design," *International Journal of Production Economics*, vol. 145, no. 1, pp. 139–149, 2013.

[59] M. Fattahi, M. Mahootchi, K. Govindan, and S. Husseini, "Dynamic supply chain network design with capacity planning and multi-period pricing," *Transportation Research Part E: Logistics and Transport. Review*, vol. 81, pp. 169–202, 2015.

[60] P. Thanh, N. Bostel, and O. Péton, "A dynamic model for facility location in the design of complex supply chains," *International Journal of Production Economics*, vol. 113, no. 2, pp. 678–693, 2008.

[61] J. Lim, B. Norman, and J. Rajgopal, "Redesign of vaccine distribution networks," *International Transactions in Operational Research*, vol. 29, no. 1, pp. 200–225, 2022.

[62] S. Abazari, A. Aghsami, and M. Rabbani, "Prepositioning and distributing relief items in humanitarian logistics with uncertain parameters," *Socioeconomic Planning Sciences*, vol. 74, p. 100933, 2021.

[63] B. Kargar, M. Pishvaee, H. Jahani, and J.-B. Sheu, "Organ transportation and allocation problem under medical uncertainty: a real case study of liver transplantation," *Transportation Research Part E: Logistics and Transport. Review*, vol. 134, p. 101841, 2020.

[64] K. Cooper, S. Hunter, and K. Nagaraj, "An epsilon-constraint method for integer-ordered bi-objective simulation optimization," in *Winter Simulation Conference (WSC) 2017*. IEEE, 2017, pp. 2303–2314.

[65] X. Yang, Z. Leng, S. Xu, C. Yang, K. Liu, Y. Song, and L. Zhang, "Multi-objective optimal scheduling for CCHP microgrids considering peak-load reduction by augmented -constraint method," *Renewable Energy*, vol. 172, pp. 408–423, 2021.

[66] E. Tirkolaee, A. Goli, A. Faridnia, M. Soltani, and G.-W. Weber, "Multi-objective optimization for the reliable pollution-routing problem with cross-dock selection using pareto-based algorithms," *Journal of Cleaner Production*, vol. 276, p. 122927, 2020.

[67] S. Moghadam, A. Aghsami, and M. Rabbani, "A hybrid NSGA-II algorithm for the closed-loop supply chain network design in e-commerce," *RAIRO: Recherche Op´erationnelle*, vol. 55, p. 1643, 2021.

[68] D. Light and J. Lexchin, "The costs of coronavirus vaccines and their pricing," *Journal of the Royal Society of Medicine*, vol. 114, no. 11, pp. 502–504, 2021.

[69] "Cost of Living Index by State 2022," https://worldpopulationreview.com/state-rankings/cost-of-living-index-by-state, accessed on 29 November 2022.

[70] T.-M. Choi, "Risk analysis in logistics systems: A research agenda during and after the COVID-19 pandemic," *Transportation Research Part E: Logistics and Transportation Review*, vol. 145, p. 102190, 2021.

[71] COVID-19 Data Tracker. https://covid.cdc.gov/covid-data-tracker/datatracker-home. Accessed on 20 November 2022.

[72] Weekly United States COVID-19 Cases and Deaths by States. https://data.cdc.gov/Case-Surveillance/Weekly-United-States-COVID-19-Cases-and-Deaths-by-/pwn4-m3yp/data. Accessed on 20 November 2022.

[73] U.S. Census Bureau, "State Population by Characteristics: 2020-2021," https://www.census.gov/data/datasets/time-series/demo/popest/2020s-statedetail.html, 2022, accessed on 20 November 2022.

[74] "Covid-19 dashboard," https://coronavirus.jhu.edu/map.html, accessed on 29 November 2022.

[75] H. T. Haider, O. H. See, and W. Elmenreich, "A review of residential demand response of smart grid," *Renewable and Sustainable Energy Reviews*, vol. 59, pp. 166–178, 2016.

[76] California Independent System Operator (CAISO), "Conditions on the grid becoming more strained as heat wave intensifies," 2022. [Online]. Available: http://www.caiso.com/Documents/conditions-on-the-grid-becoming-more-strained-as-heat-wave-intensifies.pdf

[77] H. Ming, B. Xia, K.-Y. Lee, A. Adepoju, S. Shakkottai, and L. Xie, "Prediction and assessment of demand response potential with coupon incentives in highly renewable power systems," *Protection and Control of Modern Power Systems*, vol. 5, no. 1, pp. 1–14, 2020.

[78] G. Le Ray, E. M. Larsen, and P. Pinson, "Evaluating price-based demand response in practice—with application to the EcoGrid EU Experiment," *IEEE Transactions on Smart Grid*, vol. 9, no. 3, pp. 2304–2313, 2016.

[79] H. Mohsenian-Rad, "Optimal demand bidding for time-shiftable loads," *IEEE Transactions on Power Systems*, vol. 30, no. 2, pp. 939–951, 2014.

[80] C. Chen, S. Kishore, Z. Wang, M. Alizadeh, and A. Scaglione, "How will demand response aggregators affect electricity markets?—A Cournot game analysis," in *2012 5th International Symposium on Communications, Control and Signal Processing*. IEEE, 2012, pp. 1–6.

[81] L. Xie and H. Zheng, "Demand elasticity analysis by least squares support vector machine," in *2013 6th International Congress on Image and Signal Processing (CISP)*, vol. 2. IEEE, 2013, pp. 1085–1089.

[82] X. Xu, C.-f. Chen, X. Zhu, and Q. Hu, "Promoting acceptance of direct load control programs in the united states: Financial incentive versus control option," *Energy*, vol. 147, pp. 1278–1287, 2018.

[83] M. Wang, Y. Mu, T. Jiang, H. Jia, X. Li, K. Hou, and T. Wang, "Load curve smoothing strategy based on unified state model of different demand side resources," *Journal of Modern Power Systems and Clean Energy*, vol. 6, no. 3, pp. 540–554, 2018.

[84] J. Luft, "Bonus and penalty incentives contract choice by employees," *Journal of Accounting and Economics*, vol. 18, no. 2, pp. 181–206, 1994.

[85] P. Cappers, C. Goldman, and D. Kathan, "Demand response in US electricity markets: Empirical evidence," *Energy*, vol. 35, no. 4, pp. 1526–1535, 2010.

[86] S. Ghosh, J. Kalagnanam, D. Katz, M. Squillante, X. Zhang, and E. Feinberg, "Incentive design for lowest cost aggregate energy demand reduction," in *2010 First IEEE International Conference on Smart Grid Communications*. IEEE, 2010, pp. 519–524.

[87] H. Aalami, M. P. Moghaddam, and G. Yousefi, "Demand response modeling considering interruptible/curtailable loads and capacity market programs," *Applied Energy*, vol. 87, no. 1, pp. 243–250, 2010.

[88] H. Zhong, L. Xie, and Q. Xia, "Coupon incentive-based demand response: Theory and case study," *IEEE Transactions on Power Systems*, vol. 28, no. 2, pp. 1266–1276, 2012.

[89] D. S. Kirschen, G. Strbac, P. Cumperayot, and D. de Paiva Mendes, "Factoring the elasticity of demand in electricity prices," *IEEE Transactions on Power Systems*, vol. 15, no. 2, pp. 612–617, 2000.

[90] A. Asadinejad, A. Rahimpour, K. Tomsovic, H. Qi, and C.-f. Chen, "Evaluation of residential customer elasticity for incentive based demand response programs," *Electric Power Systems Research*, vol. 158, pp. 26–36, 2018.

[91] Q. Shi, C.-F. Chen, A. Mammoli, and F. Li, "Estimating the profile of incentive-based demand response (IBDR) by integrating technical models and social-behavioral factors," *IEEE Transactions on Smart Grid*, vol. 11, no. 1, pp. 171–183, 2019.

[92] X. Lu, X. Ge, K. Li, F. Wang, H. Shen, P. Tao, J. Hu, J. Lai, Z. Zhen, M. Shafie-khah *et al.*, "Optimal bidding strategy of demand response aggregator based on customers' responsiveness behaviors modeling under different incentives," *IEEE Transactions on Industry Applications*, vol. 57, no. 4, pp. 3329–3340, 2021.

[93] V. C. Pandey, N. Gupta, K. Niazi, A. Swarnkar, and R. A. Thokar, "Modeling and assessment of incentive based demand response using price elasticity model in distribution systems," *Electric Power Systems Research*, vol. 206, p. 107836, 2022.

[94] N. Li, L. Gan, L. Chen, and S. H. Low, "An optimization-based demand response in radial distribution networks," in *2012 IEEE Globecom Workshops*. IEEE, 2012, pp. 1474–1479.

[95] N. Li, L. Chen, and S. H. Low, "Exact convex relaxation of opf for radial networks using branch flow model," in *2012 IEEE Third International Conference on Smart Grid Communications (SmartGridComm)*. IEEE, 2012, pp. 7–12.

[96] M. E. Baran and F. F. Wu, "Optimal capacitor placement on radial distribution systems," *IEEE Transactions on Power Delivery*, vol. 4, no. 1, pp. 725–734, 1989.

[97] B. Subhonmesh, S. H. Low, and K. M. Chandy, "Equivalence of branch flow and bus injection models," in *2012 50th Annual Allerton Conference on Communication, Control, and Computing (Allerton)*. IEEE, 2012, pp. 1893–1899.

[98] M. Baran and F. F. Wu, "Optimal sizing of capacitors placed on a radial distribution system," *IEEE Transactions on Power Delivery*, vol. 4, no. 1, pp. 735–743, 1989.

[99] S. Kumar and M. Sushama, "Strategic demand response framework for energy management in distribution system based on network loss sensitivity," *Energy and Environment*, vol. 31, no. 8, pp. 1385–1402, 2020.

[100] T. V. Vu, C. S. Edrington, and R. Hovsapian, "Distributed demand response considering line loss for distributed renewable energy systems," in *2017 IEEE Power & Energy Society General Meeting*. IEEE, 2017, pp. 1–5.

[101] J. M. Arroyo, L. Baringo, A. Baringo, R. Bolaños, N. Alguacil, and N. G. Cobos, "On the use of a convex model for bulk storage in MIP-based power system operation and planning," *IEEE Transactions on Power Systems*, vol. 35, no. 6, pp. 4964–4967, 2020.

[102] PJM Data Miner, "Real-Time Day-Ahead Monthly Locational Marginal Prices (LMPs)," 2018. [Online]. Available: https://dataminer2.pjm.com/feed/rt$_d a_m onthly_l mps$

[103] C. Xu, B. Liu, and Y. Zhao, "Offline reinforcement learning for price-based demand response program design," in *57th Annual Conference on Information Sciences and Systems (CISS)*. IEEE, 2023, pp. 1–6.

[104] J. van Tilburg, L. C. Siebert, and J. L. Cremer, "MARL-iDR: Multi-agent reinforcement learning for incentive-based residential demand response," *arXiv preprint arXiv:2304.04086*, 2023.

[105] S. Nolan and M. O'Malley, "Challenges and barriers to demand response deployment and evaluation," *Applied Energy*, vol. 152, pp. 1–10, 2015.

[106] J. S. Vardakas, N. Zorba, and C. V. Verikoukis, "A survey on demand response programs in smart grids: Pricing methods and optimization algorithms," *IEEE Communications Surveys and Tutorials*, vol. 17, no. 1, pp. 152–178, 2014.

[107] R. Lu, S. H. Hong, and X. Zhang, "A dynamic pricing demand response algorithm for smart grid: Reinforcement learning approach," *Applied Energy*, vol. 220, pp. 220–230, 2018.

[108] B. Shen, G. Ghatikar, Z. Lei, J. Li, G. Wikler, and P. Martin, "The role of regulatory reforms, market changes, and technology development to make demand response a viable resource in meeting energy challenges," *Applied Energy*, vol. 130, pp. 814–823, 2014.

[109] P. Siano, "Demand response and smart grids—a survey," *Renewable and Sustainable Energy Reviews*, vol. 30, pp. 461–478, 2014.

[110] P. T. Baboli, M. Eghbal, M. P. Moghaddam, and H. Aalami, "Customer behavior based demand response model," in *2012 IEEE Power and Energy Society General Meeting*. IEEE, 2012, pp. 1–7.

[111] Z. Wang, H. Li, N. Deng, K. Cheng, B. Lu, B. Zhang, and B. Wang, "How to effectively implement an incentive-based residential electricity demand response policy? experience from large-scale trials and matching questionnaires," *Energy Policy*, vol. 141, p. 111450, 2020.

[112] Y.-C. Hung and G. Michailidis, "Modeling and optimization of time-of-use electricity pricing systems," *IEEE Transactions on Smart Grid*, vol. 10, no. 4, pp. 4116–4127, 2018.

[113] K. Vanthournout, B. Dupont, W. Foubert, C. Stuckens, and S. Claessens, "An automated residential demand response pilot experiment, based on day-ahead dynamic pricing," *Applied Energy*, vol. 155, pp. 195–203, 2015.

[114] C. Li, C. Liu, K. Deng, X. Yu, and T. Huang, "Data-driven charging strategy of pevs under transformer aging risk," *IEEE Transactions on Control Systems Technology*, vol. 26, no. 4, pp. 1386–1399, 2017.

[115] M. Yu and S. H. Hong, "Incentive-based demand response considering hierarchical electricity market: A stackelberg game approach," *Applied Energy*, vol. 203, pp. 267–279, 2017.

[116] A. Gholian, H. Mohsenian-Rad, and Y. Hua, "Optimal industrial load control in smart grid," *IEEE Transactions on Smart Grid*, vol. 7, no. 5, pp. 2305–2316, 2015.

[117] B.-G. Kim, Y. Zhang, M. Van Der Schaar, and J.-W. Lee, "Dynamic pricing and energy consumption scheduling with reinforcement learning," *IEEE Transactions on Smart Grid*, vol. 7, no. 5, pp. 2187–2198, 2015.

[118] X. Kong, D. Kong, J. Yao, L. Bai, and J. Xiao, "Online pricing of demand response based on long short-term memory and reinforcement learning," *Applied energy*, vol. 271, p. 114945, 2020.

[119] Z. Wen, D. O'Neill, and H. Maei, "Optimal demand response using device-based reinforcement learning," *IEEE Transactions on Smart Grid*, vol. 6, no. 5, pp. 2312–2324, 2015.

[120] A. Mathew, A. Roy, and J. Mathew, "Intelligent residential energy management system using deep reinforcement learning," *IEEE Systems Journal*, vol. 14, no. 4, pp. 5362–5372, 2020.

[121] A. Ghasemkhani and L. Yang, "Reinforcement learning based pricing for demand response," in *2018 IEEE International Conference on Communications Workshops (ICC Workshops)*. IEEE, 2018, pp. 1–6.

[122] D. Jang, L. Spangher, T. Srivistava, M. Khattar, U. Agwan, S. Nadarajah, and C. Spanos, "Offline-online reinforcement learning for energy pricing in office demand response: lowering energy and data costs," in *Proceedings of the 8th ACM International Conference on Systems for Energy-Efficient Buildings, Cities, and Transportation*, 2021, pp. 131–139.

[123] R. Lu and S. H. Hong, "Incentive-based demand response for smart grid with reinforcement learning and deep neural network," *Applied energy*, vol. 236, pp. 937–949, 2019.

[124] L. Wen, K. Zhou, J. Li, and S. Wang, "Modified deep learning and reinforcement learning for an incentive-based demand response model," *Energy*, vol. 205, p. 118019, 2020.

[125] H. Xu, W. Kuang, J. Lu, and Q. Hu, "A modified incentive-based demand response model using deep reinforcement learning," in *2020 12th IEEE PES Asia-Pacific Power and Energy Engineering Conference (APPEEC)*. IEEE, 2020, pp. 1–5.

[126] R. S. Sutton and A. G. Barto, *Reinforcement learning: An introduction*. MIT press, 2018.

[127] A. Oğuzkağan and Ü. B. Filik, "Optimal management of household loads based on consumer elasticity and appliance diversity," in *2020 International Conference on Smart Energy Systems and Technologies (SEST)*. Ieee, 2020, pp. 1–6.

[128] K. Ma, T. Yao, J. Yang, and X. Guan, "Residential power scheduling for demand response in smart grid," *International Journal of Electrical Power & Energy Systems*, vol. 78, pp. 320–325, 2016.

[129] L. Buşoniu, R. Babu**v**ska, and B. De Schutter, "Multi-agent reinforcement learning: An overview," *Innovations in Multi-agent Systems and Applications-1*, pp. 183–221, 2010.

[130] R. Crites and A. Barto, "Improving elevator performance using reinforcement learning," *Advances in Neural Information Processing Systems*, vol. 8, 1995.

[131] M. J. Matarić, "Reinforcement learning in the multi-robot domain," *Robot colonies*, pp. 73–83, 1997.

[132] H. T. Tse and H.-f. Leung, "Exploiting semantic epsilon greedy exploration strategy in multi-agent reinforcement learning," *arXiv preprint arXiv:2201.10803*, 2022.

[133] J. Fan, Z. Wang, Y. Xie, and Z. Yang, "A theoretical analysis of deep q-learning," in *Learning for Dynamics and Control*. PMLR, 2020, pp. 486–489.

[134] Y. Li, "Deep reinforcement learning: An overview," *arXiv preprint arXiv:1701.07274*, 2017.